AFRL-AFOSR-UK-TR-2023-0060

Non-Foster Networks for Tunable and Wideband RF Devices

Hrabar, Silvio
FAKULTET ELEKTROTEHNIKE I RACUNARSTVA
UNSKA 3
ZAGREB, , 10000
HR

03/30/2023
Final Technical Report

DISTRIBUTION A: Distribution approved for public release.

Air Force Research Laboratory
Air Force Office of Scientific Research
European Office of Aerospace Research and Development
Unit 4515 Box 14, APO AE 09421

REPORT DOCUMENTATION PAGE

PLEASE DO NOT RETURN YOUR FORM TO THE ABOVE ORGANIZATION.

1. REPORT DATE
20230330

2. REPORT TYPE
Final

3. DATES COVERED

START DATE
20191201

END DATE
20221130

4. TITLE AND SUBTITLE
Non-Foster Networks for Tunable and Wideband RF Devices

5a. CONTRACT NUMBER

5b. GRANT NUMBER
FA8655-20-1-7008

5c. PROGRAM ELEMENT NUMBER
61102F

5d. PROJECT NUMBER

5e. TASK NUMBER

5f. WORK UNIT NUMBER

6. AUTHOR(S)
Silvio Hrabar

7. PERFORMING ORGANIZATION NAME(S) AND ADDRESS(ES)
FAKULTET ELEKTROTEHNIKE I RACUNARSTVA
UNSKA 3
ZAGREB 10000
HR

8. PERFORMING ORGANIZATION REPORT NUMBER

9. SPONSORING/MONITORING AGENCY NAME(S) AND ADDRESS(ES)
EOARD
UNIT 4515
APO AE 09421-4515

10. SPONSOR/MONITOR'S ACRONYM(S)
AFRL/AFOSR IOE

11. SPONSOR/MONITOR'S REPORT NUMBER(S)
AFRL-AFOSR-UK-TR-2023-0060

12. DISTRIBUTION/AVAILABILITY STATEMENT
A Distribution Unlimited: PB Public Release

13. SUPPLEMENTARY NOTES

14. ABSTRACT

As a short summary, the realized outcomes of the project are:

• We have shown that all electronic circuits that mimic negative immittance (NICs and NIIs) rely on the superposition of the original signal and assisting signal. Since these signals must be coherent, all classical circuits use positive feedback, which often leads to instability. It is extremely important to make a clear distinction between electronic admittance (associated with SCS properties) and electronic impedance (associated with OCS properties). We have also shown that a simple one-pole model of the NIC/NII amplifier is a useful approximation for both prediction of dispersion properties for frequencies below the pole frequency and for stability predictions. It was found that the dispersion of all the circuits analyzed is negligible when the maximum operating frequency is below one-tenth of the frequency of the first pole. The "parasitic" real part of the input impedance/admittance of the negative capacitor/inductor is negative in the SCS design and positive in the OCS design. This "parasitic" conductance/resistance can be compensated by an additional passive load network.

• We have reviewed all known methods of stability prediction and proposed a simple, straightforward method to develop simple equivalent circuits for all one-pole non-Foster and negative elements. We have also studied the most common realizations of NIC/NII circuits and performed a very thorough analysis of their stability properties. As expected, the stability properties were found to depend on both the NIC/NII topology and the passive external network topology. It was found that both OCS and SCS DC coupled negative capacitors/inductors/resistors based on NICs or NIIs always have an unstable DC pole that degrades the stability robustness. In addition, the DC coupled negative OCS capacitor and negative SCS inductor have a pole at the origin that causes DC offset at the input. The overall conclusion is that there is no such thing as the "most robust NIC/NII topology", per se.

• We have investigated the possibilities of improving the stability properties and found that the introduction of a bandpass mode significantly improves the stability properties. It turns out that the operating bandwidth is always inversely proportional to the range of allowable external impedances, i.e., to the stability robustness. We have applied this finding to the well-known Linvill NIC and shown that the stability characteristics can be improved by adjusting the operating bandwidth through proper selection of cross-coupling capacitors. We have also developed a very simple and accurate equivalent circuit for this modified Linvill negative capacitor.

• We have presented a novel design of non-Foster and Negative elements based on some very simple LP and HP passive series/shunt networks that exhibit non-Foster ‘inverse’ dispersion such that they behave as band-limited ‘lossy negative capacitors/inductors. The losses of these passive ‘negative’ networks can be compensated by an additional negative series/shunt resistance/conductance. These novel non-Foster elements have shown stability properties better than the stability properties of all classical (NIC/NIVbased) non-Foster elements in the literature. The correctness of the proposed approach has been verified using four independent designs of negative capacitors and negative inductors in L and X frequency bands, in 40-nm CMOS technology. The generated negative capacitance capacitances and negative inductance ranged from -0.5 pF to -1 pF and -1 nH to -5 nH, respectively.

• In addition, we have shown applications of the proposed non-Foster elements in some RF tunable/broadband devices. We have designed and fabricated a general negative Miler capacitor using HCBT technology that produces capacitance from -0.3 pF to -0.1 pF in the frequency range from DC to 2GHz. We have also developed a tunable negative inductor that can be tuned between -100 pH and -300 pH in the range of 5-15 GHz. Finally, we have developed a tunable non-Foster-based bandpass filter for the 2.5-GHz band using 40-nm CMOS technology. We have demonstrated tunability of the center frequency up to 20% and bandwidth up to 30%, with return loss of more than 15 dB. A very important feature is that the symmetry of the bandpass curve is maintained over the tuning bandwidth, which is not possible with a standard passive design.

In addition to applications in RF tunable/broadband networks, we have found that the developed methodology can be extended to self-oscillating active antennas, PT -symmetric systems, and
time-varying systems. In future research projects, we plan to develop a general, unified methodology that can be used to design all of these systems .

15. SUBJECT TERMS

16. SECURITY CLASSIFICATION OF:			**17. LIMITATION OF ABSTRACT**	**18. NUMBER OF PAGES**
a. REPORT U	**b. ABSTRACT** U	**c. THIS PAGE** U	SAR	157

19a. NAME OF RESPONSIBLE PERSON
ATTILA SZEP

19b. PHONE NUMBER *(Include area code)*
314 235 6044

FINAL REPORT FOR CONTRACT FA8655-20-1-7008

Non-Foster Networks for Tunable and Wideband RF Devices

by

Silvio Hrabar
Igor Krois
Ante Brizic
Dominik Zanic
Katarina Lebo
Darin Nozina
Boris Okorn

SUBMITTED BY: Prof. Silvio Hrabar
Faculty of Electrical Engineering and Computing
University of Zagreb
Unska 3
Zagreb, HR-10000, Croatia

28th February 2023

TABLE OF CONTENTS

Chapter 1. INTRODUCTION: NEGATIVE ELEMENTS IN RF ELECTRONICS

Introduction: Negative elements in RF electronics

There is a clear trend toward increasing the bandwidth of radio frequency (RF) communications, radar, surveillance, and electronic warfare systems. It applies both to RF electronic devices used as building blocks and to the associated antennas. This trend is driven not only by ever-increasing modulation data rates, but also by the requirements for "smart" systems capable of reconfiguring themselves to achieve maximum performance in a harsh electromagnetic environment with interfering signals [1]. All these systems share the same basic physical background: radiation, propagation, and guiding of electromagnetic waves and the subsequent processing of the information signals impressed into them. Typical electronic devices used in RF system include amplifiers, oscillators, filters, couplers, and combiners/splitters, to name a few [2].

The need for larger bandwidth has led to a shift in operating frequencies to higher microwave and millimeter frequency bands. For active devices, this shift introduces an additional problem, namely the maximum available (and sustainable) RF power. Therefore, a trade-off between bandwidth, reconfigurability, and available RF power level is a key problem for the transmit blocks of modern radio frequency systems.

In recent years, the power-frequency problem has been studied very thoroughly and with remarkable success, mainly thanks to available semiconductor technologies [3]. Among the promising examples, III -V compounds such as GaAs and GaN technology can handle up to several watts in the L (1-2 GHz), C (5-8 GHz), and Ku (12-18 GHz) bands with power efficiency of 40% [3]. However, for some special applications, an even broader behavior is required, which can range from L to Ku bands. In this context, it should be understood that the amplifier characteristics depend not only on the active element but also on the associated broadband reactive network. Although this fact is obvious and well known, research on broadband reactive networks lags far behind the semiconductor field [3].

Most commercial amplifiers and antenna systems use ‘classical’ passive matching networks that have been known for many years. This is surprising since the bandwidth and reconfigurability/tunability characteristics of current RF systems are primarily limited by the characteristics of embedded reactive networks.

A passive reactive network consists only of ordinary energy-storing reactive elements such as capacitors and inductors (Figure 1-1).

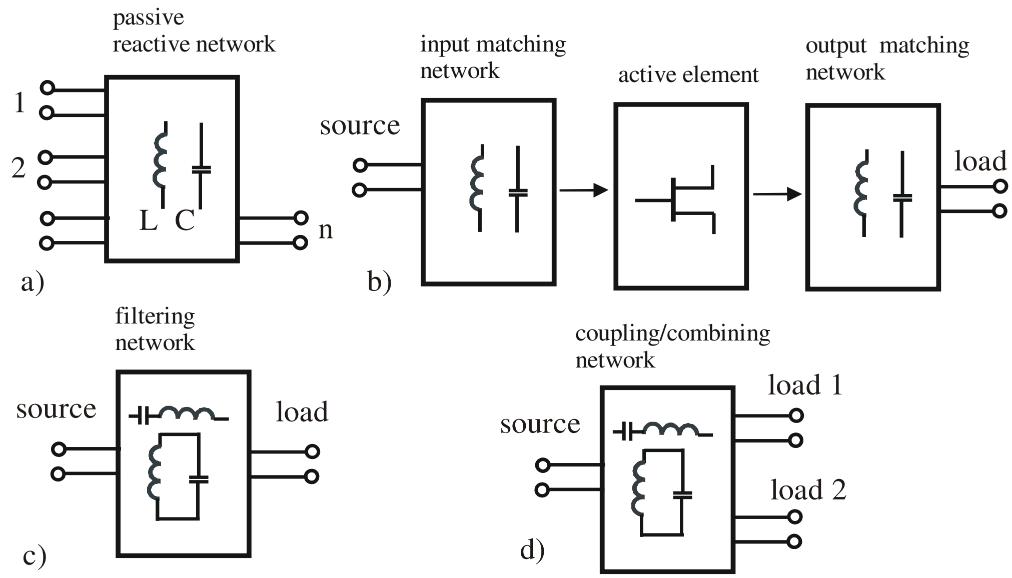

Figure 1-1 a) Definition of a passive reactive network, b) Reactive network as a matching block in an RF amplifier, c) Reactive network as a filtering structure, d) Reactive network as a coupling/splitting/combining structure

A reactive network may also contain segments of lossless transmission lines, which can be viewed (within a finite bandwidth) as a ladder network composed of inductors and capacitors. The absence of losses allows complete control of the energy transmitted through a system as well as the energy reflected back to the source.

In a familiar case of RF power amplifier (Figure 1-1b), reactive networks operate as matching blocks, the purpose of which is the maximization of signal power delivered by a source to an active element and, subsequently, the maximization of a signal power delivered by an active element to a load. A matching network converts an active element's input (output) complex impedance $Z_A=R_A+jX_A$ into a real system impedance Z_0. This process includes cancellation of the imaginary part of active element impedance (X_A) by its ''negative image'' ($-X_A$) and transformation of remaining real part (R_A) into real system impedance Z_0. Obviously, a matching process should be effective across the whole operation bandwidth. Again, an identical approach is used for resonant matching of an antenna to a transmitter output power amplifier or receiver input amplifier.

A slightly modified matching mechanism is used in RF filters (Figure 1-1c). An RF filter is actually a special kind of matching network. It obtains either a good matching or nearly total reflection within some predetermined bands (band-pass or band-stop filter). It is worth noting that the phase characteristic of a filtering network is very important since it directly affects group delay (and, therefore, the signal distortion). Again, the effective matching mechanism is needed across a whole operating bandwidth.

Yet another very common application of reactive networks is in signal combining/splitting and coupling structures such as directional couplers and hybrid junctions (Figure 1-1d). These are multi-port reactive networks that employ frequency-dependent matching mechanism across the signal paths between different ports. By clever superposition of several multi-port matching paths, it is possible to split or combine signals, even with directional properties.

From the brief review given above, one concludes that the basic physics of matching, filtering and splitting/combining RF devices is essentially the same. It is based on impedance transformation properties of reactive network across some predetermined bandwidth.

Unfortunately, the matching bandwidth of passive reactive network is *inherently narrowband,* which seriously limits its applications. Classical matching based on ordinary positive (passive) reactance is a frequency-dependent resonance process. Physically, the energy that was stored in a reactive matching element during the previous cycle of a signal "feeds" the load, until there is no energy in its own reactance. Mathematically, two imaginary functions (reactance functions of source and load) have opposite signs, but the same modulus at a certain frequency (resonance frequency).

The fundamental question is whether it is possible for these two functions to have the same modulus but opposite signs over some bandwidth? It can be shown that the signs of the reactances of the source and load are always different (i.e., the capacitive character versus the inductive character) when the load is matched to the source, and the slope of the reactance frequency is always positive, as well. This conclusion follows from the fundamentals of electromagnetics. The reactive energy stored in the differential volume of any lossless (electric and/or magnetic) material is given by the well-known expression [4]:

$$W = \frac{1}{2}\frac{\partial[\omega\cdot\varepsilon(\omega)]}{\partial\omega}|E|^2 + \frac{1}{2}\frac{\partial[\omega\cdot\mu(\omega)]}{\partial\omega}|H|^2. \tag{1.1}$$

Here, ε and μ stand for permittivity and permeability, respectively. Irrespective of the internal structure, the overall reactive energy stored in any passive lossless material (1.1) is always greater than the energy stored in vacuum (as nicely noted in [5], some work should be done in order to polarize the material). This fact, together with the causality requirements, leads to the strong form of basic energy-dispersion constraints [4]:

$$\frac{\partial[\omega\cdot\varepsilon(\omega)]}{\partial\omega} > \varepsilon_0, \quad \frac{\partial[\omega\cdot\mu(\omega)]}{\partial\omega} > \mu_0, \tag{1.2}$$

where ε_0 and μ_0 are free-space permittivity and permeability. Inspection of (1.1 ,1.2) immediately reveals that:

$$\frac{\partial\epsilon}{\partial\omega} > 0, \qquad \frac{\partial\mu}{\partial\omega} > 0\,. \tag{1.3}$$

Equation (1.3) is a very fundamental fact that is valid for every lossless dielectric or magnetic material. Obviously, every reactive lumped element (i.e. circuit theory element) assumes presence of either dielectric material (a case of a capacitor) or magnetic material (a case of an inductor). Therefore, the requirements (1.3) can directly be transferred to the circuit-theory equivalent known as the Foster reactance theorem [6]:

$$\frac{\partial X}{\partial \omega} > 0, \qquad \frac{\partial B}{\partial \omega} > 0\,. \tag{1.4}$$

Here, X and B stand for reactance and susceptance, respectively. Foster theorem is valid for every network that contains ordinary (positive) reactive elements such as capacitors or inductors, (please see solid curves in Figure 1-2 [7]).

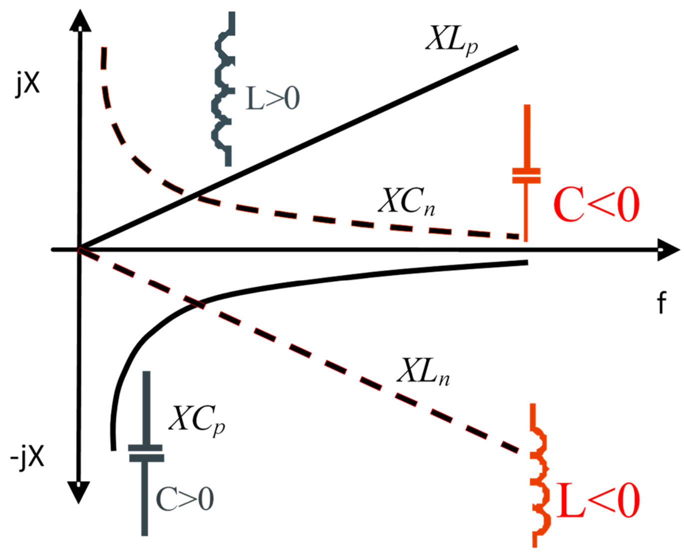

Figure 1-2 Solid: Reactance of positive (Foster) reactive elements, Dashed: Reactance of negative (non-Foster) reactive elements (taken from [7]).

Due to Foster theorem, a perfect cancellation of jX_A with $-jX_A$ is possible *at only one frequency*. In other words, maximal matching/filtering/combining bandwidth (the bandwidth with some predetermined maximal modulus of reflection coefficient) *is always fundamentally constrained* (well-known Bode-Fano constraints [2]).

This problem is well-known in the antenna community [8]. Specifically, a short antenna has predominantly reactive impedance. It should be matched to a real impedance of the feeding transmitter. Similar problem occurs in matching of high FET input impedance in RF power amplifier [3]. A simple model that describes both scenarios is sketched in the left part of Figure 1-3.

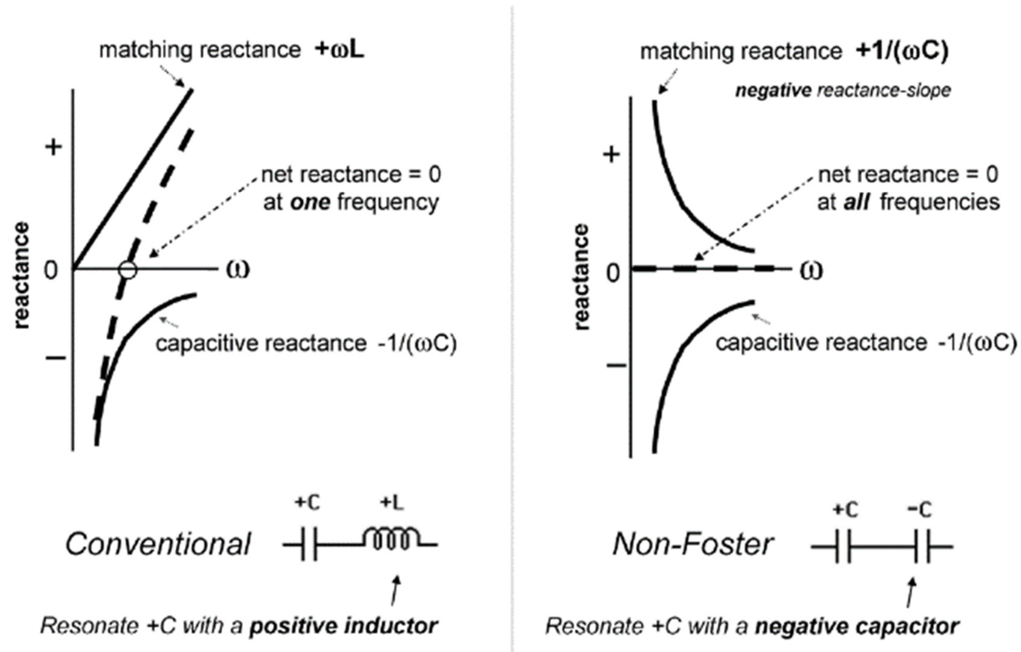

Figure 1-3 Comparison of passive matching (left) and active non-Foster matching (right) of a highly capacitive load (Figure copied from [8], copyrighted to IEEE)

As it can be seen, perfect cancellation (net reactance equal to zero) occurs at only one frequency. Predominantly capacitive character of a load ($X_A >> R_A$) inevitably leads to a rather high Q factor and, in turn, to an inevitable narrow matching bandwidth (usually defined by maximal return loss of 10 dB). Obviously, this behavior is not compatible with the requirement for wideband operation. One might turn to resistive matching that would decrease Q factor and enlarge the matching bandwidth, but it would also decrease the efficiency [3].

Similar problem occurs in filter applications (Figure 1-1c). Quite often, a narrow pass-band characteristic with high out-of-band rejection is desirable. Obviously, the Bode-Fano constraints [2] limit achievable stiffness of the filter characteristic and associated out-of-band rejection. In addition, the possibility of broad-band tuning (and, possibly, reconfiguration of the filter order) is high desirable in modern systems [1][9]. Unfortunately, there are (at least) two serious problems related to tunability and reconfigurability. Normally, one would like to maintain the shape of the filter transfer characteristic across the tuning bandwidth. For this purpose, tuning of both capacitance and inductance is required (due to Foster theorem). Second, there is a lack of suitable tuning elements, especially in microelectronics technology. One can use a varactor, but the ratio between maximum and minimum capacitance is usually too small, so additional improvements are needed. On the other hand, the technology of microelectronic variable inductance is still in infant phase.

Finally, the matching bandwidth constraints appear in the case of combining/coupling structures, as well (Figure 1-1d). In this case, the usual goal is a broad bandwidth with a good phase tracking between the output ports. A common approach is optimization of the parameters of the embedded reactive ladder networks (or lengths of coupled transmission lines), which may lead to multi-octave bandwidth. However, the wideband operation is accompanied with inevitable ‘ripples’ in the transfer characteristic, associated again with the limitations of background physics (Bode-Fano criteria and Foster’s theorem [2]). This problem becomes more important if one wants to design a device with a fixed phase shift between output ports (a quadrature hybrid, for instance) [2].

From the above discussion, it appears that the problem of complex broadband matching, related to Foster's and Bode-Fano constraints, is still not adequately solved. It is interesting to note that this matching bandwidth problem is well known in antenna technology, while its importance in RF /microwave electronics has not yet been fully recognized.

Above discussion presumes a 'traditional approach', in which the electromagnetic and electronic subsystems of wireless communication/radar systems, such as antennas, feeding networks, amplifiers, mixers, oscillators, etc., have been developed separately [2]. However, recent advances in active electromagnetic structures in general, and smart antenna systems in particular, are changing this approach and bringing together the fields of electromagnetics, radio frequency and microwave electronics. Some of the RF system components such as amplifiers, filters, couplers, etc. are now embedded in radiating structures to form an active electromagnetic system. In this "modern" approach, broadband complex matching becomes even more important as it affects not only the signal processing characteristics but also the electromagnetic (radiation) properties of a given system.

All the scenarios discussed assumed ordinary positive capacitances and inductances. On the other hand, there are active circuits that mimic the behavior of hypothetical negative capacitors and negative inductors (so-called non-Foster elements) [7][8][10][11][12][13][14][15][16] (dashed curves in Figure 1-2). The reactance of non-Foster elements has a negative slope with frequency (i.e., negative dispersion) (red dashed curves in the graph in Figure 1-2). This unusual property allows compensation for the positive dispersion of ordinary elements over a (theoretically) infinite bandwidth (right part of Figure 1-3). This "non-Foster compensation" uses a reactive network containing both positive and negative capacitors. Due to negative capacitance/inductance, the terminal current of non-Foster elements is negative (it flows outward from the positive terminal). Thus, a negative capacitor and a negative inductor behave as (reactive) sources, i.e. they are inevitably active devices.

It is important to notice that energy-dispersion constraints (and Foster's theorem) have been derived assuming that there are no losses present. So, strictly speaking, hypothetical negative resistor (an active element that delivers real power) should not be termed as a 'non-Foster element'. However, one might say that a negative capacitor, a negative inductor, together with a negative resistor form a complete group of (hypothetical) 'Negative elements'.

Although a basic idea of non-Foster elements was introduced almost hundred years ago [10][11][12][13][14], there have been very few practical applications. These mainly deal with broadband matching of small antenna systems [8][17][18][19][20][21][22][23][24][25][26][27][28][29][30][31][32][33][34][35]. In the technology of electronic RF devices and subsystems, non-Foster elements are occasionally used to cancel parasitic capacitances in power amplifiers [36] and to extend the VCO (voltage controlled oscillator) tuning range [37][38][39]. Both applications involve a network whose total capacitance is positive. Only recently has the possibility of using non-Foster-based matching networks with positive and negative capacitance in power amplifiers [40][41] and tunable filters [42] been pointed out, and it is still a matter of "speculation".

The main bottleneck preventing the widespread use of non-Foster circuits is the inherent stability problem (the non-Foster networks are susceptible to unwanted self-oscillations). As a quick hint, the ideal complete cancelation outlined in the right part of Figs. 1-3 would lead to instability. Thus, the ideal frequency-independent matching does not seem to be feasible in practice. But even if one accepts a non-ideal (partial) cancelation, stability problems are very common and severe in practice.

The stability problem occurs in both kinds of non-Foster circuitry: the ‘negative impedance converters’, (NIC) and ‘negative impedance inverters’, (NII) [10][11][12][13][14][15][16][17][27][43][44]. In essence, these circuits are specially designed amplifiers with positive feedback. Positive feedback is needed in other to assure sign flipping in the case of NICs (Z_{in} ~ -Z_{load}) or sign flipping accompanied with the inversion (Z_{in} ~ -1/Z_{load}), Z_{in} and Z_{load} being input and load impedances, respectively.

In the literature, the instability is almost always attributed to non-ideal fabrication process and the occurrence of parasitic capacitance and inductance [27].

In our recent EOARD/AFRL-funded projects (FA 8655-10-1-3030, FA8655-12-1-208, and FA9550-15-1- 0120) [27][43][44], we conducted a very thorough investigation of possible use of non-Foster elements in artificial electromagnetic structures (“metamaterials” and “metasurfaces” [45][46][47][48]). The main idea was to compensate for the inevitable scattering of the artificial structure by non-Foster elements with ‘inverse’ dispersion [5][49][50][51][52][53][54][55][56][57][58][59][60][61][62][63][64][65][66][67][68][69][70][71][72][73][74][75][76][77][78]). Unexpectedly, we found that the main problem does not lie in the inadequacies of the available production technology (as is usually believed). The main problem lies in the incorrect stability prediction during the design phase, caused by the misinterpretation of the non-intuitive physical principles of non-Foster elements [60]. Shortly, it was postulated that non-Foster elements (and, more generally, Negative elements) are dispersionless and linear. This is not correct. Dispersionless negative capacitance or negative inductance would presume the existence of dispersionless negative permittivity and negative permeability, which would not be compatible with causality [60]. Therefore, every practical non-Foster or negative element must be dispersive. Although this ‘drawback’ limits operating bandwidth, it improves stability properties [27][43]. On the other hand, nonlinearity limits the allowable amplitude of the input signal in "classical" applications such as wideband matching. For non-Foster-based self-oscillating devices, nonlinearity is crucial because it stabilizes the amplitude of the oscillating signal [44].

It is important to mention that these conclusion are compatible with all published theoretical and experimental results [79][80][81][82][83][84][85][86][87][88][89][90][91][92][93][94][95].

In above-mentioned projects, we have developed a self-consistent theoretical framework for the design of stable non-Foster networks and verified it by both numerical simulations and experiments. In addition, we initiated a new research area of active non-Foster artificial structures, that is widely investigated nowadays [7]. Briefly, using a transmission line periodically loaded with negative capacitors or/and negative inductors it is possible to obtain an arbitrary low value of equivalent permittivity and permeability. Using this idea, we experimentally demonstrated several practical broadband metamaterial-inspired devices such as: the first active broadband ENZ non-Foster metamaterial in the world [50][51] and related ‘superluminal’ guiding structures [61][62], the reconfigurable active ENZ/MNZ non-Foster metamaterial unit cell [43], and the first stable band-pass non-Foster capacitor in the world [96]. The bandwidth of these devices spans from one 1:10 to 1:7000, which surpasses all known passive metamaterial structures (typical bandwidth of 1:1.2).

In our last EOARD/AFRL-funded project (FA9550-15-1-0120), we have also shown that the widely accepted stability criterion of positive 'mesh' capacitance fails for a parallel combination of positive and ideal negative capacitor followed by transmission line [91][95]. Such a network is always unstable, regardless of the line length and the capacitance values of the positive and negative capacitors. However, the inherent dispersion of a realistic negative capacitor (usually considered a disadvantage) can be adjusted to ensure stable operation. Furthermore, we found that the concept of an unstable 'mixed distributed network" can be used in an active self-oscillating non-Foster Fabry-Pérot (FP) antenna [35]. Experimental results proved the correctness of the basic idea of a broadband active self-oscillating FP antenna (antenna-transmitter system). We have also developed a novel topology of a "bandpass" non-Foster capacitor intended for use in active metamaterials/metasurfaces and antennas [96]. Analytical and numerical results have shown that the stability properties of a "bandpass" negative capacitor are significantly better than those of classical designs. Finally, we have investigated a well-known problem of using non-Foster elements for matching the transmitting antenna [97][98]. To circumvent the problem of nonlinearity, we introduced the idea of a non-Foster source ("non-Foster antenna transmitter") and built an experimental demonstrator based on two crossed dipoles and demonstrated oscillations that can be tuned within a 1:2 bandwidth [99][100][101]. In addition, the simulations showed that a tuning bandwidth larger than 1:10 can be achieved by using different tuning elements. All of the above demonstrators were produced manually, using commercially available components, and their operating frequency was in the lower RF band (up to 1 GHz), since there is no microelectronic fabrication technology at UNIZG.

One can conclude that all our projects so far have shown that the construction of a stable system with negative elements is feasible, but still an extremely challenging engineering task.

Chapter 2. PROJECT OBJECTIVE AND REALIZED OUTCOMES

Project objective and realized outcomes

2.1 Problem identification

From Introduction it is evident that the matching bandwidth achievable by passive reactive networks (networks that comprise positive capacitors and inductors) is limited by fundamental (and not technological!) constraints. Very similar constraints limit the tuning properties of passive reactive networks. These facts slow down development of broadband and tunable/reconfigurable RF devices such as amplifiers, filters and coupling/combining networks.

On the other hand, there has been a significant development of non-Foster elements (negative capacitors and negative inductors) for metamaterial applications [5][49][50][51][52][53][54][55][56][57][58][59][60][61][62][63][64][65][66][67][68][69][70][71][72][73][74][75][76][77][78].

Therefore, the purpose of this 24-month research effort is to extend the principles revealed in previous EOARD/AFRL-funded projects [27][43][44]. The final goal is a straightforward methodology for a design of *stable broadband non-Foster matching networks for tunable RF devices such as filters and/or power amplifiers.* The research methodology includes analytical and numerical theoretical study, complemented with manufacturing of experimental demonstrators.

The work in the project has been divided in the following tasks:

- **Identification of the most robust NIC/NII topologies**

In our previous EOARD/AFRL-funded projects [27][43][44], we have shown that many methods of stability prediction that are routinely used in microwave engineering (such as Rollet method, Stern method, mu-factor method, etc.) fail in the case of non-Foster networks. This is because these methods either do not pay attention to transient states or are unable to detect instability at the input port in the presence of hidden modes. Briefly, only methods that use analysis in the Laplace domain (or in the time domain) or use frequency domain but for all the frequencies from $-\infty$ to $+\infty$, and, at the same time, take into account all the meshes and nodes of the analyzed network (the analysis of system determinant, the NDF function, etc.) are always reliable and cannot result with incorrect stability prediction. We also found that the presence of an arbitrarily long transmission line segment fundamentally changes the stability scenario. Finally, we have proposed and practically implemented a novel bandpass-like circuit with significantly improved stability properties [96]. In all these efforts, a generic single-pole amplifier model of a non-Foster circuit was used.

However, it remains unclear which kind of NIC (or NII) would be the most appropriate choice for practical realization, from the stability and non-linearity point of view. Although the monolithic microwave integrated circuit (MMIC) implementations almost exclusively use Linvill crossed-transistor topology [16], there is no study that shows whether it is the best solution or not. It is particularly important because most MMIC devices employ non-Foster-based parasitic cancellation or extension of the VCO tuning range [37][38][39], that needs positive overall capacitance [36]. At the moment, it is unclear whether Linvill topology can be used for ‘negative’ matching networks, proposed for wideband power amplifier (PA) design [41].

Therefore, we investigate stability properties of representative NIC-NII topologies [10][11][12][13][14][15][16][24][26][33][39][102][103][104][105][106]. Once the most robust topology is selected, an attempt is made to further improve its stability properties by the recently proposed bandpass-like design [96] that eliminates the existence of the unstable DC RHP pole (Figure 2-1). This should allow for an overall negative capacitance (which is inherently unstable in classical designs).

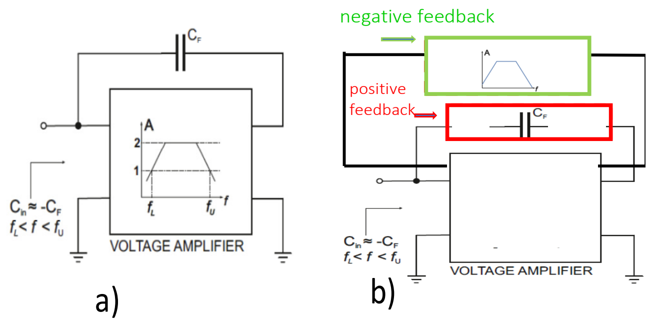

Figure 2-1 a) A basic idea stable ‘bandpass’ negative b) possible practical implementation [96]

a) Design of novel non-Foster-based fixed/tunable inductance

A vast majority of published non-Foster circuits deals with negative capacitance. On the contrary, the literature on negative inductance is sparse [43]. In order to implement negative inductance, classical NIC design requires ordinary inductance located within a positive feedback loop [43]. This may be impractical in MMIC realization. However, the use of Meunier-Kolev NII topology would enable transformation of ordinary capacitance into negative inductance [39]. This approach can be extended to tunable positive/negative inductance (Figure 2-2 a). In this way, it would be possible to design tunable non-Foster reactive network that can be used for tunable band-pass and band-stop filters (Figure 2-2 b [42]). To the best of our knowledge, there are no similar studies available in the literature.

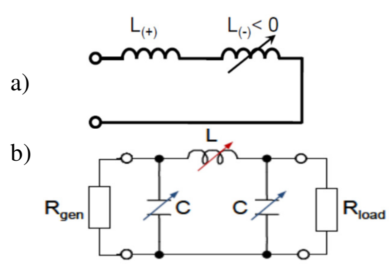

Figure 2-2 a) An idea of tunable non-Foster inductor, b) possible implementation in band-pass filter [42]

Therefore, we perform an analytical/numerical investigation of the stable bandpass NIC/NII topology selected in step a) and develop a suitable design to be tested by simulations in the L or Ku microwave band.

b) Novel non-Foster element topology with significantly improved stability robustness

All our efforts from previous projects, as well as the results from the literature, show that neither a system based on non-Foster elements nor a system based on Negative elements can be stable for any external passive network. Thus, absolute stability does not seem to be possible. The above systems can be stable for some types of external passive networks. Of course, it makes sense to keep the group of admissible external networks (which guarantee stable operation) as large as possible. Unfortunately, there is no theory that could predict the types of external networks allowed for a given operating bandwidth. There are so-called unilateral non-Foster designs based on compensated lossy networks with anomalous dispersion [72][73]. However, there is no clear theoretical relationship between stability and operating bandwidth. Moreover, the achievable bandwidth seems to be rather limited. Finally, the requirement for unilateral operation severely limits the possible applications. Recently, there has been a theoretical proposal for bandpass non-Foster elements that were claimed to be absolutely stable [102]. These elements are similar in some sense to the bandpass non-Foster capacitors proposed in our earlier EOARD/AFRL-funded projects [27][43]. However, there is no clear physical connection between these two approaches. Intuitively, one might expect that the presence of resistive components (even if their losses are compensated by additional negative resistance/conductance) would improve stability properties. We believe that using a passive structure with loss compensation by negative resistance, it is possible to design a non-Foster element with a range of allowable external impedances (admittances) larger than the circuits available in the literature.

Based on all these hypotheses, we decided to investigate this issue and try to find a novel topology of non-Foster/negative elements with significantly improved stability robustness.

c) Possible applications in RF tunable/wideband devices

The knowledge gained in step (b) is used to design a reactive non-Foster network for tunable bandpass/bandstop filters. Different strategies based on transmission line resonators loaded with tunable negative capacitance/inductance, tunable ladder networks with lumped elements connected in the form of series and parallel circuits, and an approach based on non-Foster immittance inverters [9][42] are compared and the most suitable topology is selected. Special attention is paid to a trade-off of required Q-factor and the achievable tuning bandwidth. To mitigate potential stability issues, this investigation will be limited to positive total inductance/capacitance, which mimics the characteristics of classical mechanically tunable microwave filters. The developed principle is verified by circuit simulations.

2.2 Novelty and uniqueness of the proposed research

Proposed research is certainly novel and unique since it tries to give the answers on several long-standing questions in non-Foster technology of broadband matching:

- Which NIC/NII topology is the most appropriate from stability point of view?
- Is it possible to construct a stable tunable negative inductance?
- Is it possible to construct a stable non-Foster reactive matching network for wideband tunable MMIC filters?

As far as we know, there are almost no publicly available studies that try to provide an answer to any of the above questions. In particular, the idea of a tunable broadband microwave non-Foster filter has not even been mentioned in the literature. If successful, the proposed efforts could pave the way for fabrication of broadband non-Foster-based RF devices such as filters, combiners, splitters, hybrid junctions, and PAs.

2.3 Realized outcomes

The main realized outcomes of the project are:

- We have shown that all electronic circuits that mimic negative immittance (NICs and NIIs) rely on the superposition of the original signal and assisting signal. Since these signals must be coherent, all classical circuits use positive feedback, which often leads to instability. It is extremely important to make a clear distinction between electronic admittance (associated with SCS properties) and electronic impedance (associated with OCS properties). We have also shown that a simple one-pole model of the NIC/NII amplifier is a useful approximation for both prediction of dispersion properties for frequencies below the pole frequency and for stability predictions. It was found that the dispersion of all the circuits analyzed is negligible when the maximum operating frequency is below one-tenth of the frequency of the first pole. The "parasitic" real part of the input impedance/admittance of the negative capacitor/inductor is negative in the SCS design and positive in the OCS design. This "parasitic" conductance/resistance can be compensated by an additional passive load network.
- We have reviewed all known methods of stability prediction and proposed a simple, straightforward method to develop simple equivalent circuits for all one-pole non-Foster and negative elements. We have also studied the most common realizations of NIC/NII circuits and performed a very thorough analysis of their stability properties. As expected, the stability properties were found to depend on both the NIC/NII topology and the passive external network topology. It was found that both OCS and SCS DC coupled negative capacitors/inductors/resistors based on NICs or NIIs always have an unstable DC pole that degrades the stability robustness. In addition, the DC coupled negative OCS capacitor and negative SCS inductor have a pole at the origin that causes DC offset at the input. The overall conclusion is that there is no such thing as the "most robust NIC/NII topology", per se.
- We have investigated the possibilities of improving the stability properties and found that the introduction of a bandpass mode significantly improves the stability properties. It turns out that the operating bandwidth is always inversely proportional to the range of allowable external impedances, i.e., to the stability robustness. We have applied this finding to the well-known Linvill NIC and shown that the stability characteristics can be improved by adjusting the operating bandwidth through proper selection of cross-coupling capacitors. We have also developed a very simple and accurate equivalent circuit for this modified Linvill negative capacitor.
- We have presented a novel design of non-Foster and Negative elements based on some very simple LP and HP passive series/shunt networks that exhibit non-Foster ‘inverse’ dispersion such that they behave as band-limited ‘lossy negative capacitors/inductors. The losses of these passive ‘negative’ networks can be compensated by an additional

negative series/shunt resistance/conductance. These novel non-Foster elements have shown stability properties better than the stability properties of all classical (NIC/NIV-based) non-Foster elements in the literature. The correctness of the proposed approach has been verified using four independent designs of negative capacitors and negative inductors in L and X frequency bands, in 40-nm CMOS technology. The generated negative capacitance capacitances and negative inductance ranged from -0.5 pF to -1 pF and -1 nH to -5 nH, respectively.

- In addition, we have shown applications of the proposed non-Foster elements in some RF tunable/broadband devices. We have designed and fabricated a general negative Miler capacitor using HCBT technology that produces capacitance from -0.3 pF to -0.1 pF in the frequency range from DC to 2GHz. We have also developed a tunable negative inductor that can be tuned between -100 pH and -300 pH in the range of 5-15 GHz. Finally, we have developed a tunable non-Foster-based bandpass filter for the 2.5-GHz band using 40-nm CMOS technology. We have demonstrated tunability of the center frequency up to 20% and bandwidth up to 30%, with return loss of more than 15 dB. A very important feature is that the symmetry of the bandpass curve is maintained over the tuning bandwidth, which is not possible with a standard passive design.

Chapter 3. ELECTRONIC CIRCUITS THAT MIMIC NEGATIVE IMMITTANCE

Electronic circuits that mimic negative immittance

3.1. Basic ideas on artificial electronic immittance

Immittance (impedance and admittance) is a fundamental property of any circuit-theory element (one-port network). Very often, immittance is loosely taken as a simple ratio of voltage and current (or current and voltage) in the Laplace domain, without mentioning any kind of driving source. As will be shown later, this definition is rather misleading for nonlinear elements. In particular, it is very inconvenient in the development of artificial immittance elements such as non-Foster or negative elements.

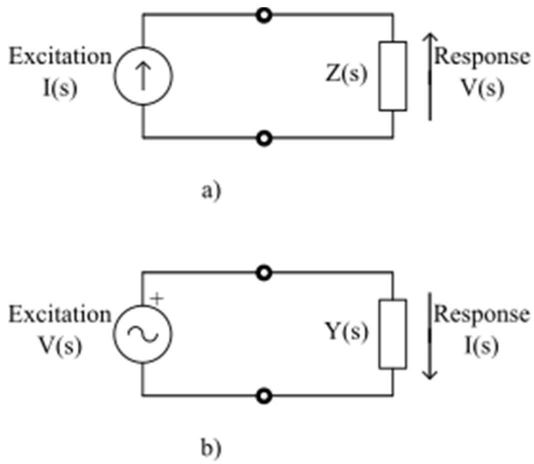

Rigorous definition takes immittance as special type of transfer function (Figure **3**-**1**).

When an element is excited by an ideal current source, it can be assumed that the element responds with developed voltage. In this case, the transfer function, defined as the ratio of response and excitation signal, is therefore the impedance Z(s):

$$\text{Transfer function}=\frac{\text{Response signal}}{\text{Excitation signal}}=\frac{V(s)}{I(s)}=Z(s). \tag{3.1}$$

Figure 3-1 Definition of one-port immittance transfer functions. a) Definition of impedance; b) Definition of admittance

Here, s stands for complex frequency (s=σ+jω) (Figure **3**-**1**a).

An element can also be excited by an ideal voltage source and the current developed across the element is the response. In this case, the transfer function is an admittance Y(s):

$$\text{Transfer function}=\frac{\text{Response signal}}{\text{Excitation signal}}=\frac{I(s)}{V(s)}=Y(s). \tag{3.2}$$

Above rigorous definitions are valid for any kind of both linear and non-linear elements (which will later be shown in detail in paragraph 3.1.2.)

3.1.1. Superposition of source signal and 'asissting source' signal

These rigorous definitions from the previous paragraph are also valid in the case of active element that contains a source, the signal of which opposes to the original signal producing so-called *artificial immittance*. This idea is sketched in Figure **3-2**.

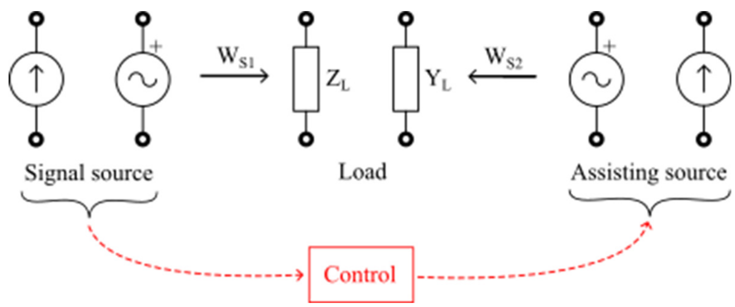

Figure 3-2 Basic idea of generation of electronic immittance by superposition of source signal and 'assisting source' signal. Here WS1 and WS2 denote energy flows caused by signal source and assisting source, respectively.

Let us assume that we have a load that is described by its impedance Z_L (or its admittance Y_L). This load is excited by either current signal source or voltage signal source. Let us further assume the existence of some assisting source (again either of voltage or current type) that is controlled by original signal source. Because of the presence of control circuitry, the assisting source is obviously a type of controlled source. The net voltage seen by excitation current source is a superposition of the voltage caused by the original signal and the voltage caused by assisting signal. Similarly, the net current of the excitation voltage source is a superposition of the current caused by the original signal and the current caused by assisting signal. Because of this superposition, the source "sees" a new effective immittance that is different from the original load immittance. This effective immittance is called the "electronic immittance" and can be of almost any value, which can be adjusted by changing the magnitude and phase of the assisting source.

One of the simplest implementations of the described principle concerns an ideal voltage amplifier with a load (Y_L) in its positive feedback loop (Figure 3-3).

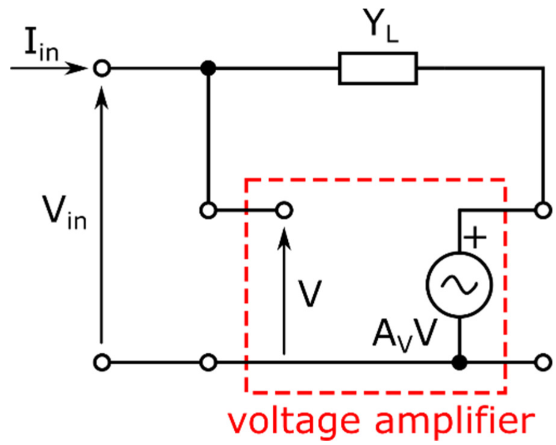

Figure 3-3 System for the generation of electronic immittance based on ideal voltage amplifier with load in positive feedback

The potential of the left terminal of the load (Y_L) is defined by original excitation source V_{in} while the potential of the right terminal is given by the amplifier output voltage ($A_v V_i$, A_v being the voltage gain). A very simple analysis yields effective input admittance Y_{in}:

$$Y_{IN} = Y_L(1 - A_V)\,. \tag{3.3}$$

A common choice in practice is A_V =2. This choice leads to unitary negative conversion of a load admittance into its 'negative image': $Y_L \rightarrow -Y_L$. If a load has a purely reactive character (a capacitor or an inductor), the whole device behaves as a negative capacitor or a negative inductor. One notes that the input current of the circuit in Figure **3**-**3** is the same as the load current (due to infinite input impedance of an ideal voltage amplifier). At the same time the input voltage is a negative image of the load voltage. So, it can be said that a circuit in Figure **3**-**3** does *voltage inversion*.

It is easy to imagine a dual implementation based on an ideal current amplifier with a load impedance located in the positive feedback loop Figure 3-4.

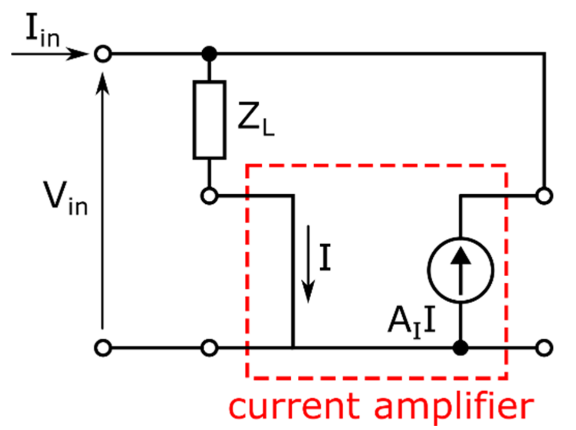

Figure 3-4 System for generation of electronic immittance based on ideal current amplifier with a load located in the positive feedback loop

Again, it is a simple task to derive an expression for equivalent input impedance Z_L:

$$Z_{IN} = Z_L(1 - A_I)\,. \tag{3.4}$$

Here, A_I stands for current gain of an amplifier. It can be seen that equation (3.4) is of the same form as (3.2). The only difference is that admittance is replaced by impedance and voltage gain by current gain. This is a direct consequence of duality. The duality is also found in the basic principle of operation. The input voltage of the circuit in Figure **3**-**4** is the same as the output voltage (due to zero-valued voltage present at the input of an ideal current amplifier). At the same time the input current is a negative image of the load current. So, a circuit in Figure 3-4 does current inversion.

3.1.2. Non-linearity of 'assisting source' – distinction between impedance and admittance

In the previous section, the amplifiers were considered perfectly linear. Due to linearity, it is possible to use the Thevenen's representation of a controlled source (Figure **3**-**3**) or the Norton's representation (Figure **3**-**4**), and either of them gives the same result. So, one may conclude that impedance and admittance are inverse quantities, as it is usually considered. However, this is correct only for passive linear elements and not for active elements and circuits like those in Figure **3**-**3** and Figure **3**-**4**.

Clearly, linearity is only an approximation of any amplifier since operating point inevitably enters non-linear regime at high levels of input signal. Due to this effect, a value of effective input impedance/admittance in non-linear region depends on the amplitude of input signal. It is well-known in the theory of negative resistance oscillators [2]. Negative conductance/resistance can also be thought as generated by circuits from Figure **3**-**3** and Figure

3-**4** (with purely resistive load in the feedback loop). The oscillator based on such negative conductance/resistance can be considered as being linear only for a very low amplitude of the generated signal. In addition, such a system has low efficiency. Indeed, the signal generated in any efficient oscillator inevitably enters the non-linear region of voltage-current characteristics of an active element. The amplitude grows up to the point at which the generated power equals the power dissipated at the load [2]. This process can be described by the well-known negative conductance/resistance properties of so-called N and S curves.

Briefly, all negative elements with real impedance can be classified into a voltage-driven type ('N' curve depicted in Figure 3-5 (a)) and a current-driven tape ('S' curve depicted in Figure 3-5 (b)). The 'bending' in the curves occurs because of saturation properties of a given element. In other words, the voltage and current cannot grow above the values limited by feeding DC power source. Either maximum voltage across an active element or maximum current flowing through it, will be limited by saturation. In the case of 'N -type' element (Figure 3-5 (a)), it is convenient to connect it in a parallel with a load. In the implementation of an oscillator, there is also an additional parallel LC circuit that determines the frequency of oscillations. A quantity that is common for this parallel combination is the voltage, which gives only one (stable) operating point in current-voltage curve [2]). While the amplitude of oscillations grows up, it 'climbs' along the curve and enters the non-linear part. Due to the change of negative differential conductance, the growth stops when the generated power equals the power dissipated at the load (stable operating point). However, if the point is unstable, it will move over the 'hill top', enter the region with positive differential conductance and the oscillations will cease. If a series combination were used instead the parallel one, the common quantity would be the current and it would give two operating (unstable) points. Thus, the N element should be voltage-driven and it is described by *admittance*, which is consistent with a rigorous definition in Figure **3**-**1**(a).

At this point it is appropriate to briefly consider the stability of the N element. Let us assume that one excites (wrongly!) the N element with a current source which is connected to a constant current line parallel to the x-axis in the graph in Figure 3-5. There are two intersections between a line and an N curve (two operating points. The system state keeps jumping back and forth between these two operating points, even when a current source is turned off and the input terminals are left open. Clearly, this system is unstable if the input terminals are left open. On the contrary, when the input terminals are shorted (which is the case for excitation with an ideal voltage source), the system is stable. Due to this property, the system with the N-element is called and short-circuit-stable (SCS) system. This also the reason why it is incorrect to describe the system with N element with impedance.

In the case of an 'S-type' element (Figure 3-5 (b)), the situation is exactly opposite. It is convenient to connect this element in series with a load. Here, a quantity that is common for this series combination is the current. It gives only one (stable) operating point in current-voltage curve (the intersection between 'S' curve and the load line [2]. Again, the operating point 'climbs' along the curve during the oscillations growth and enters the non-linear part. Due to the change of negative differential resistance, the growth stops when the generated power equals the power dissipated at the load (stable operating point). Similarly to the previous case, there is an additional series LC circuit that determines the frequency of oscillations. If the point is unstable, it will move over the 'hill top', enter the region with positive differential conductance and again cause the oscillations diminishing. If a parallel combination were used, the common quantity would be voltage and it would give two operating (unstable) points. Thus, the ‘S -type’ element should be current-driven, which is consistent with a rigorous definition in Figure **3-1**(b).

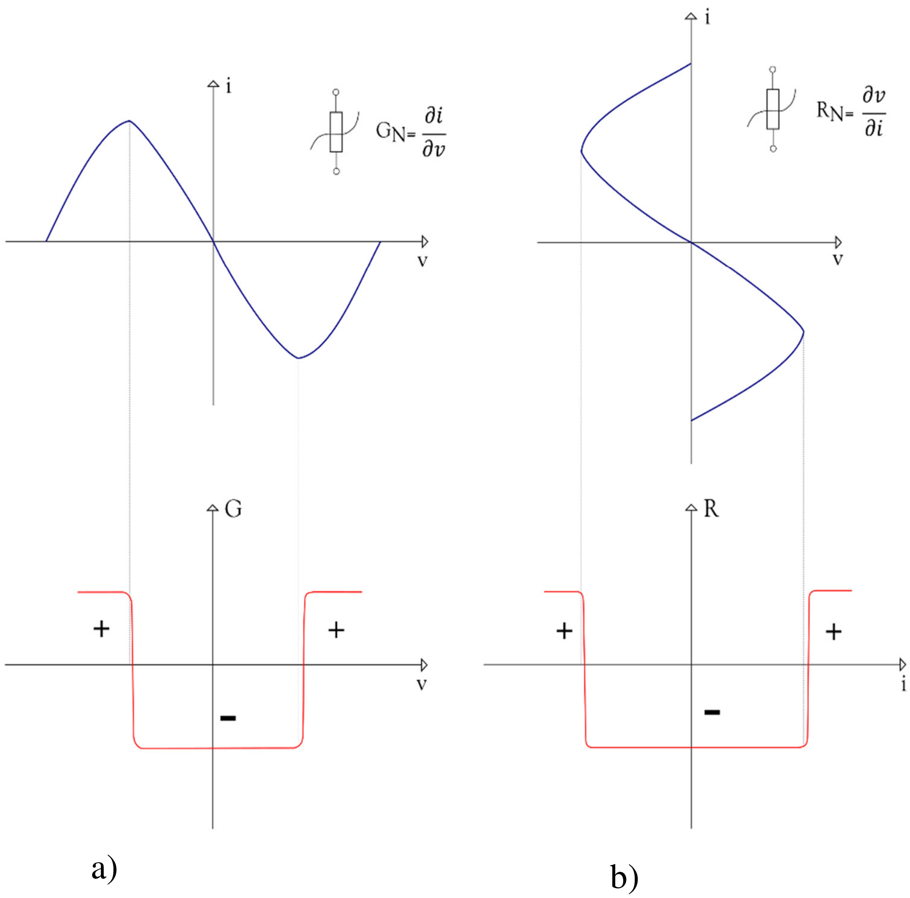

Figure 3-5 Voltage-current curves of negative conductance/resistance elements a) ‘N’ curve, b) ‘S’ curve (adapted from [44])

Similar to the previous discussion, excitation of the S-element with an ideal voltage source leads to instability. Excitation with an ideal current source (which has infinite impedance when off) leads to a stable system. Therefore, any system with an S-element is inherently an open stable system (OCS) and must be described by impedance (not admittance).

Colloquially, both types of elements are usually referred to as negative resistors. However, as emphasized in [103] it would be more correct to term ‘N -type’ element as a ‘negative conductor’ and ‘S -type’ element as a ‘negative resistor’.

3.1.3 Extension of a concept of N and S curves to non-Foster elements

The non-linear behavior of non-Foster networks is highly unexplored. Therefore, it would be very convenient to revise extension of the familiar concept of ‘N’ and ‘S’ curves to negative capacitance and negative inductance (non-Foster reactance) [44] (Figure 3-6, Figure 3-7). Keeping the current/voltage dependence for plotting does not seem to be appropriate since the current is a complex number over here (due to phase shift associated with negative capacitance/inductance). It would be better to define some new variable that is a real number (‘effective quantity’ [44]). We have chosen the differential electric charge and differential magnetic charge (magnetic flux) as effective quantities. They are related to capacitance and inductance by basic relations:

$$C(v) = \frac{\partial D}{\partial v} = \frac{\partial Q_e}{\partial v} \Rightarrow Q_e = \int C(v)\, dv \tag{3.5}$$

$$L(i) = \frac{\partial \varphi}{\partial i} = \frac{\partial Q_m}{\partial i} \Rightarrow Q_m = \int L(i) di \tag{3.6}$$

Here, D and φ are electric and magnetic fluxes while Q_e and Q_m stand for electric and magnetic charges, respectively. It is clear that all of these quantities would have their inherent physical meaning only in the case of some real negative non-linear capacitors and inductors (for instance in semiconductor technology and in inductors with ferromagnetic cores). In the case of electronic circuitry that emulate behavior of hypothetical negative capacitors and inductors the effective quantities are primarily mathematical tools that simplify analysis. Using discussed approach it is possible to plot generalized N and S curves of non-linear negative capacitors and inductors (Figure 3-6 and Figure 3-7).

Quick analysis of these figures reveals that the use of non-linear negative capacitor in a parallel circuit and the use of non-linear negative inductor in a series circuit assures smooth transition between positive and negative values at the ends of linear region of the operating curve (‘hill top’ points). On the contrary the use of non-linear negative capacitor in series circuits and the use of non-linear negative inductor in parallel circuits causes abrupt, pole-like change between positive and negative values at the ends of linear region of the operating curve.

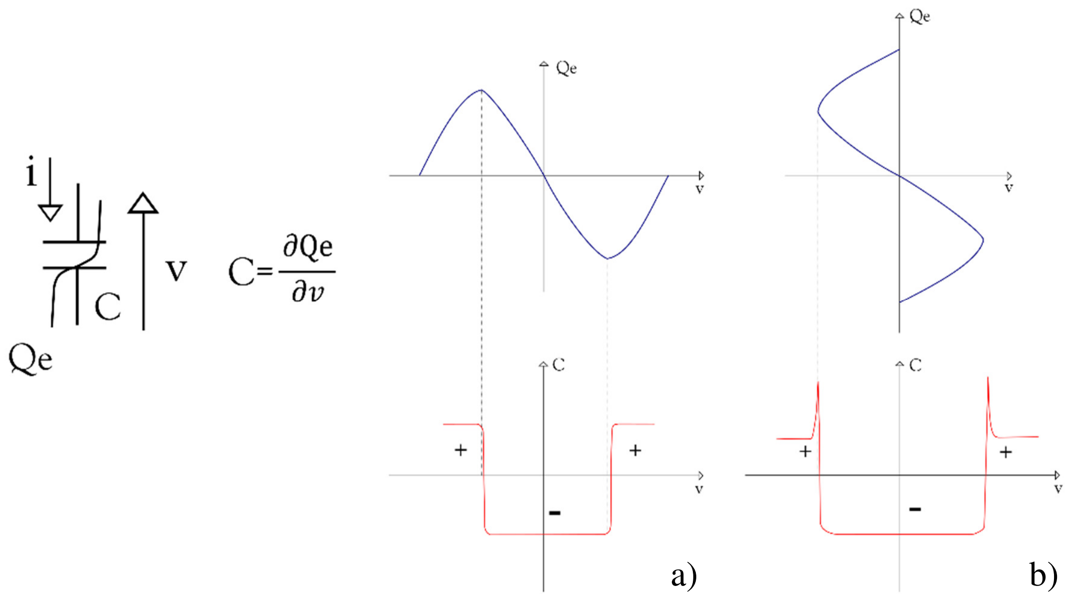

Figure 3-6 Generalized curves of non-linear negative capacitor a) 'N' curve, b) 'S' curve (taken from [44])

.

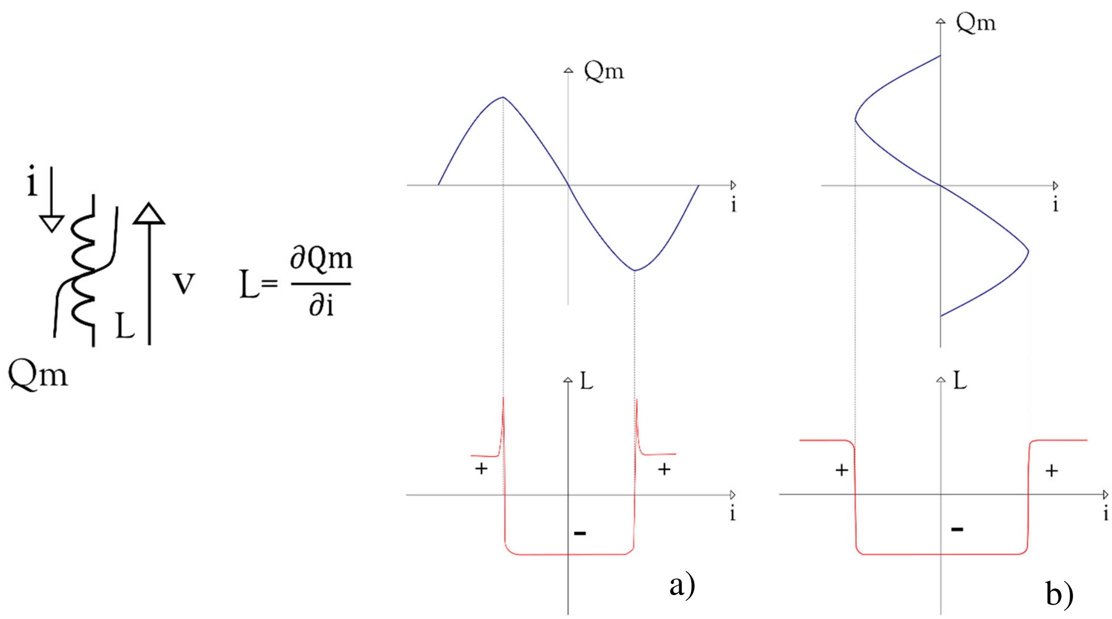

Figure 3-7 Generalized curves of a non-linear negative inductor a) 'N' curve, b) 'S' curve (taken from [44])

Let us analyze the N and S curves of negative capacitors and negative inductors generated by two basic types of systems : the voltage-conversion type and the current-conversion type , sketched in Figure **3-3** and Figure **3-4**, respectively. As discussed before, they employ voltage-dependent and current-dependent sources (voltage and current amplifiers) with inverting loads in positive feedback loops.

It is very instructive to analyze basic 'conversion equations' (3.3, 3.4) for the case of negative capacitor. Clearly, both gain functions (A_V and A_I) should decrease when the input signal drives circuit into a non-linear regime (this is a familiar phenomenon of gain compression, Figure 3-8). The analysis (3.3, 3.4), in the region of compression shows that the input impedance/admittance change is, in a way, described by generalized curves of non-Foster elements (Figure 3-6 and Figure 3-7). The difference between 'N' and 'S' types of non-linearity (for the case of a capacitive load) is sketched in Figure 3-9. For the 'N' type of non-linearity, the input capacitance smoothly changes from negative to positive values with the increase of input signal level, crossing zero-capacitance for A_V=1. On the other hand, for the 'S' type of non-linearity, there is divergent behavior of input capacitance with a pole at the frequency for which A_I=1 (Figure 3-9).

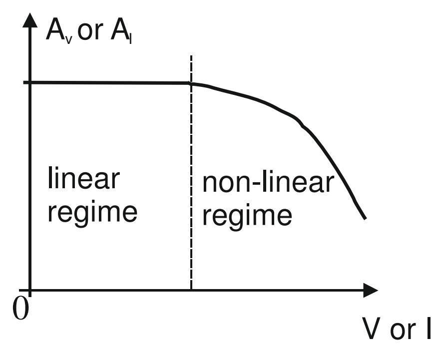

Figure 3-8 Gain-input characteristic of active element (amplifier) of realistic circuits in Figure 3-3 and Figure 3-4 (modified from [44])

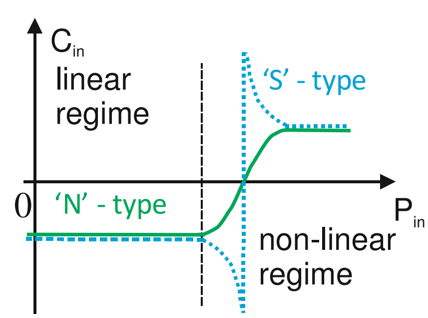

Figure 3-9 Dependence of input capacitance on input signal for circuits in Figure 3-3 and Figure 3-4 , assuming the 'N' and 'S' types of non-linearity, respectively (taken from [44])

3.2. 'Negative Impedance Converter' (NIC)

The basic idea of systems that are capable of generating negative admittance based on ideal voltage amplifier with positive feedback (Figure **3-3**) and those based on ideal current amplifier with positive feedback (Figure **3-4**) can be further generalized and formalized. This leads to definition of dedicated electronic circuit called '**N**egative **I**mpedance **C**onverter' [10][11][12][15][16]. The first NICs was introduced almost hundred years ago [10]. In spite of this, the design of reliable and stable NIC circuits is still one of the most challenging engineering tasks in RF electronics.

3.2.1. Basic OCS and SCS NIC circuits

If one assumes that an ideal voltage amplifier from Figure **3-3** has independent input and output terminals (there is no common electrode), it is possible to construct a two-port NIC (Figure 3-10) [103]. One of the NIC ports is always SCS, while the other is OCS. Which port plays a particular role can be determined from the sensing signal. For instance, in the circuit in Figure 3-10 (a), zero-valued sensing signal causes zero-valued amplitude of the assisting signal. In other words, when input voltage signal is switched off, the system is stable. Thus, the left port in Figure 3-10 (a) is SCS. Very similar analysis shows that the right port in Figure 3-10(b) is OCS. So, with an ideal voltage amplifier, it is possible to build a NIC that can produce both negative admittance and negative impedance (depending on the choice of ports).

Again, very similar conclusion can be drawn for two-port NIC that contains ideal current amplifier from Figure **3-3** (with independent input and output terminals). This scenario is sketched in Figure 3-11. Here, the left port is OCS (Figure 3-11 (a)), while the right port is SCS (Figure 3-11 (a)).

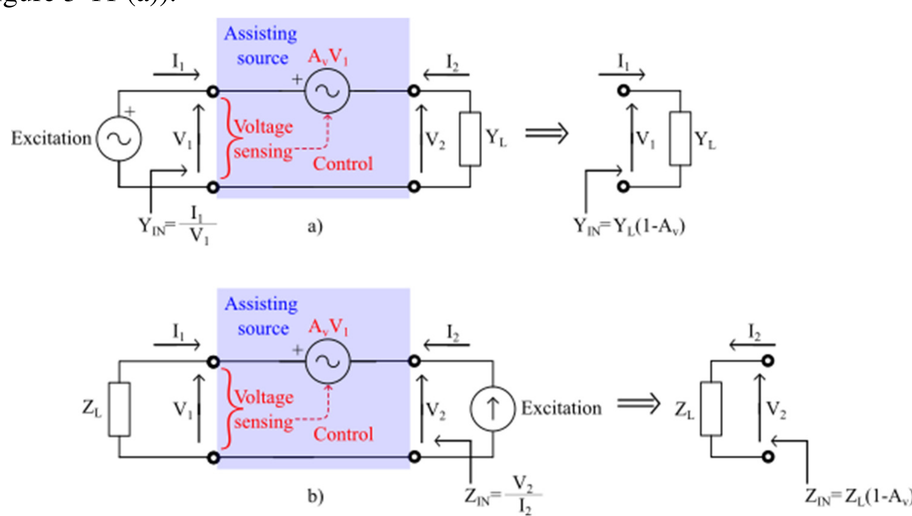

Figure 3-10 Basic schematics of grounded current inversion NICs (INIC) based on ideal voltage amplifier. a) SCS implementation, b) OCS implementation

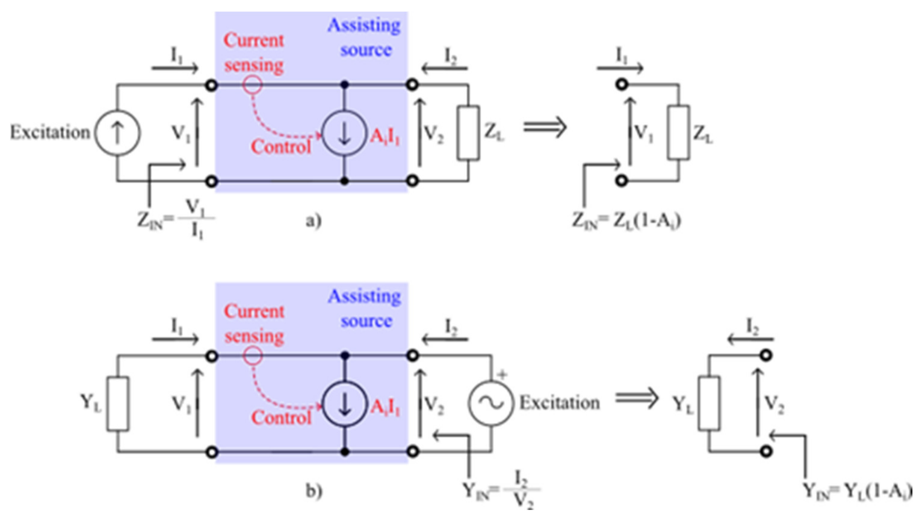

Figure 3-11 Basic schematics of grounded voltage inversion NICs (VNIC) based on ideal current amplifier. a) SCS implementation, b) OCS implementation

Both of NIC basic schematics presented so far (Figure 3-10, Figure 3-11) are of grounded type (lower input terminal is connected to lower load terminal). This is inconvenient for some applications with symmetrical (differentially driven) devices such as simple dipole antennas. In this case, one may use floating versions of the same NIC (Figure 3-12 , Figure 3-13 [103]). It is important to notice that each amplifier has a gain that is one half of the gain required by basic equations (3.3, 3.4). So, minimal gain of each amplifier needed for negative conversion is 1. This may be very convenient for practical implementations since one can simply use two BJTs (or FETs) in CC (CS) configuration with A_V~1 for floating NIC based on two voltage amplifiers (Figure 3-12). Similarly, one can use two BJTs (or FETs) in CB (CG) configuration with A_i~1 for floating NIC based on two current amplifiers (Figure 3-12). Latter approach is used in very popular Linvill NIC ([16]), discussed in detail in section 3.5.

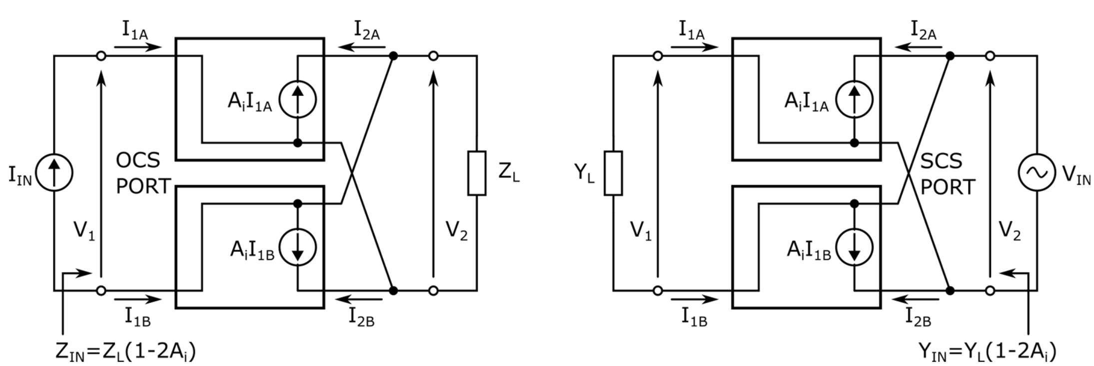

Figure 3-12 Basic schematics of floating voltage inversion NICs (VNIC) based on two ideal current amplifiers. a) OCS implementation, b) SCS implementation

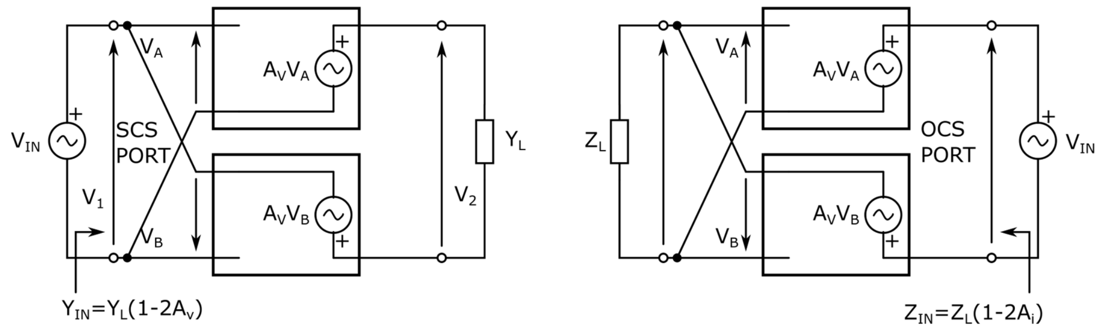

Figure 3-13 Basic schematics of floating current inversion NICs (INIC) based on two ideal voltage amplifiers. a) SCS implementation, b) OCS implementation

3.2.2. Dispersion properties

In the simplified analysis from the previous section, it was assumed that the voltage gain A_V (in 3.3), and the current gain A_i (in 3.4), are real numbers. For instance, let us take example of voltage amplifier from Figure **3**-**3**, with capacitor C_F in positive feedback loop. It resembles Miller effect in classical CS amplifiers, so we will call it Miller NIC. Inserting $Y_L = sC_F$ into (3.3) yields:

$$Y_{\mathrm{IN}}(s) = \frac{I_{\mathrm{IN}}(s)}{V_{\mathrm{IN}}(s)} = [1 - A_V]C_F \;, \qquad C_{\mathrm{IN}} = [1 - A_V]C_F. \tag{3.7}$$

It can be seen that generated negative capacitance (when A_V=2) is entirely dispersionless. This is a consequence of assumption that A_V is a real number. In other words, the amplifier should have a perfectly 'flat' dispersionless gain curve from DC to infinite frequency, with no signal delay at all. Obviously, this behavior would violate causality [7][27][43][44].

In order to investigate influence of inevitable non-ideality of the amplifier, let us first briefly review simple intuitive analysis in the frequency domain ($s = j\omega$) from [27]. The operation of this NIC is described by phasor diagram (Figure 3-14), which shows idealized case without dispersion with A_V=2. In this case, the input current lags the input voltage by 90 degrees, thus the input impedance is a pure negative capacitance (Figure 3-14 (a)).

However, every realistic amplifier always introduces some delay or (in the frequency domain) some phase shift Φ (in other words, the gain A is a complex number). The phasor diagram for this case is sketched in Figure 3-14 (b). A very simple analysis shows that in this case there is a component of the input current that is 180 degrees out of phase in respect to input voltages. Thus, the inevitable phase shift of the used active element causes 'parasitic' negative input conductance.

Above brief analysis shows importance of a phase shift (or, more generally, complex gain) of the active element, will cause dispersion of input negative susceptance and occurrence of (also dispersive) parasitic negative conductance. So, the non-ideality of active element (an amplifier) cannot be neglected.

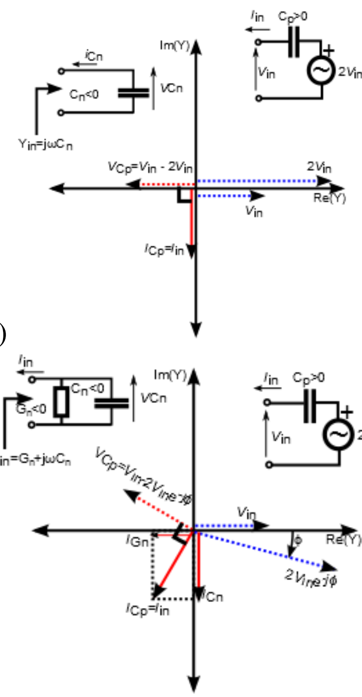

a)

b)

Figure 3-14 Phasor diagram for a negative capacitor based on SCS grounded INIC in **Figure 3-10** (a). **a**) ideal case with zero-valued time delay (there is no phase shift in dependent voltage source) **b**) realistic case with finite time delay (there is a phase shift in dependent voltage source) (taken from [27]).

In order to analyze a more realistic case, the amplifier in Figure **3-3**, can be modeled using a low-pass one-pole gain function:

$$A(s) = \frac{A_0}{1 + s\tau}, \quad \omega_{\mathrm{P}} = \frac{1}{\tau}. \tag{3.8}$$

Here τ stands for the amplifier time constant, associated with pole frequency ω_{P} (cut-off frequency of an amplifier). If $\tau = 0$ ($\omega_P = \infty$), the model reduces to the ideal non-dispersive case with infinite bandwidth. Using (3.3) and (3.8) one finds the input admittance:

$$Y_{IN} = \frac{1 + s\tau - A_0}{1 + s\tau} sC_{\mathrm{F}}. \tag{3.9}$$

The steady-state ($s = \mathrm{j}\omega$) input admittance ($Y_{\mathrm{IN}}(\omega) = G_{\mathrm{IN}}(\omega) + \mathrm{j}\omega C_{\mathrm{IN}}(\omega)$) consists of a parallel combination of a dispersive capacitance $C_{\mathrm{IN}}(\omega)$ and a dispersive conductance $G_{\mathrm{IN}}(\omega)$:

$$C_{\mathrm{IN}} = C_{\mathrm{F}}\left[1 - \frac{A_0}{1 + \omega^2\tau^2}\right], \quad G_{\mathrm{IN}} = -\frac{A_0 C_{\mathrm{F}} \omega^2 \tau}{1 + \omega^2\tau^2}. \tag{3.10}$$

Quick analysis of (3.10) shows that generated capacitance becomes zero at frequency where gain drops to unity. By further increase of the frequency, input capacitance approaches (positive) capacitance C .On the other hand, the delay of the amplifier causes the occurrence of dispersive negative input conductance, which becomes more and more pronounced with the increase of the frequency. Of course, this negative conductance degrades the performance of a negative capacitor. It can be shown that the 'Q factor' decreases with frequency and it reaches value of 10 at the frequency equal to approximately one tenth of the pole frequency ($\omega \approx 0.1/\tau$) (Figure 3-17).

Of course, it is possible to use higher-order amplifier models (two-pole and three-pole models [27]), which would give more realistic dispersion prediction for higher frequencies. In practice, however, non-Foster elements are used for frequencies where the operating frequency is lower than the frequency of the first pole (or even lower than one-tenth of it). So, it seems that the use of one-pole model is a sufficient approximation for initial design. More importantly, the one-pole approximation is sufficient for predicting the stability properties (as it will be shown in detail in the Section 3.4).

Thus, we decided to perform dispersion analysis for all basic SCS and OCS NIC terminated by three representative loads: a capacitor, an inductor, and resistor. These NICs should behave as negative capacitance, negative inductance, and negative conductance/resistance. We paid particular attention of correct modelling of input immittance taking into account associated SCS/OCS properties. We used input admittance for OCS NIC and input impedance for SCS NIC. The models of equivalent input networks are briefly explained in Table 3-1

NIC type	Load type	Equivalent input network	Analysis presented in:
SCS	capacitor	dispersive C shunted by 'parasitic' dispersive G	Figure 3-15 Figure 3-16 Figure 3-17 Figure 3-18
OCS	capacitor	dispersive C in series with 'parasitic' dispersive R	
SCS	inductor	dispersive L shunted by 'parasitic' dispersive G	Figure 3-19 Figure 3-20 Figure 3-21 Figure 3-22
OCS	inductor	dispersive L in series with 'parasitic' dispersive R	
SCS	resistor	dispersive G shunted by 'parasitic' dispersive C	Figure 3-23 Figure 3-24 Figure 3-25 Figure 3-26
OCS	resistor	dispersive R in series with 'parasitic' dispersive L	

Table 3-1 Models of input admittance/impedance used in dispersion analysis of various one-pole NICs

For each analyzed case, we calculated both ‘desired’ input quantity and ‘parasitic’ input quantity, Q factor, and relative error of generated ‘desired’ input quantity. All these values are defined as a function of the frequency normalized on the pole frequency.

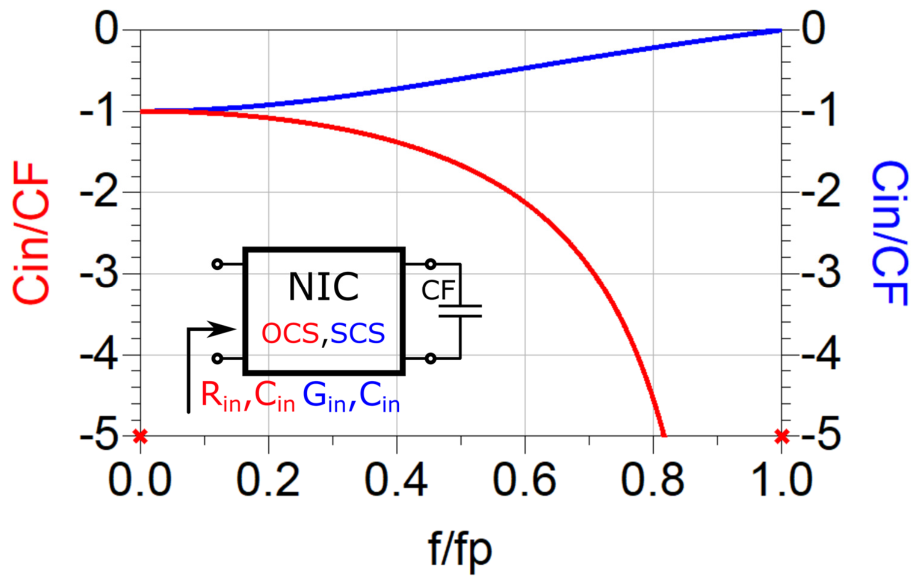

Figure 3-15 Dispersion of capacitance of OCS/SCS negative capacitor (OCS/SCS NIC terminated by ordinary capacitor)

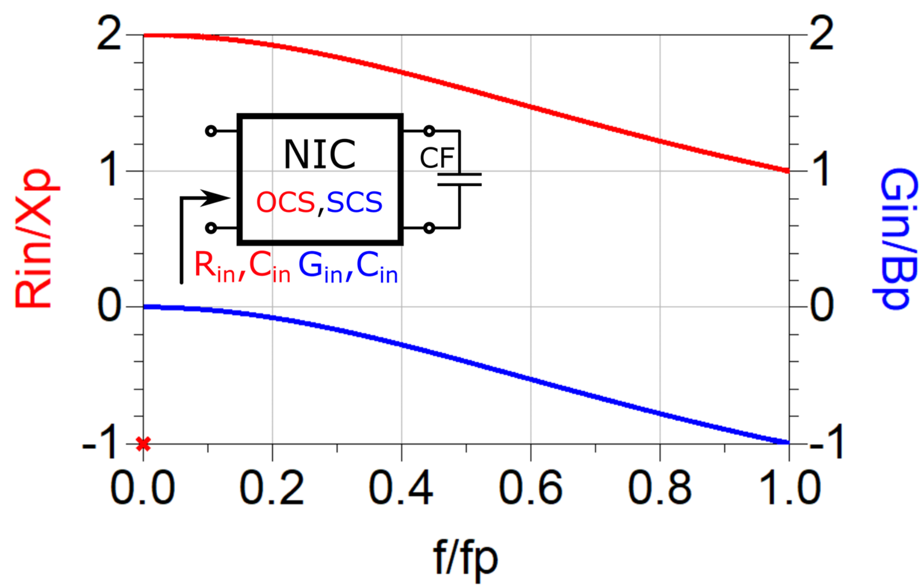

Figure 3-16 Dispersion of ‘parasitic’ resistance/conductance of OCS/SCS negative capacitor (OCS/SCS NIC terminated by ordinary capacitor)

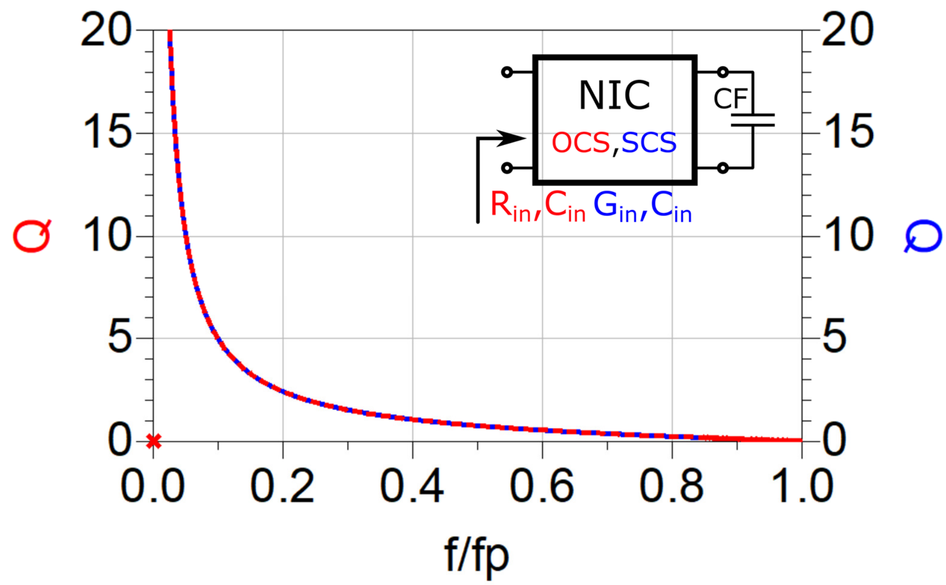

Figure 3-17 Q factor of OCS/SCS negative capacitor (OCS/SCS NIC terminated by ordinary capacitor)

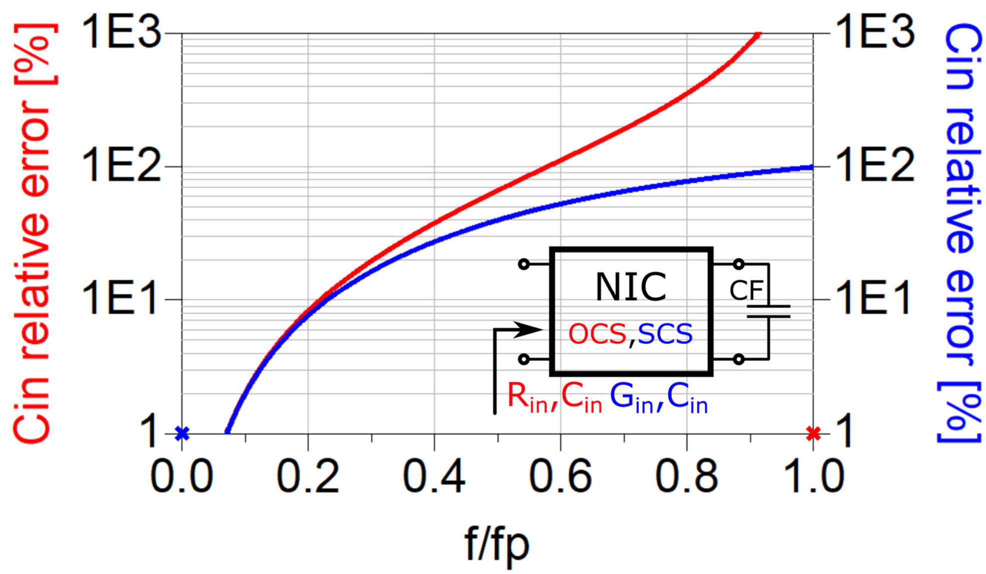

Figure 3-18 Relative error of capacitance of OCS/SCS negative capacitor (OCS/SCS NIC terminated by ordinary capacitor)

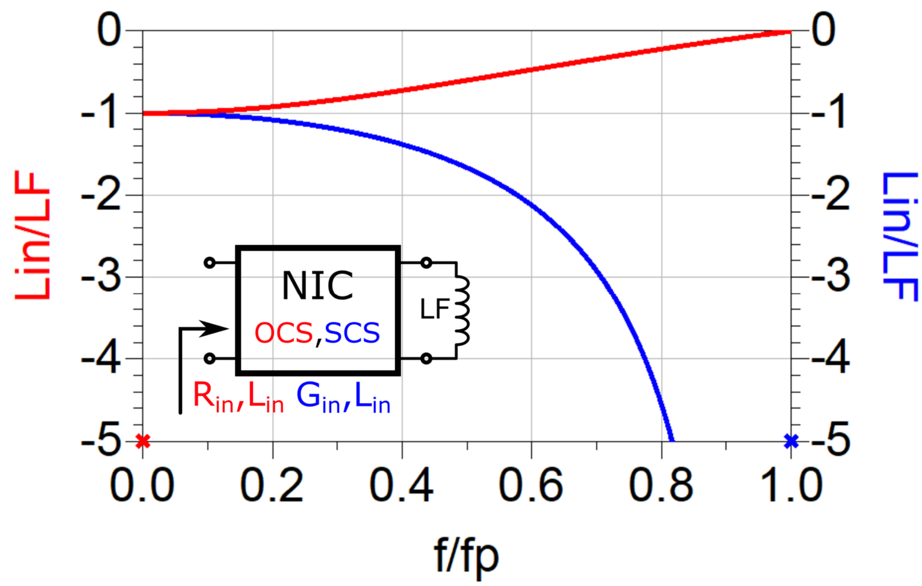

Figure 3-19 Dispersion of inductance of OCS/SCS negative inductor (OCS/SCS NIC terminated by ordinary inductor)

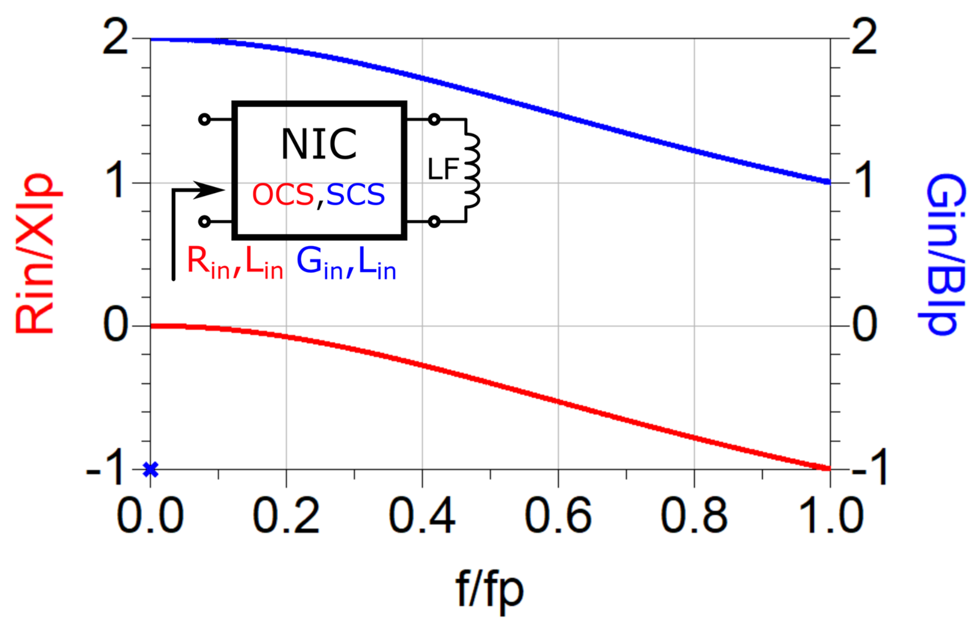

Figure 3-20 Dispersion of 'parasitic' resistance/conductance of OCS/SCS negative inductor (OCS/SCS NIC terminated by ordinary inductor)

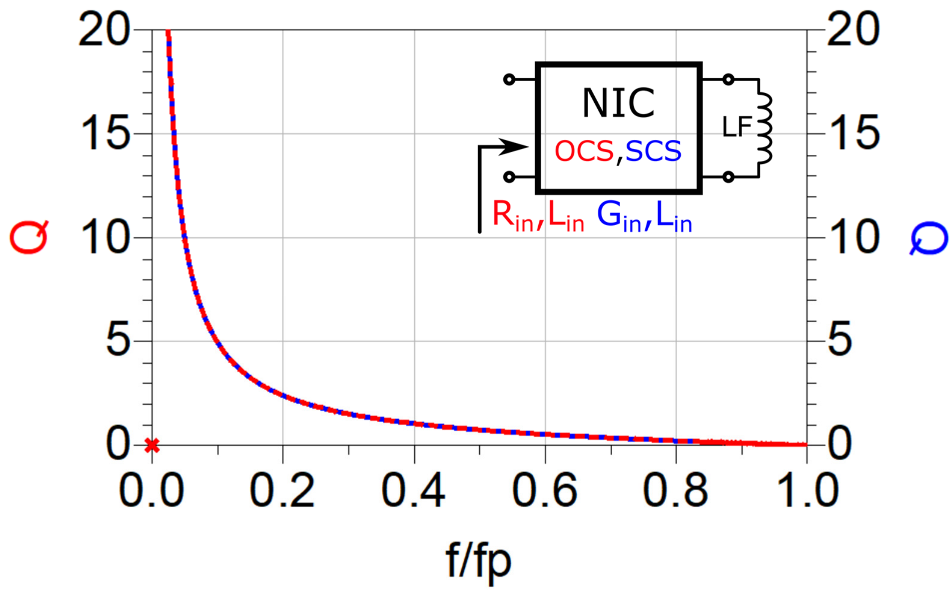

Figure 3-21 Q factor of OCS/SCS negative inductor (OCS/SCS NIC terminated by ordinary inductor)

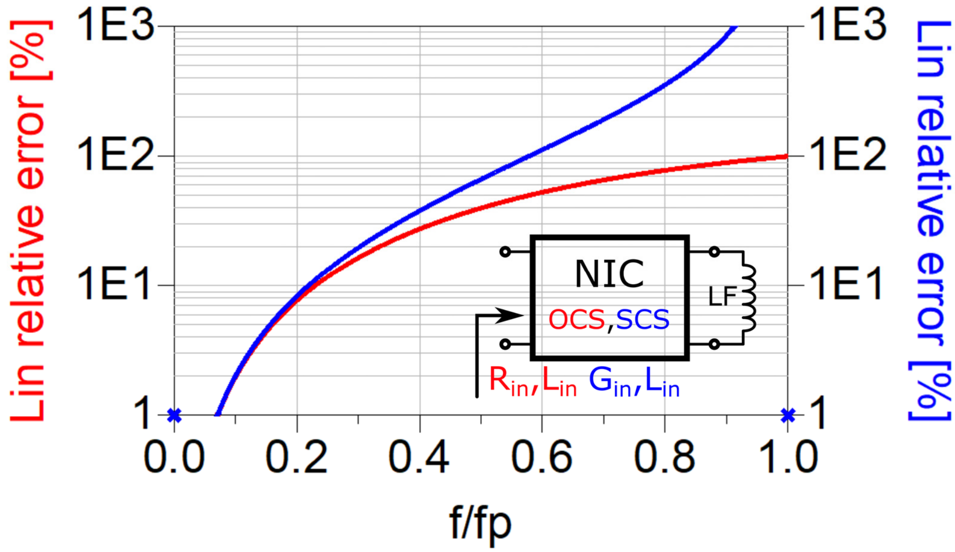

Figure 3-22 Relative error of inductance of OCS/SCS negative inductor (OCS/SCS NIC terminated by ordinary inductor)

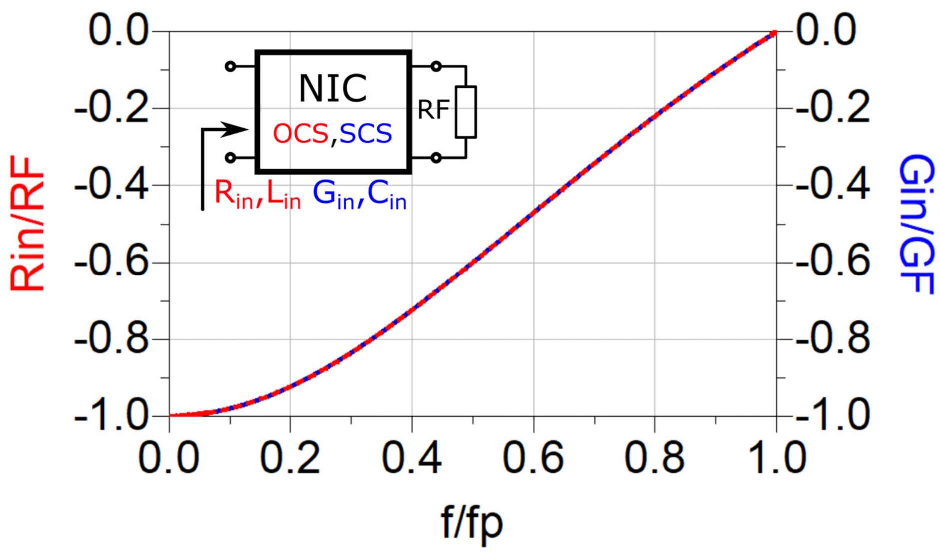

Figure 3-23 Dispersion of resistance/conductance of OCS/SCS negative resistor (OCS/SCS NIC terminated by ordinary resistor)

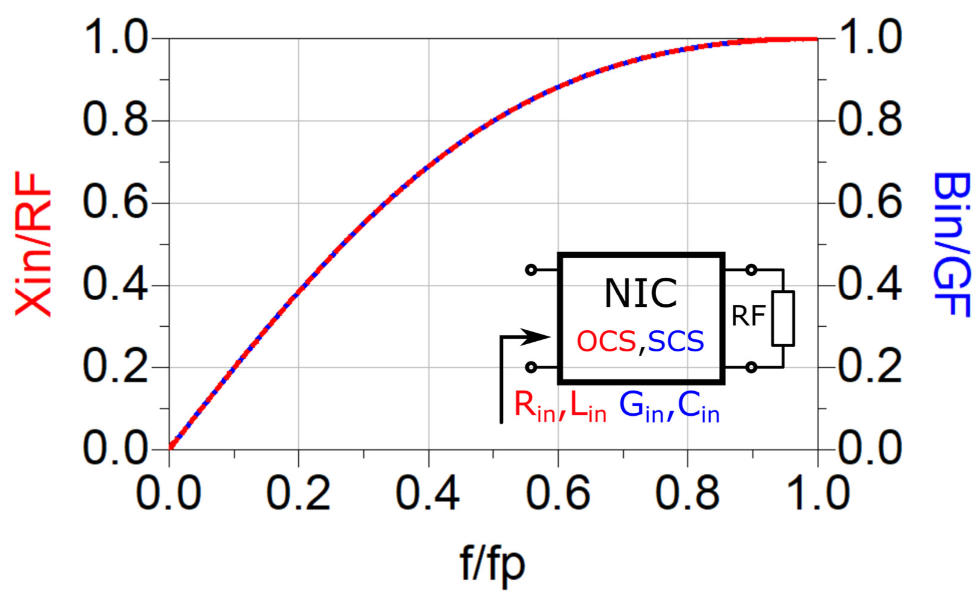

Figure 3-24 Dispersion of 'parasitic' reactance/susceptance of OCS/SCS negative resistance (input 'parasitic' reactance/susceptance of OCS/SCS NIC terminated by ordinary resistor)

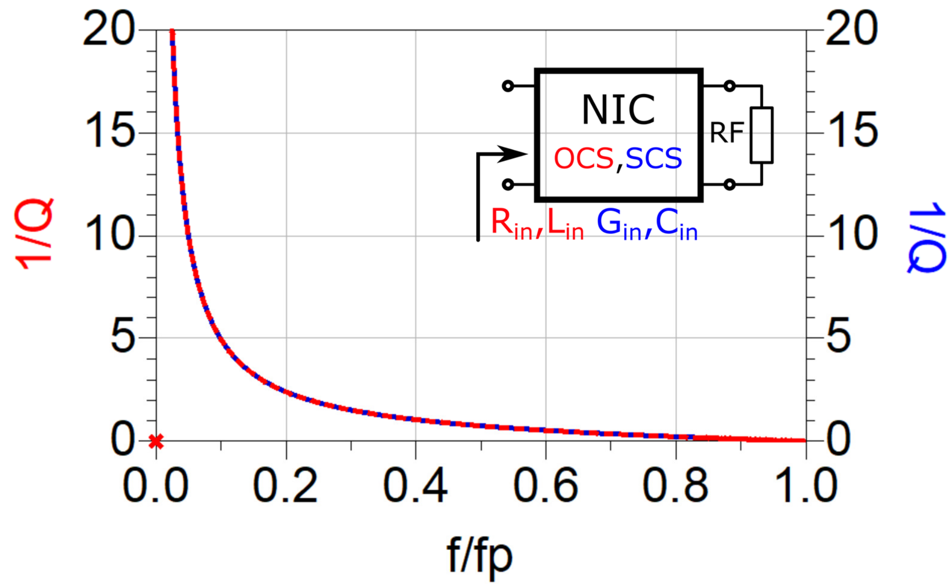

Figure 3-25 Q factor of OCS/SCS negative resistor (OCS/SCS NIC terminated by ordinary resistor)

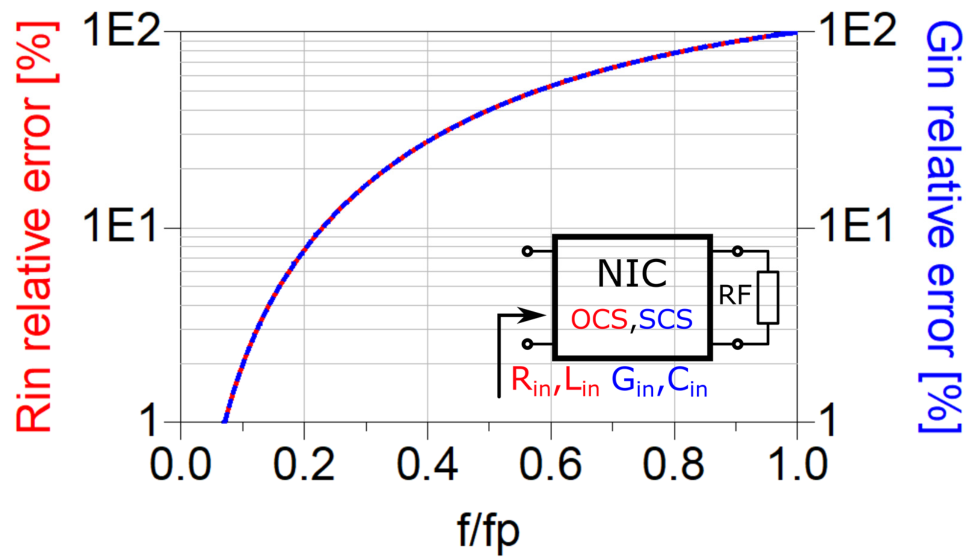

Figure 3-26 Relative error of resistance/conductance of OCS/SCS negative resistor (OCS/SCS NIC terminated by ordinary resistor)

Several important conclusions can be drawn from presented simplified dispersion analysis of the basic NIC circuits:

- The negative SCS capacitor produces an ideal negative input capacitance at zero frequency. As the frequency increases, the capacitance also increases and becomes zero at the pole frequency. In addition, the negative SCS capacitor produces a negative input conductance that causes additional gain that can lead to stability problems. The OCS negative capacitor also produces an ideal negative input capacitance at zero frequency. However, as the frequency increases, the capacitance decreases and reaches a negative infinite value at the pole frequency. In addition, the negative OCS capacitor produces a positive parasitic input resistance that causes additional losses. Both SCS and OCS negative capacitors have negligible dispersion (with a relative capacitance error of less than 2% up to one tenth of the pole frequency, where the value of associated Q factor drops to 5). At frequencies higher than one tenth of the pole frequency, the negative SCS capacitor has a smaller error than the negative OCS capacitor.
- The behavior of the negative inductor is a dual of the behavior of the negative capacitor. The negative OCS inductor produces an ideal negative input inductance at zero frequency. As the frequency increases, the inductance also increases and becomes zero at the pole frequency. In addition, the negative OCS inductor produces a negative input resistance that causes additional gain that can lead to stability problems. The SCS negative inductor also produces an ideal negative input inductance at zero frequency. However, as the frequency increases, the inductance decreases and reaches a negative infinite value at the pole frequency. In addition, the negative SCS inductor produces a positive parasitic input resistance that causes additional losses. Both OCS and SCS negative capacitors have negligible dispersion (with a relative capacitance error of less than 2% up to one tenth of the pole frequency, where the value of associated Q factor drops to 5). At frequencies higher than one tenth of the pole frequency, the negative OCS inductor has a smaller error than the negative SCS inductor.
- For negative resistors/negative conductors, there is no difference in dispersion between OCS and SCS types. This is a direct consequence of the fact that the N and S curves (Section 3.13.) are identical in their linear parts. The only difference is that the OCS type has a parasitic positive series inductance, while the SCS type has a parasitic positive shunt capacitance.

3.2.3. Non-ideal NIC circuits – rigorous analysis

Discussion presented so far was largely intuitive. The analysis can simply be formalized using familiar hybrid h-parameters ([27], Figure 3-27).

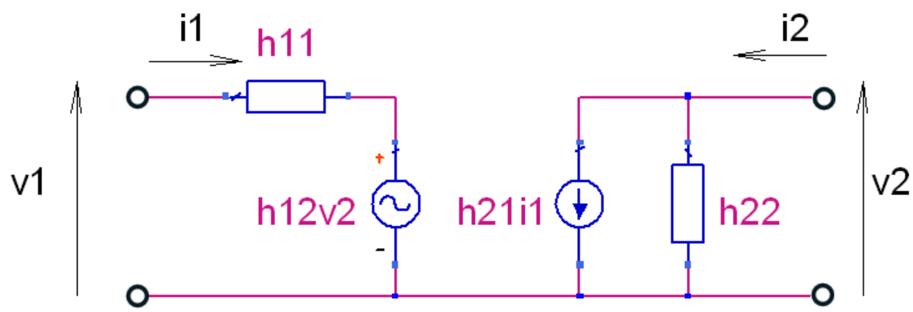

Figure 3-27 General NIC modelled with h-parameters

The h-parameter model is defined by well-known equations:

$$V_1 = h_{11} \cdot I_1 + h_{12} \cdot V_2 \tag{3.11}$$

$$I_2 = h_{21} \cdot I_1 + h_{22} \cdot V_2 \tag{3.12}$$

If the port 2 is terminated with impedance Z_F, the input impedance (seen into the port 1) reads as:

$$Z_{in} = \frac{V_1}{I_1} = h_{11} - \frac{k \cdot Z_F}{1 + h_{22} \cdot Z_1}, \quad k = h_{12} \cdot h_{21}. \tag{3.13}$$

Here, k stands for the conversion ratio [103]. An ideal NIC should have k=1. Inspection of (3.13) shows that this will be achieved if the following conditions are satisfied:

$$h_{11} = h_{22} = 0, \tag{3.14}$$

$$h_{12} \cdot h_{21} = 1. \tag{3.15}$$

As already mentioned in the Section 3.2.1., two basic types of NIC are realizable in accordance with (3.14, 3.15) depending on whether current or voltage inversion occurs. The first type is referred to as a current inverting NIC or INIC, and it does current inversion without affecting the polarity of input and output voltages. If the load Z_F is connected to port 2, the inversion of port current generates voltage V_1 that now enforces current flow in the opposite direction such as to oppose the applied voltage (Figure 3-28). Thus, the input impedance is negative while $I_1=I_2$, $V_1=V_2$. This can be written in matrix form as:

$$\begin{bmatrix} h_{11} & h_{12} \\ h_{21} & h_{22} \end{bmatrix} = \begin{bmatrix} 0 & 1 \\ 1 & 0 \end{bmatrix}. \tag{3.16}$$

Equation (3.16) defines an ideal INIC.

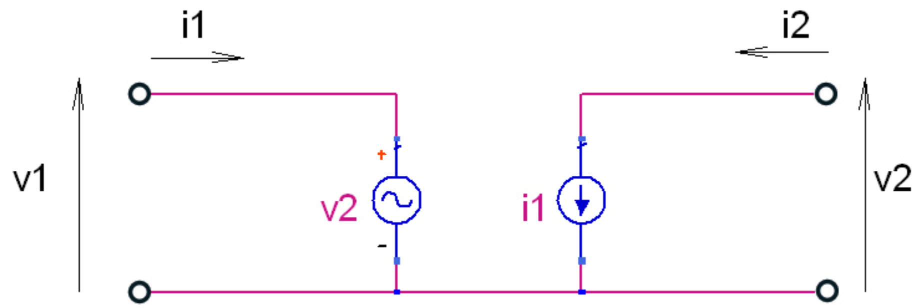

Figure 3-28 h-parameter model of an ideal INIC

It can be seen that the load voltage V_2 is actually 'transferred' to the input port voltage V_1 without change of sign. On the contrary, the input port current I_1 is transferred to the load with reversed sign.

Another possible way of achieving negative input impedance is to reverse one port voltage leaving polarity of currents unchanged. Thus, I_1=-I_2, V_1=-V_2, which again leads to a simple matrix equation:

$$\begin{bmatrix} h_{11} & h_{12} \\ h_{21} & h_{22} \end{bmatrix} = \begin{bmatrix} 0 & -1 \\ -1 & 0 \end{bmatrix} \qquad (3.17)$$

The device defined by (5.17) is referred to as a voltage inverter or VNIC (Figure 3-29).

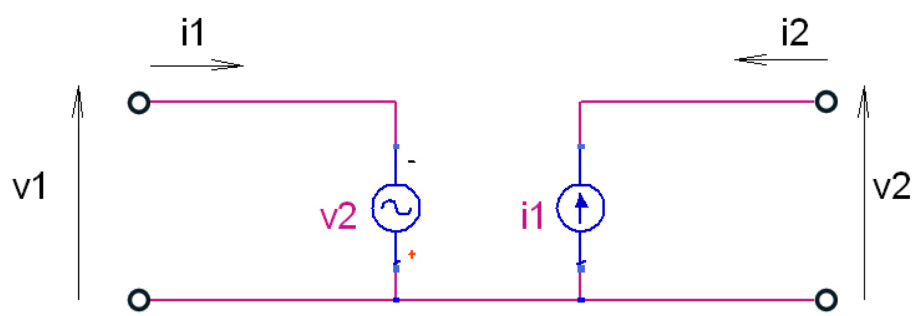

Figure 3-29 h-parameter model of an ideal VNIC

Basic INIC (Figure 3-28) and VINIC (Figure 3-29) models have two controlled (dependent) sources. At first glance, this seems impractical. However, these circuits can be reduced to those using a single dependent source by very simple transformations.

In the case of basic INIC circuit (left part of Figure 3-30) the upper input terminal and upper output terminal have equal potentials (referring to the common lower terminals) due to V_1= V_2. Thus, it is possible to connect upper input terminal to upper output terminal. The dependent voltage source will be connected in parallel to the dependent current source. In the next step, the voltage source can be dropped out if the current source amplitude is changed to $2I_1$. This leaves port voltages and port currents unchanged, thus the circuit in the right part of

(Figure 3-28) represents and INIC equivalent circuit that contains single (dependent) current source. Since the lower terminal of this current source is connected to the common point (ground), a floating source is not needed here.

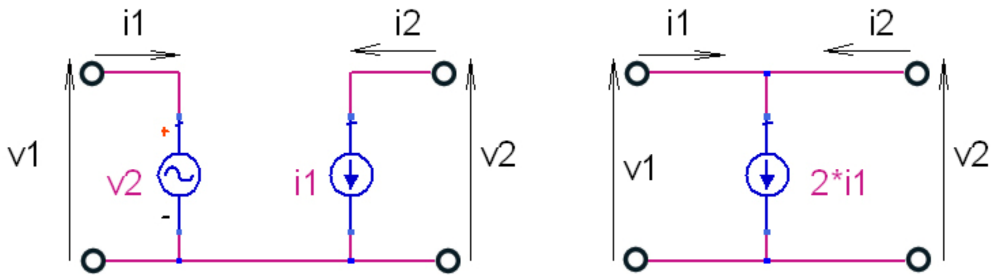

Figure 3-30 Transformation of basic INIC into with single current source

It can be seen that transformed circuit (right part of Figure 3-30) is identical to basic system in Figure 3-10, used initial intuitive analysis.

Very similar approach can be applied to the case of VNIC circuit (Figure 3-31).

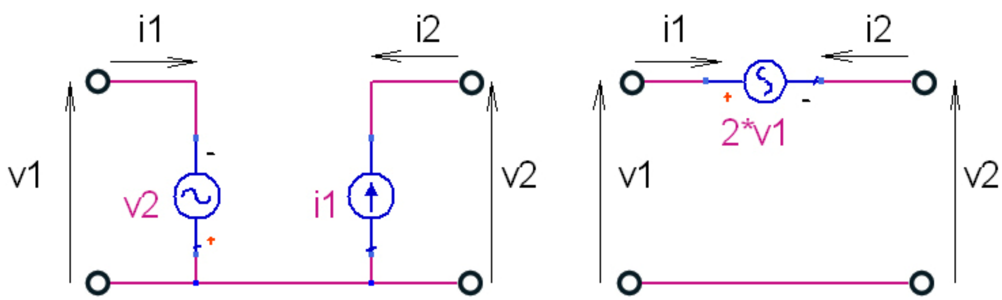

Figure 3-31 Transformation of basic VNIC into VNIC with single voltage source

It can be seen that the potential of the upper input terminal is equal to the potential of the upper output terminal, but with the opposite sign. At the same time, the port currents are the same but flow in different directions. Therefore, it is possible to omit the original voltage and current sources and replace them with a single series voltage source with amplitude $2V_1$ (right part of **Figure 3-31).**

Figure 3-31 uses a floating voltage source, which would lead to a complicated practical implementation with some three-terminal devices. Looking from the input port, a floating source is connected in series with the load (left part of Figure 3-32). Of course, the input current and voltage do not change when the positions of the voltage source and load are reversed (right part of Figure 3-32). Here the voltage source is no longer floating (the lower terminal is connected to ground). This 'trick' is very often used in grounded low-frequency NICs with OPamps [27][100][101].

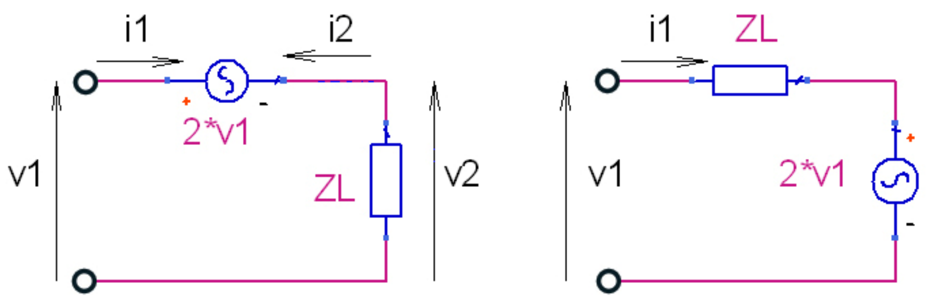

Figure 3-32 Two possible equivalent circuits of VNIC with single voltage source

Now, let us analyze the influence of non-idealities. At first one should be aware that basic requirements on NIC h-parameters (3.14, 3.15) describe the entire NIC (active element together with all the parasitics and eventual negative feedback used for gain management). Formally, the net h-matrix that can be decomposed into h-matrix of the active element (NIC amplifier) and h-matrix of the remaining passive network [107]. This yields the *h*-matrix of an ideal active two-port ($h_{\mathrm{a,\,ideal}}$), which can be written as:

$$h_{\mathrm{a,\,ideal}} = \begin{bmatrix} 0 & 0 \\ 1 & 0 \end{bmatrix}. \tag{3.18}$$

So, the parameters of ideal NIC amplifier are zero-valued input impedance, infinity-valued output impedance, and unity-valued current gain. This conclusion is, in a sense, similar to the requirements for generation of the negative resistance and conductance based on the ideal current 'transactors' (zero-input-impedance and infinite-input-impedance current amplifiers with unity gain) [103]. As already mentioned, this is the characteristic of ideal CB-configured BJT amplifier (or CG-configured FET amplifier). As detailed in [103] (and consistent with Figure 3-13), the NIC can also be constructed using the ideal volage 'transactors' (infinite-input-impedance and zero-input-impedance voltage amplifiers with unity gain). Clearly, this is the characteristic of ideal CC-configured BJT amplifier (or CD-configured FET amplifier).

In practice, the negative impedance conversion operation described above is affected by the influence of non-idealities of practical transistors and associated biasing networks. Recently, it has been shown that a small change in the bias point can significantly improve the conversion accuracy [107]. It was also found that in addition to the magnitude of the h_{12} parameter (which describes the non-unilaterality), its phase angle also plays an important role. Moreover, it is generally believed that the use of transistors with a sufficiently high transit frequency f_T (much higher than the operating frequency) allows for a low conversion error. However, practical guidelines are not available. Although the influence of all the above parameters can be considered analytically, this is usually considered too complicated for practical purposes. In the absence of a simple analytical approach, numerical circuit optimization is usually applied to achieve the desired design characteristics (usually minimum conversion error and 'apartment' dispersion curve). This is an iterative and lengthy process, where the complexity of the system makes it difficult to gain physical insight into the influence of individual components on the overall system.

On the other hand, low frequency NICs based on OPamps are known to have characteristics very close to the ideal ones. This is, of course, a consequence of the large open-loop gain and the strong negative feedback applied. It is interesting to note that almost all studies on RF and microwave NICs (including microelectronic implementations) use 'bare transistors' without negative feedback at all. Those studies try to optimize their technological parameters to achieve near-ideal behavior. There are very few papers on NICs, the amplifier of which employs both positive and negative feedback, although it allows easy implementation of reconfigurability issue [108][112][113]. Therefore, in the experimental part (Section 6.1), we try to construct a Miller-type of NIC that mimics classical OPamps. It is based on a rudimentary differential amplifier with strong negative feedback, designed in HCBT technology.

3.3. 'Negative Impedance Inverter' (NII)

Basic principle of NIC circuits is 'flipping' the sign of input current or input voltage ('negative conversion'), which, in turn, causes the impedance or admittance 'negation'. So, $\mathrm{Z_{IN}}. \sim -\mathrm{Z_{LOAD}}$ or $\mathrm{Y_{IN}}. \sim -\mathrm{Y_{LOAD}}$. Therefore, a positive capacitance is converted to a negative capacitance and a positive inductance is converted to a negative inductance. There is also a class of different circuits usually called Negative Impedance Inverters (NII). Such a circuit, 'swaps' the role of voltage and current and flips the sign of one of them. So, $\mathrm{Z_{IN}} \sim -1/\mathrm{Z_{LOAD}}$ or $\mathrm{Y_{IN}} \sim -1/\mathrm{Y_{LOAD}}$. In this case, a positive capacitance is converted to a negative inductance and a positive inductance is converted to a negative capacitance. The use of NII circuits with 'negative inversion' is in some cases more advantageous than the use of NIC circuits with 'negative conversion'. This is especially the case with MMIC circuits where it can be difficult to build a high quality inductor.

3.3.1. Basic OCS and SCS NIC circuits

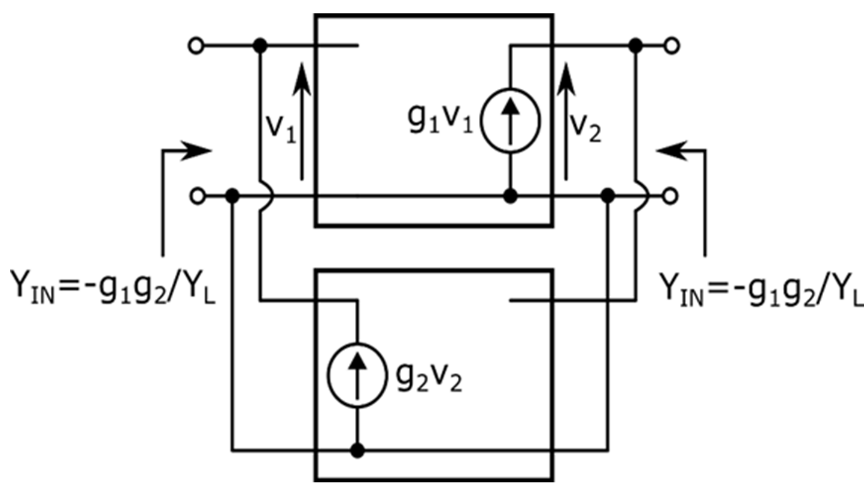

Figure 3-33 Basic SCS NII based on two trans-conductance amplifiers [103]

A basic SCS NII comprises two trans-conductance amplifiers (Figure 3-33). Let u suppose that a load with admittance (Y_L) (not shown in the figure) is connected to the right port. Upper amplifier 'inverts' the input voltage (V_1) at left port into output current (g_1V_1). This current gives rise to the load voltage (g_1V_1/Y_L), which is, in turn, 'inverted' into input current at the left port ($-g_1g_2V_1/Y_L$). Therefore, input admittance is a scaled inverse of the load admittance with flipped sign:

$$Y_{IN(left)} = -\frac{g_1 g_2}{Y_L} \tag{3.19}$$

Since the circuit in Figure 3-33 is symmetrical, the same expression applies if the locations of the input and load ports are swapped:

$$Y_{IN(right)} = -\frac{g_1 g_2}{Y_L} \tag{3.20}$$

'Classical' realization of this SCS NII is Kolev-Meuinier design[39] [110] (Section 3.5.2), based on two FETs.

There is also a basic OCS NII, shown in Figure 3-34.

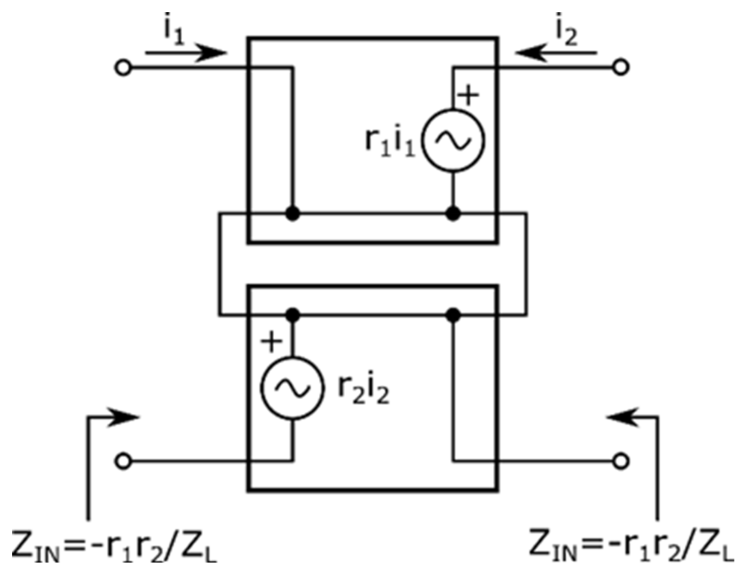

Figure 3-34 Basic OCS NII based on two trans-resistance amplifiers [103]

This circuit is a direct dual of the SCS NII from Figure 3-33, and it comprises two trans-resistance amplifiers.

Let u suppose that a load with impedance (Z_L) (not shown in the figure) is connected to the right port. Upper amplifier 'inverts' the input current (I_1) at left port into output voltage($r_1 I_1$). This voltage gives rise to the load current ($r_1 I_1 / Z_L$), which is, in turn, 'inverted' into input voltage at the left port ($- r_1 r_2 I_1 / Z_L$). Therefore, input impedance is a scaled inverse of the load impedance with flipped sign:

$$Z_{IN(left)} = -\frac{r_1 r_2}{Z_L} \tag{3.21}$$

Since the circuit in Figure 3-33 is symmetrical, the same expression applies if the locations of the input and load ports are swapped:

$$Z_{IN(right)} = -\frac{r_1 r_2}{Z_L} \tag{3.22}$$

3.3.2. Dispersion properties

Similarly to the dispersion analysis of NICs (Section 3.2.2), one can model non-ideality of the NIIs amplifiers using a low-pass one-pole gain function. Thus, the one-pole model of trans-conductance amplifier reads:

$$g(s) = \frac{g_0}{1 + s\tau}, \quad \omega_{\mathrm{P}} = \frac{1}{\tau}, \tag{3.23}$$

while the trans-resistance amplifier is described by:

$$r(s) = \frac{r_0}{1 + s\tau}, \quad \omega_{\mathrm{P}} = \frac{1}{\tau}, \tag{3.24}$$

Here, τ stands for the amplifier time constant, associated with pole frequency ω_{P} (cut-off frequency of an amplifier). Symbol g_0 and r_0 stand for the trans-conductance and trans-resistance at zero frequency, respectively. If, $\tau = 0$ the models reduce to the ideal non-dispersive case with infinite bandwidth.

For example, let us analyze the SCS NII from Figure 3-33 loaded with inductor L, assuming one-pole model of the trans-conductance amplifiers. Following the procedure from Section 3.2.2. , one finds the input admittance:

$$G_{IN} = Re\{Y_{IN}\} = -\omega L g_0^2 \frac{\frac{2}{\omega_p}}{\left(1 - \frac{\omega^2}{\omega_p^2}\right)^2 + \left(\frac{2\omega}{\omega_p}\right)^2} \tag{3.25}$$

$$C_{IN} = \frac{Im\{Y_{IN}\}}{\omega} = -L g_0^2 \frac{1 - \frac{\omega^2}{\omega_p^2}}{\left(1 - \frac{\omega^2}{\omega_p^2}\right)^2 + \left(\frac{2\omega}{\omega_p}\right)^2} \tag{3.26}$$

Similar analysis of the OCS NII from Figure 3-34 loaded with capacitor C, assuming one-pole model of the trans-resistance amplifiers yields input impedance:

$$G_{IN} = Re\{Y_{IN}\} = -\omega L g_0^2 \frac{\frac{2}{\omega_p}}{\left(1 - \frac{\omega^2}{\omega_p^2}\right)^2 + \left(\frac{2\omega}{\omega_p}\right)^2} \tag{3.26}$$

$$C_{IN} = \frac{Im Y_{IN}}{\omega} = -L g_0^2 \frac{1 - \frac{\omega^2}{\omega_p^2}}{\left(1 - \frac{\omega^2}{\omega_p^2}\right)^2 + \left(\frac{2\omega}{\omega_p}\right)^2} \tag{3.27}$$

Of course, it is possible to use higher-order amplifier models (two-pole and three-pole models [27]), which would give more realistic dispersion prediction for higher frequencies. However, as mentioned before, non-Foster elements are used for frequencies where the operating frequency is lower of the frequency of the first pole (or even lower than one-tenth of it) and one-pole approximation is sufficient for predicting the stability properties (as it will be shown in detail in the Section 3.4).

Thus, we decided to perform dispersion analysis for all basic SCS and OCS NIIs terminated by three representative loads: a capacitor, an inductor, and resistor. These NIIs should behave as negative inductance, negative capacitance and negative conductance/resistance. We used input admittance for SCS NIC and input impedance for OCS NIC. The models of equivalent input networks are briefly explained in Table 3-2

NII type	Load type	Equivalent input network	Analysis presented in:
SCS	capacitor	dispersive L shunted by 'parasitic' dispersive G	Figure 3-35 Figure 3-36 Figure 3-37 Figure 3-38
OCS	capacitor	dispersive L in series with 'parasitic' dispersive R	
SCS	inductor	dispersive C shunted by 'parasitic' dispersive G	Figure 3-39 Figure 3-40 Figure 3-41 Figure 3-42
,OCS	inductor	dispersive C in series with 'parasitic' dispersive R	
SCS	resistor	dispersive G shunted by 'parasitic' dispersive C	Figure 3-43 Figure 3-44 Figure 3-45 Figure 3-46
OCS	resistor	dispersive R in series with 'parasitic' dispersive L	

Table 3-2 Models of input admittance/impedance used in dispersion analysis of various one-pole NIIs

For each analyzed case, we calculated both 'desired' input quantity and 'parasitic' input quantity, Q factor, and relative error of generated 'desired' input quantity. All these values are defined as a function of the frequency normalized on the pole frequency.

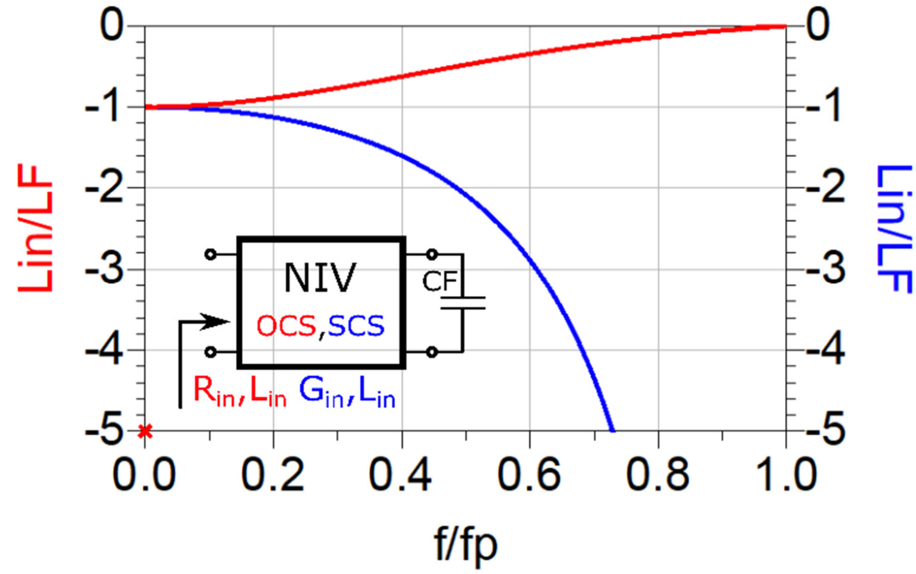

Figure 3-35 Dispersion of inductance of OCS/SCS negative inductor (OCS/SCS NIV terminated by ordinary capacitor)

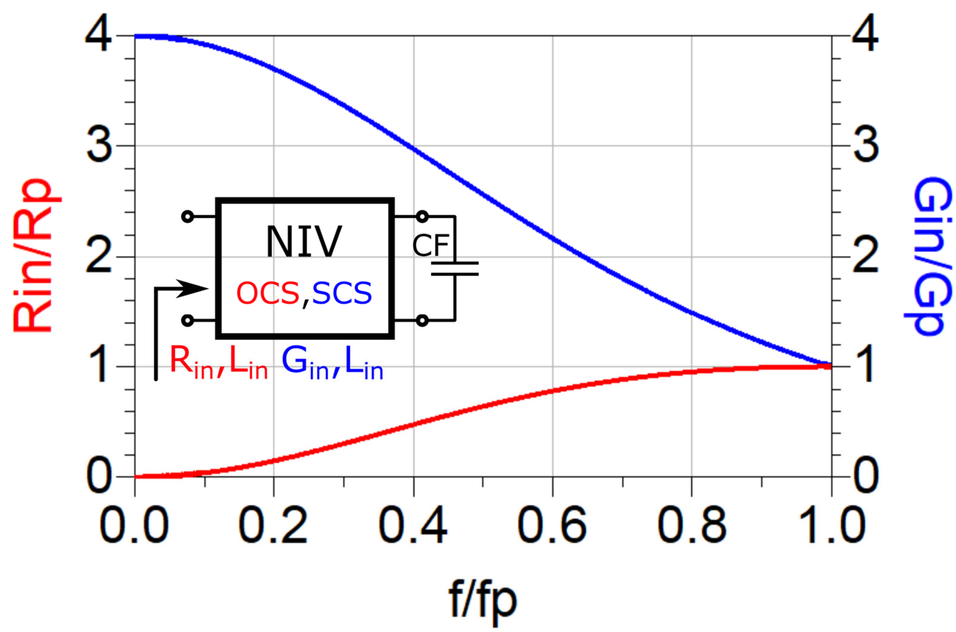

Figure 3-36 Dispersion of ‘parasitic’ resistance/conductance of OCS/SCS negative inductance (input ‘parasitic’ resistance/conductance of OCS/SCS NIV terminated by ordinary capacitor)

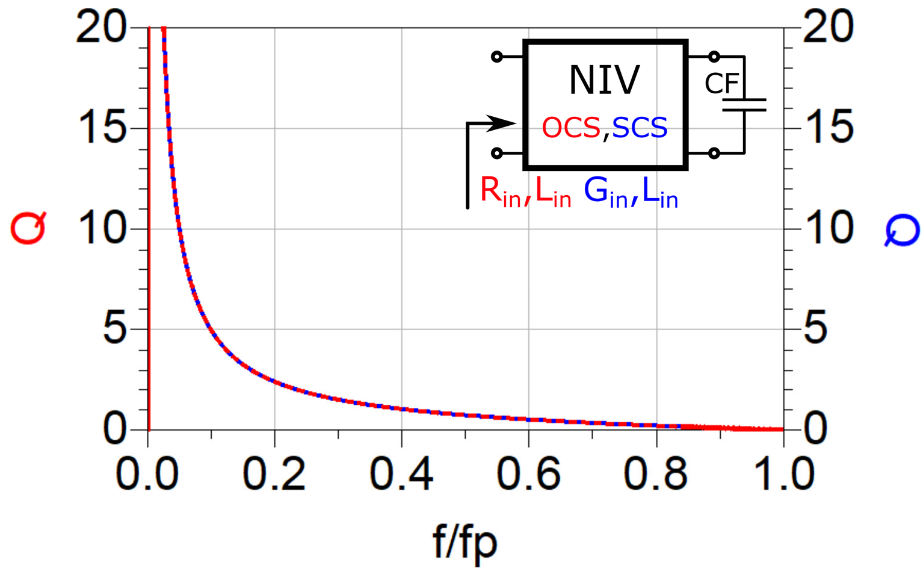

Figure 3-37 Q factor of OCS/SCS negative inductor (OCS/SCS NIV terminated by ordinary capacitor)

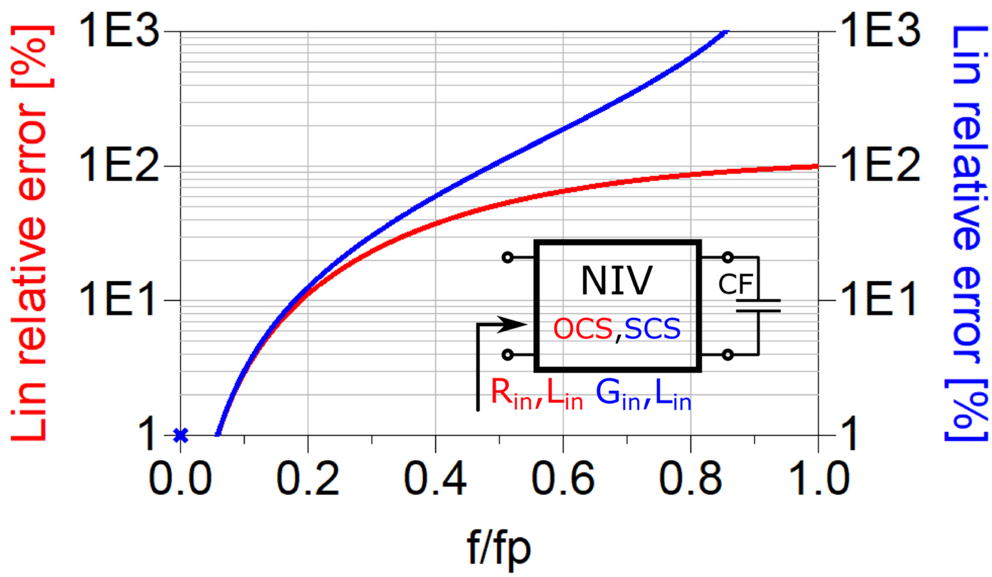

Figure 3-38 Relative error of inductance of OCS/SCS negative inductor (OCS/SCS NIV terminated by ordinary capacitor)

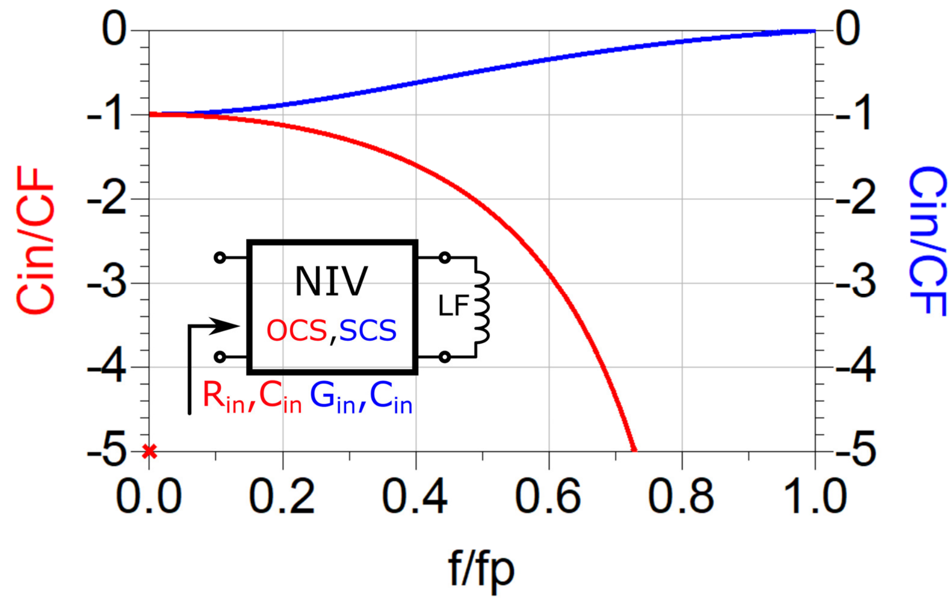

Figure 3-39 Dispersion of capacitance of OCS/SCS negative capacitor (OCS/SCS NIV terminated by ordinary inductor)

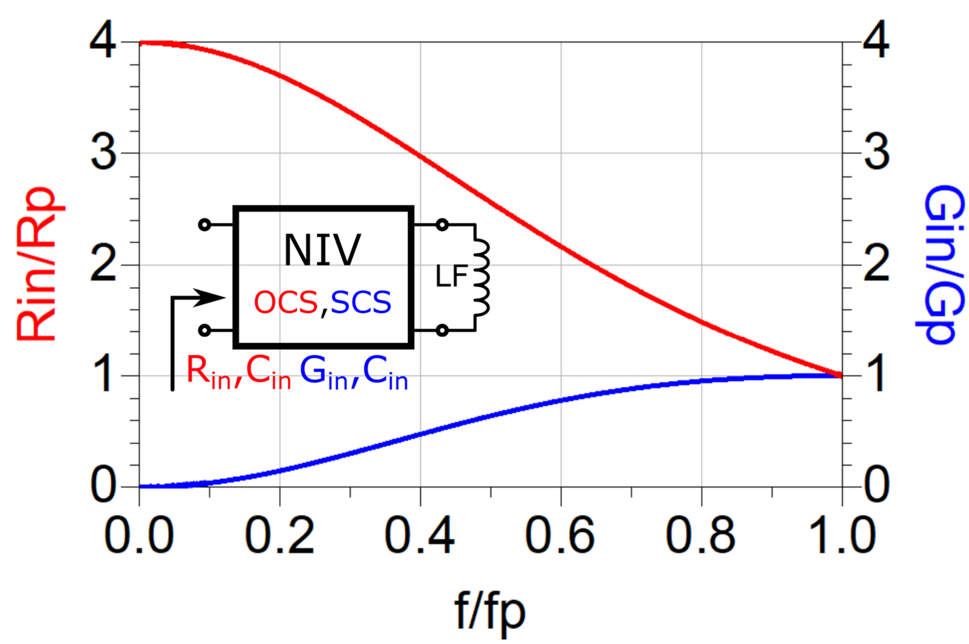

Figure 3-40 Dispersion of 'parasitic' resistance/conductance of OCS/SCS negative capacitance (input 'parasitic' resistance/conductance of OCS/SCS NIV terminated by ordinary inductor)

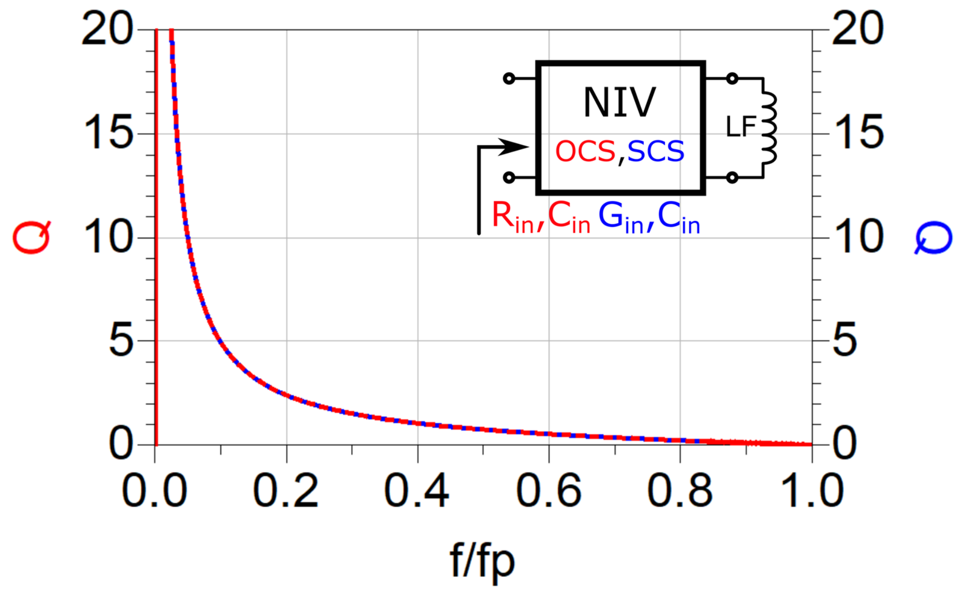

Figure 3-41 Q factor of OCS/SCS negative capacitor (OCS/SCS NIV terminated by ordinary inductor)

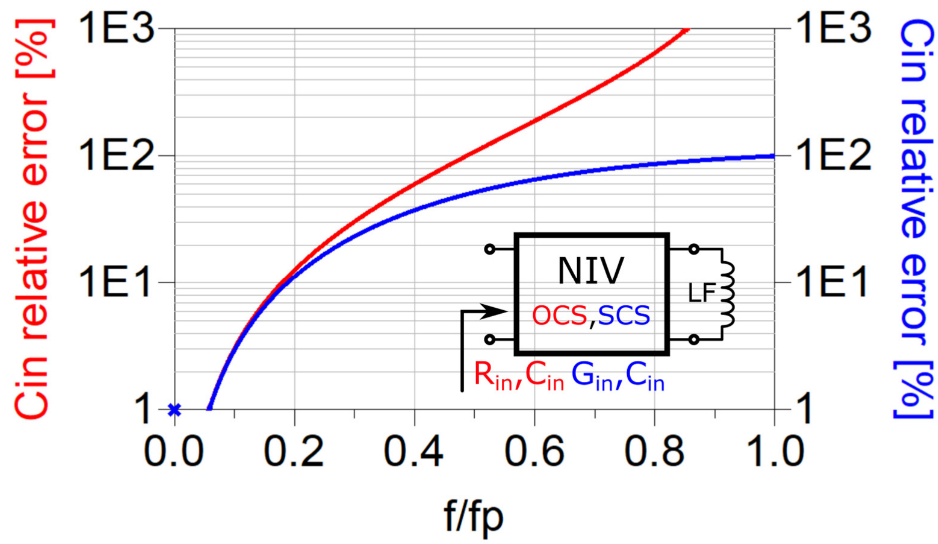

Figure 3-42 Relative error of capacitance of OCS/SCS negative capacitor (OCS/SCS NIV terminated by ordinary inductor)

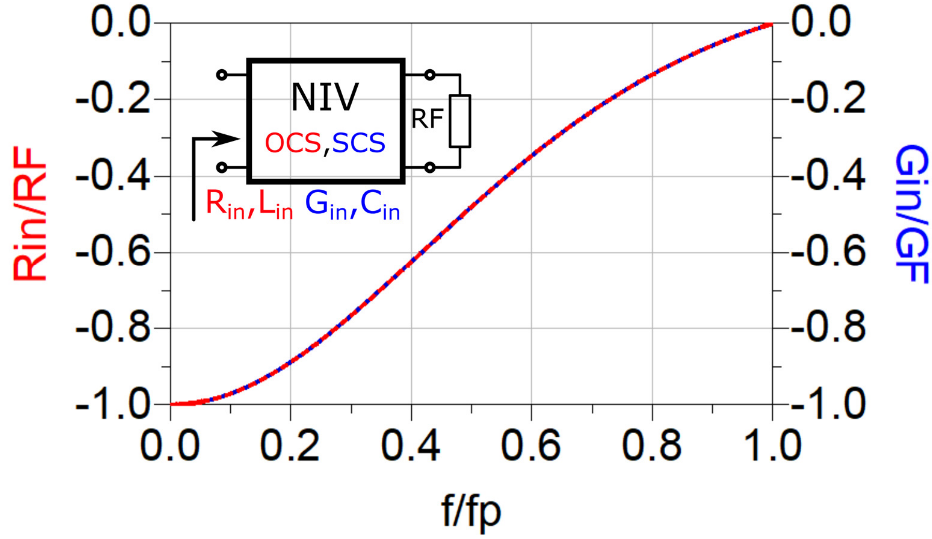

Figure 3-43 Dispersion of resistance/conductance of OCS/SCS negative resistor (OCS/SCS NIV terminated by ordinary resistor)

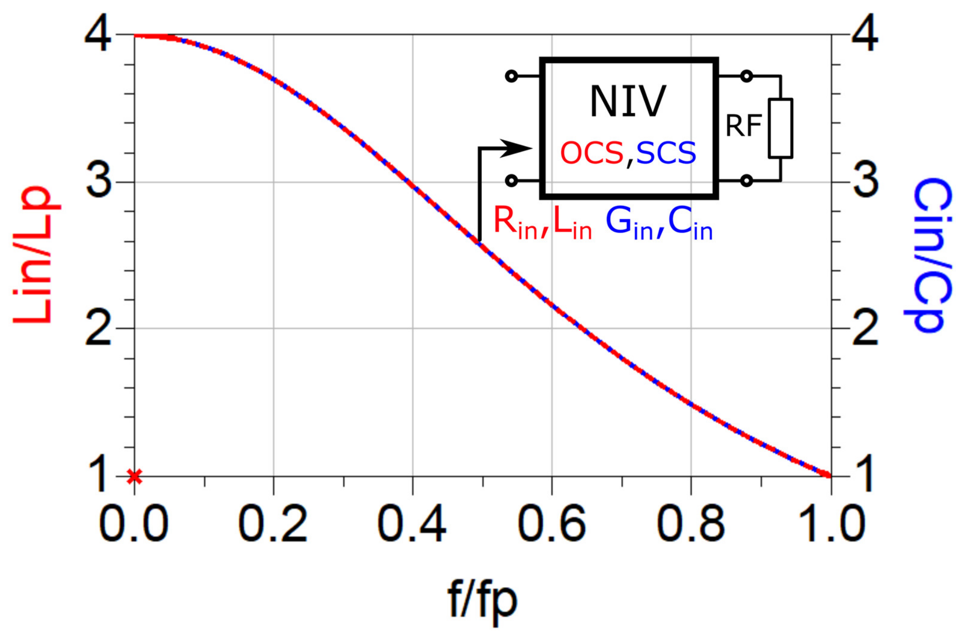

Figure 3-44 Dispersion of 'parasitic' inductance/capacitance of OCS/SCS negative resistance (input 'parasitic' inductance/capacitance of OCS/SCS NIV terminated by ordinary resistor)

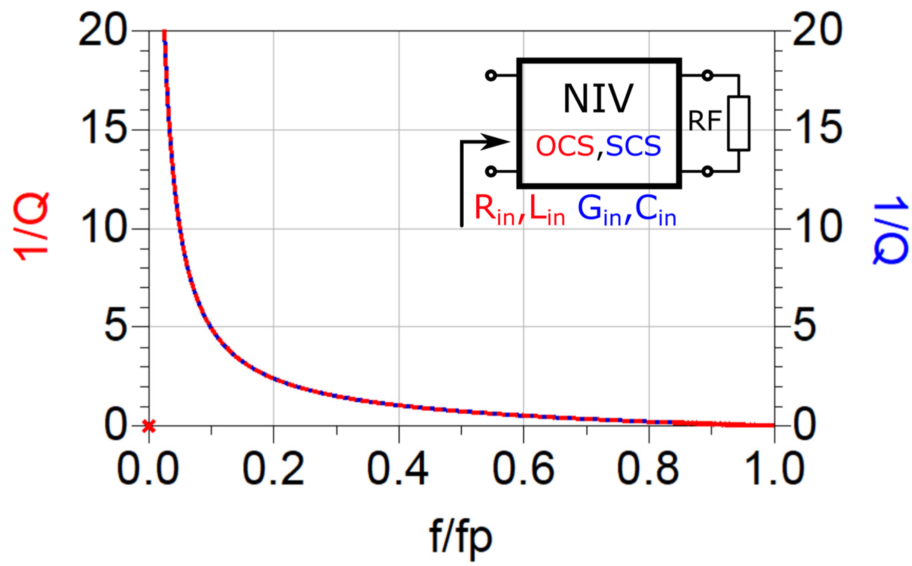

Figure 3-45 Q factor of OCS/SCS negative resistor (OCS/SCS NIV terminated by ordinary resistor)

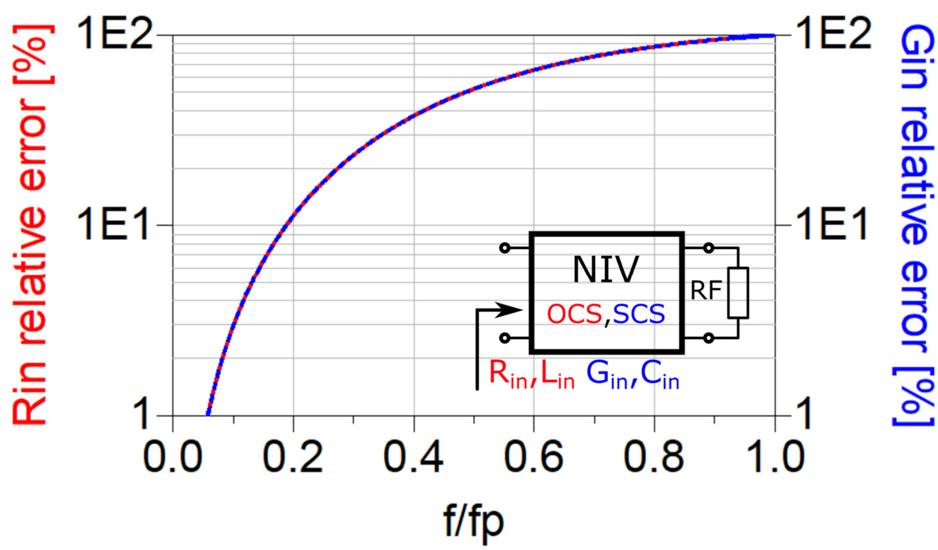

Figure 3-46 Relative error of resistance/conductance of OCS/SCS negative resistor (OCS/SCS NIV terminated by ordinary resistor)

The conclusions that can be drawn from presented simplified dispersion analysis of the basic NII circuits are analog to those from the analysis of NIC circuits (Section 3.2.2). The main difference is that the operation bandwidth defined by some predetermined impedance error is approximately 20% narrower due to use of two amplifiers.

3.3.3. Non-ideal NII circuits – rigorous analysis

The rigorous analysis of non-ideal NIC circuits, based on h parameters, was presented in Section 3.2.3. It was shown the parameters of ideal NIC amplifier are zero-valued input impedance, infinity-valued output impedance, and unity-valued current gain. In practice, one usually attempts to produce amplifier whose characteristics are close to above requirements.

The rigorous analysis of non-ideal NII circuits can be performed using Y and Z matrices [103]. It is very similar to the analysis in Section 3.2.3. This analysis is straightforward but rather lengthy and, therefore, it is not included here. We just point the main conclusions which are, in a sense, very similar to the requirements from Section 3.2.3.

In the case of SCS NII (Figure 3-33), one should try to construct trans-conductance amplifier with high (ideally, infinite-valued) input impedance and low (ideally, zero-valued) output impedance. However, there is no preferred value for trans-conductance gain (the preferred values of voltage and current gain in Section 3.2.3 was 1). For the case of OCS NII (Figure 3-34), there is a dual requirement. One should try to construct trans-resistance amplifier with low (ideally, zero-valued) input impedance and high (ideally, infinity-valued) output impedance. The value of trans-resistance gain is again selected taking into account required conversion ratio.

3.4. Stability properties of networks containing NIC and NII circuits

As it was highlighted in Introduction, all non-Foster and negative elements are prone to instability caused by inevitable use of positive feedback. Indeed, successful prediction and management of stability properties of systems with non-Foster and Negative elements is extremely difficult engineering task. In this Chapter we discuss stability properties of networks containing NIC/NII circuits.

3.4.1. Analysis based on OCS/SCS approach

So far, it was shown that common non-Foster or Negative 'element' comprises NIC (or NII), terminated with some appropriate load. In many applications, this 'element' is then connected to some external passive network. For instance, this is the scenario of matching a small antenna or cancellation of some parasitic capacitance, using non-Foster negative capacitance.

Thus, the simplest practical system comprises an external network connected to the input impedance at port 1 (or port 2) (for some particular termination at port 2 (or port 1) of some NIC (NII) and the NIC/NII itself.

Choosing the short-circuit or open-circuit as a load impedance leads to so-called SCS/OCS analysis. Historically, it was observed that a practical NIC has the SCS properties at one port, and (simultaneously) the OCS properties at the other port (and vice versa).

Brownlie [79], Hoskin [80], and Schwarz [81] proposed three separate proofs to justify this stability phenomenon by considering the existence of poles or zeros in the right hand side

(RHS) of the complex plane. All three authors introduced some prerequisite conditions. Brownlie [99] assumed the existence of 'parasitic' parameters in the NIC h-matrix. Hoskin [100] assumed the existence of time delay in the NIC circuit. Schwarz [101] assumed that either right-half-plane poles or right-half-plane zeros are introduced during the conversion process. In other words, in all three approaches, the NIC is considered being non-ideal (conditions 3.14 and 3.15 are not satisfied).

Deeper physical explanation, based on two different approaches, was given in [102]. The first approach analyzed the NIC and its terminating networks as a linear frequency dependent system. In order to prove that the practical NIC is SCS at one port, and OCS at the other port it was found necessary to prove that the input impedance at one port has no right-half-plane pole but has right-half-plane zero and that the input admittance at the other port has no right-half-plane pole but has right-half-plane zero. The second approach analyzed the practical NIC, when terminated in resistors, as a nonlinear system. More precisely, the saturation region of used active elements (bipolar transistors or FETs) was taken into account. To prove that the practical NIC is SCS at one port and OCS at the other port it was necessary to prove that the negative input resistance of the NIC was voltage-controlled ('N' type of non-linearity) at one port and current-controlled ('S type of non-linearity) at the other port.

It is very important to stress that whether a practical NIC will remain stable or not in a system depends on the properties of *networks that are connected to the NIC*. To investigate the stability of the NIC, it is necessary to consider the NIC and its terminating networks (or the system) as a whole. Usually it is assumed that (practically speaking) OCS means, that if a very large resistance terminates the port 1 on NIC, then the overall network will be stable. Similarly, it is usually considered that SCS means that overall network will be stable if a very large conductance is placed across the input. Originally, Linvill [16] suggested that OCS versions should be used only as series elements, while SCS versions should be used as shunt elements. This 'recipe', based on the selection of SCS/OCS type, is widely used in many studies [63][108][109][110][111][112][113].

However, one should be very careful in interpretation of above common assumptions. Firstly, it comes from the analysis of purely resistive (conductive) loads and nothing is said about the reactive parts. Indeed, even a pure negative (non-Foster) reactance when connected to a positive resistance leads to instability [40]. Secondly, if some system is SCS (or OCS) *it does not necessary mean* that it will be stable for some very low resistance (or some very low conductance). For instance, there are two very interesting examples presented in [83]. The first example deals with a one-port network that is SCS but unstable for any resistance between 0.5Ω and 1Ω. The second example presented in [83] shows a two-port network with SCS/OCS ports that is unstable if either port is terminated with 1 Ω resistor.

One concludes that, although widely used for the first selection of NIC/NIV type, the SCS/OCS method is strictly valid only for short-circuit and open circuit termination and it is uninformative for the case of arbitrary termination.

3.4.2. Analysis based on ideal dispersionless negative elements

The SCS/OCS method usually does not analyze the generalized non-Foster network *per se*. Instead, it deals with the NIC circuit terminated with networks that contain ordinary positive lumped elements. Many authors use the next level of abstraction and analyze the lumped networks that contain ordinary (positive) elements and ideal generalized non-Foster elements (ideal negative resistor, ideal negative capacitor, and ideal negative resistor). Is this a physically correct approach? Clearly, idealized dispersion-free models of negative elements are not physical. Several examples of predicted non-physical behavior can be found in the literature [2,41,90]. Thus, the answer to the question above is surely 'no'. However, the question 'Can the analysis based on idealized dispersionless elements give any useful information?' is more complex and the answer is not so clear. Let us discuss this point in some more details.

There are two groups of non-physical behavior observed in stability analysis: the unbounded signal growth associated with the infinite energy and incompatibility of predicted signal with causality. The unbounded signal growth neglects inherent saturation (i.e. the non-linearity) that is inevitably present in every practical active element. Nevertheless, every non-linear instability effect started as a linear effect (for early time and small signal levels), so *the occurrence of instability* will be predicted correctly. Of course, since the gain compression and saturation effects are neglected, the waveform of predicted signal will be incorrect. As far as the causality problems concern, they are inevitable connected to networks with delay (transmission lines). Unfortunately, available public literature is sparse of such studies.

It is important that the use of idealized dispersionless elements may (sometimes) predict behavior that is *physical* (within the limits given by linear stability analysis) and compatible with causality, but *still incorrect*. ([91]). This happens due to the unwanted ('parasitic') conductance and reactance of realistic non-Foster and Negative elements. Thus, the issue of usefulness of stability prediction using idealized dispersion-free models of negative elements can be summarized as follows. If the network does not contain transmission lines and it is only important to predict whether it is stable or not, the analysis with ideal elements *might* give a correct answer and *might* help in identifying the 'problematic' parts. However, this result should be cross-checked by realistic models of negative elements.

The widely accepted stability criterion in networks with ideal elements is that *the overall 'mesh'* capacitance or inductance must be a positive number [91]. A very thorough instigation reported in [27] confirmed this assumption for many simple combinations that contained not only reactive (L, C) elements but also resistive (R) elements. Thus, above criterion is extended *to overall 'mesh' resistance*, which should also be a positive number. Counter-intuitively, the same analysis showed stable behavior if the overall 'mesh' capacitance, inductance, and resistance *is negative.*

Finally, let us briefly review some of the methods of stability analysis and their connection to ideality (or non-ideality) of negative elements. Every negative element contains some kind of a controlled source (in practice, it is usually some active element such as BJT, FET or OPamp that acts as an amplifier). If an ideal amplifier with infinite bandwidth existed, a generated negative capacitance, inductance or resistance would also be ideal (i.e. dispersionless). However, the gain of every realistic amplifier (regardless of used technology) will always be band-limited and its amplitude and phase transfer functions must be connected via Hilbert transform (Kramers-Kronig relations). One may argue that a phase shift is negligible for practical purposes if the operating frequency is far below the frequency of the first pole of active element [7]. This may be true *but it does not mean* that one could use some method of stability analysis in frequency domain within this limited bandwidth. The stability prediction in phasor domain (steady-state analysis with real frequencies) should not be used at all. This approach neglects the transient response that is (as discussed in previous paragraph) crucial in non-Foster circuits. This is connected to commonly used incorrect saying like 'This circuit is stable within frequency band of …'. Thus, stability analysis in the Laplace domain (with complex frequency $s = \sigma + j\omega$) or in the time domain is a first prerequisite (necessary, but not always sufficient!) for a reliable stability prediction. The methods that reduce the network to the equivalent 'black box' and then look at the properties of the 'black box' input port impedance (or reflection coefficient) may fail [27][83][84][85]. This happens due to the inherent poles located in the RHS of a complex plane, the existence of which cannot be inferred just from the analysis of the 'black box' input port reflection coefficient (the existence of so-called 'hidden modes') [87-89]). In order to avoid problems with hidden modes, one should use the method (either in the Laplace domain or in the time domain) that takes into account *all the meshes and nodes* of the analyzed network.

3.4.3. Analysis based on realistic models with dispersive controlled sources

(*The material presented in Section 3.4.3 is a review of a part of research activities of Dr. Josip Loncar during previous EOARD-funded project [44]).

In discussion in previous paragraph, it was stressed that commonly used 'mathematical' dispersionless model of an ideal non-Foster negative capacitor is nonphysical and it might be used only for the crude prediction of the qualitative behavior within a finite bandwidth. Outside this band, the model should not be used at all (even for qualitative analysis) because it gives unphysical behavior [27].

A simple, more realistic three-pole model of a dispersive negative capacitor was proposed in [27].

This model can certainly be used for stability predictions, but it is too complicated. The important fact is that in many practical situations it is sufficient to predict whether a system will be stable or unstable. The 'instability' details such as the waveform of the instability signal and its spectral content are not important (unless one develops an oscillator). For such simplified predictions, the one-pole model is 'good enough'.

In Section 3.2.2. we used one-pole model for dispersion prediction of a simple negative capacitor based on Miller NIC. Here, we use the same model to illustrate methodology of stability prediction.

A parallel combination of a positive resistor (R_{G}), a positive capacitor (C_{P}) and a negative capacitor (C_{N}) may be taken as a basic example (previously mentioned 'realistic scenario') of a non-Foster network (Figure **3**-**47**).

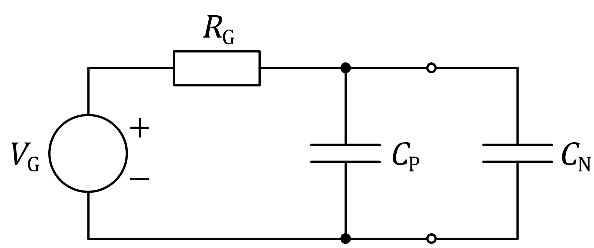

Figure 3-47 Basic network with a parallel combination of positive and negative capacitor, used in stability prediction. Negative capacitor is modelled using a realistic one-pole model

Here, one defines the transfer function as a ratio between the voltage drop across capacitors C_{P} and C_{N}, and a voltage across a 'disturbing generator' V_{G}. it is assumed that a negative capacitor has realistic behavior, given by (3.8) and (3.9). To analyze stability, one should find the complex frequencies ($s = \sigma + \mathrm{j}\omega$), for which the denominator of the transfer function becomes zero. It leads to the quadratic equation, roots of which represent the system poles:

$$s = \frac{-b \pm \sqrt{b^2 - 4ac}}{2a} \tag{3.28}$$

$$\begin{gathered} a = \tau R_{\mathrm{G}}(C_{\mathrm{P}} + C_{\mathrm{F}}), \\ b = \tau + R_{\mathrm{G}}[C_{\mathrm{P}} + (1 - A_0)C_{\mathrm{F}}], \\ c = 1. \end{gathered} \tag{3.29}$$

Analysis of (3.28) and (3.29) reveals that the network with a realistic negative capacitor has two complex poles in the most general case. By enforcing the requirement ($\mathcal{R}e\{s\} < 0$), one gets the new stability criterion:

$$|C_{\mathrm{F}}(1 - A_0)| < C_{\mathrm{P}} + \frac{\tau}{R_{\mathrm{G}}}. \tag{3.30}$$

The RHS of (3.30) contains not only the capacitance of the positive capacitor, but also an additional term (τ/R_{G}). This 'effective capacitance' is caused by one-pole low-pass behavior of the used amplifier and it (as it will be shown later) fundamentally changes the stability issue. Using (3.28) and (3.29) one finds different stability regions for different values of $|C_{\mathrm{IN}}|$ (at $\omega = 0$) and C_{P} (Figure 3-48, (a), solid curves).

In region 1, the network has stable exponential impulse response (real LHS pole, signal of $e^{\sigma t}$ form, $\sigma < 0$) and the positive capacitance is always larger than the negative capacitance. Thus, this region is convenient for applications in antenna matching systems and for cancellation of parasitic capacitance in various active RF devices. With the decrease of the time constant τ, region 1 becomes larger (the system is more similar to ideal dispersionless case). In region 2, the network has stable response with damped diminishing oscillations (complex LHS poles, signal of $e^{(\sigma + j\omega)t}$ form, $\sigma < 0$).

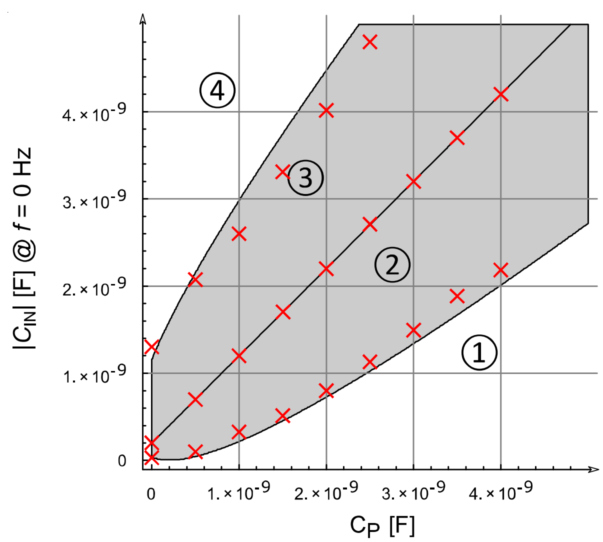

Figure 3-48 (adapted from [91]). Stability regions for lumped network (Fig. 3-2 (a)) containing parallel combination of an ideal positive and a realistic negative capacitor. Solid curves: Results obtained using analytical expressions (3.22, 3.23) and one-pole amplifier model, ($R_{\mathrm{G}} = 50\ \Omega$, $\tau = 10$ ns, $A_0 = 2$, parameters C_{P} and C_{F} are varied). Crosses: Results obtained by ADS-SPICE simulation of negative capacitor based on operation amplifier THS 4303 [91] .

It can be seen that the overall capacitance can be negative (for some values of C_{P} and C_{F}). Of course, with the decrease of time constant τ region 2 becomes smaller. The boundary between region 2 and region 3 is associated with loss-free oscillatory behavior (purely imaginary poles, signal of $e^{j\omega t}$ form, $\sigma = 0$). Above this boundary there are two unstable regions. Region 3 causes unstable growing oscillatory response (complex RHS poles, signal of $e^{(\sigma+j\omega)t}$ form, $\sigma > 0$). Region 4 supports unstable exponential response (real RHS pole, signal of $e^{\sigma t}$ form, $\sigma > 0$).

The methodology discussed is straightforward and accurate. Therefore, it has been used extensively in this project ([115][116][117][119]). There are two drawbacks. First, the characteristic equation of complicated networks may be a polynomial whose degree is higher than four. In this case, the methodology (using the Hurwitz approach) still correctly predicts the stability properties. However, the boundaries between stable and unstable regions cannot be determined analytically, so additional numerical effort is required. Second, it is difficult to immediately 'guess' what type of passive external network is required for stable operation.

3.4.4. Analysis based on equivalent circuits that contain ideal positive/negative elements

As it was discussed so far, dispersionless non-Foster and Negative elements are not causal, and, therefore non-physical. Alternatively, one may construct the 'subnetworks' comprising both ideal negative elements and ideal positive elements that together give behavior similar to behavior of a realistic dispersive negative element [90][103]. In other words, one can construct equivalent circuit of realistic non-Foster (or Negative) element that contains both ideal negative elements and ideal positive elements. This approach is actually an extension of approach with dispersive controlled source. Once the equation for input impedance/admittance is derived, one rearranges it into the appropriate from that can be interpreted as a combination of familiar lumped elements allowing negative values, as well. This method has the same mathematical problems if the degree of involved polynomials is higher than four. However, its advantage is that developed equivalent circuits are often intuitive, which may help in 'guessing' the type of passive external network is required for stable operation.

The method is illustrated by examination of stability properties of Miller negative capacitor [120]. We start from (3.9) and assume steady-state behavior ($s = j\omega$):

$$Y_{IN} = j\omega\,\frac{1 + j\omega\,\tau - A_0}{1 + j\omega\tau}\,C_{\mathrm{F}}\,. \tag{3.31}$$

This form can be further rearranged into:

$$Y_{IN} = j\omega\left[1 - \frac{A_0}{1 + j\omega\tau}\right]C_{\mathrm{F}} = j\omega\left[C_{\mathrm{F}} - \frac{1}{\dfrac{1 + j\omega\tau}{C_{\mathrm{F}}A_0}}\right] = j\omega C_{\mathrm{F}} + \frac{1}{\dfrac{1}{j\omega(-C_{\mathrm{F}}A_0)} + \left(-\dfrac{\tau}{C_{\mathrm{F}}A_0}\right)}\,. \tag{3.32}$$

Now, it is straightforward to recognize physical interpretation of particular terms in the most outright form as one positive capacitor ($\boldsymbol{C}_{\mathbf{F}}$), one negative capacitor ($-\,\boldsymbol{C}_{\mathbf{F}}\boldsymbol{A}_{\mathbf{0}}/\boldsymbol{\tau}$), and one negative resistor ($-\boldsymbol{C}_{\mathbf{F}}\boldsymbol{A}_{\mathbf{0}}$). They are connected in the way shown in Figure 3-39.

Since all the elements of this equivalent circuit are dispersionless one can use very well known rule of 'positive mesh capacitance' in order to examine stability in an intuitive way. For instance, let us suppose that external network is a simple capacitor C_{E},. It is connected in parallel with C_{F}, their net capacitance is $C_{\mathrm{E}} + C_{\mathrm{F}}$. This combination is connected in series with $-C_{\mathrm{F}}A_0$. Since the net mesh capacitance must be positive for stable operation, one immediately concludes that is external capacitor must obey the inequality $C_{\mathrm{E}} < C_{\mathrm{F}}$.

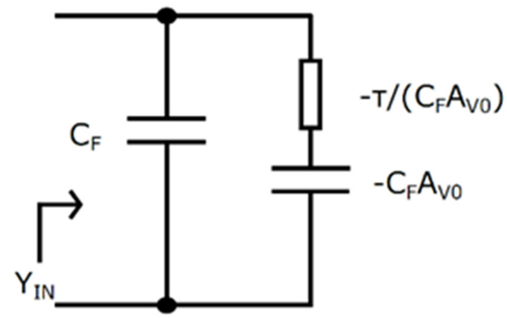

Figure 3-49 Equivalent circuit of SCS negative capacitor based on one-pole Miler NIC

Of course, external network may be so complicated that ‘intuitive’ approach is not so straightforward. In this case, one can set the determinant of Y matrix to zero and apply Hurwitz criterium to find parameters that avoid unstable RHP poles. For instance, one may suppose that there is as additional external resistor C_{E}, connected in parallel to C_{E}. Straightforward calculation yields following stability condition:

$$(R_E > \ 0 \ \&\& \ C_E \geq C_F) \ \cup \ \left(0 < C_E \ < C_F \ \ \&\& \ R_E < \frac{\tau}{C_F - C_E} \right). \tag{3.33}$$

This result is consistent with one from previous section (equation 3.30 and Figure 3-48).

Using explained approach, we have developed equivalent circuits for all SCS and OCS NIC-based elements and they are sketched in.

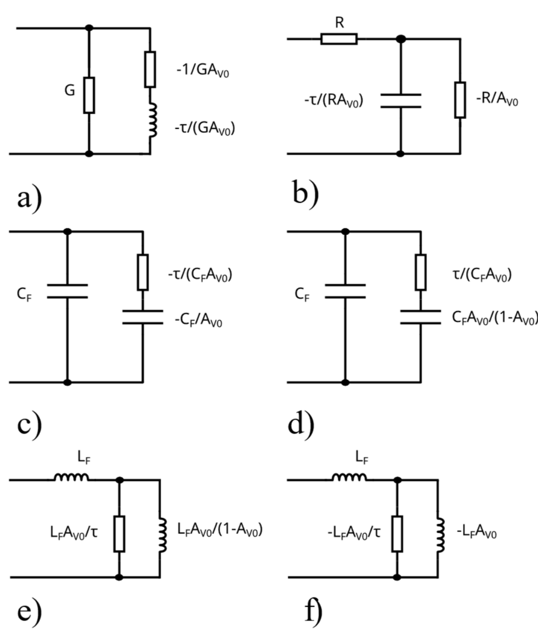

Figure 3-50 Equivalent circuits of various SCS/OCS non-Foster and Negative elements generated using one-pole NICs. (a) SCS negative conductance; (b) OCS negative resistance; (d) SCS negative capacitance; (e) SCS negative inductance; (f) OCS negative inductance

We have extended this approach to SCS negative capacitor based on two-pole NIC [120]. Such a NIC is described by two-pole gain model:

$$A(s) = \frac{A_0}{(1+s\tau_1)(1+s\tau_2)}, \quad \omega_{\mathrm{P1}} = \frac{1}{\tau_1}, \omega_{\mathrm{P2}} = \frac{1}{\tau_2}, \tag{3.34}$$

where time constant τ_2 and angular frequency ω_{P2} describe the second pole. Assuming that load is again capacitor C_{F} and using (3.7), one easily finds equivalent circuit (Figure 3-51) and input admittance (Figure 3-52). It can be seen that the bandwidth of one-pole SCS negative capacitor is slightly narrower than the bandwidth of two-pole SCS negative capacitor. However, it can be also seen that introduction of the second pole causes occurrence of the additional stability area (Figure 3-53). This is very important conclusion which will be further discussed in Chapter 4.

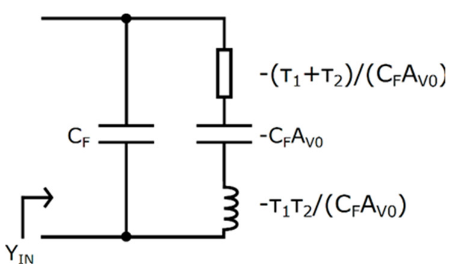

Figure 3-51 (adapted from [120]). Equivalent circuit of SCS negative capacitor based on two-pole NIC.

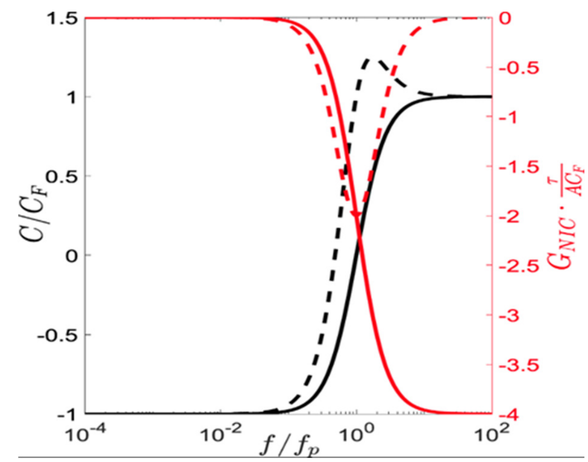

Figure 3-52 (adapted from [120]). Input capacitance (black) and conductance (red) of one-pole (solid) and two-pole (dashed) SCS negative capacitor; (A_0=2, $f_{\mathrm{p2}}/f_{\mathrm{p1}}$ =1.5).

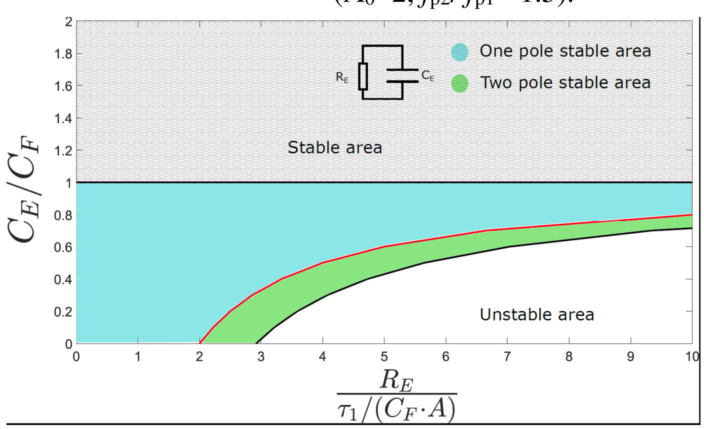

Figure 3-53 (adapted from [120]). Stability map for one-pole and two/pole negative capacitor with external shunt RC network.

Chapter 4. STABILITY IMPROVEMENT–NOVEL BAND-PASS DESIGN OF CLASSICAL NIC AND NII CIRCUITS

Stability improvement–Novel band-pass design of classical NIC and NII circuits

4.1. Comparison of most common NIC and NII circuits

At the present state of the art, the NIC circuits can be realized (in both discrete and microelectronic) BJT and FET technology.

4.1.1. Linvill NIC

Linvill circuit with two cross-coupled transistors [16] is arguably the most popular NIC realization. This circuit is very often analyzed using a simple small-signal equivalent circuit [18] [19] [63], but without emphasizing that is actually direct realization of basic idea from Figure 3-12 that employs two unity-gain current amplifiers. It is shown in Figure 4-1, taken from Schwartz's seminal work on NIC/NII circuits [103].

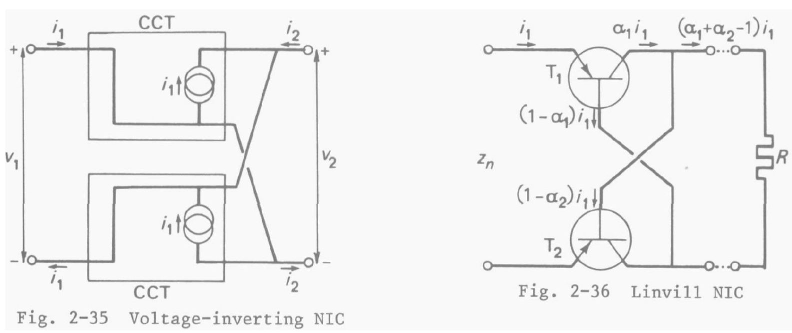

Figure 4-1 (taken from [103]). Direct comparison of differential NIC with two ideal current amplifiers with unity-gain current amplifier and Linvill NIC [16].

Looking at Figure 4-1 it becomes clear that two cross-coupled transistors in Linvill NIC operate as simple CB amplifiers (or, in the case of FET realization, CG amplifiers). If transistors were ideal, they would have unity current gain. These two unity gains add up, yielding the most basic system for negative immittance inversion (Figure 3-11,Figure 3-12).

From practice, it is known that maximal frequency of operation of Linvill NIC is higher than maximal frequency of operation of Miller NIC Figure 3-11. For instance, this was very nicely shown by detailed analysis of realistic FETs in [37]. This can also be explained in a very simple way, without any analysis. Linvill NIC uses CB (or CG) amplifiers, the cut-off frequency of which is approximately β (short-circuit current factor) higher than cut-off frequency of CE (CS) amplifiers used in Miller NIC.

Of course, non-ideality of realistic transistors introduce error in conversion gain and, therefore, 'parasitic' input admittance/impedance. For instance, let us look at very simple case of Linvill OCS negative capacitor with two FETs [43].

An approximate equation for input impedance is given by:

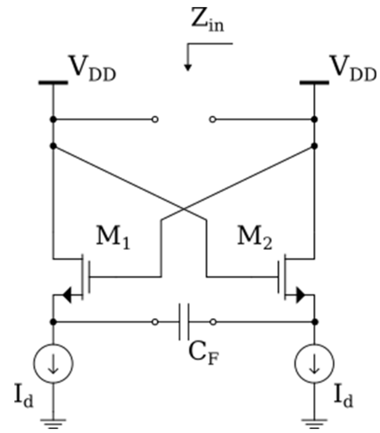

Figure 4-2 (adapted from [43]). A simplified Linvill OCS negative capacitor with two FETs

$$Z_{in} = -\frac{1}{j\omega C}\frac{g_m - j\omega\left(C_{gs} + 2C_F\right)}{g_m} = -\frac{1}{j\omega C} + \frac{\frac{C_{gs}}{C_F} + 2C_F}{g_m}. \tag{4.1}$$

Here, g_{m} is trans-conductance, C_F is load capacitance and C_{gs} stands for the internal capacitance between gate and source electrodes. Assuming $C_{gs} >> C$, (4.1) simplifies to:

$$Z_{in} \approx -\frac{1}{j\omega C} + \frac{2}{g_m}. \tag{4.2}$$

It can be seen that this result is consistent with simplified dispersion analysis in Section 3.2.2.: In OCS circuit, negative capacitance is accompanied with parasitic positive resistance. Equation (4.1) neglects some elements in small-signal FET equivalent circuit and it is valid for frequencies much lower than f_{T}. If this approximation is not valid, the equation becomes more complicated, but again, basic conclusions are consistent with the results from Section 3.2.2. There are many other examples of similar analysis in the literature [33][36][37][63][65][81][108][121][122][123][124][125] and all of them are in qualitative agreement with simplified dispersion analysis in Section 3.2.2.

Since simplified dispersion analysis in Section 3.2.2 and simplified stability analysis in Section 3.4. use the same model, the proposed stability analysis should be valid, as well.

There are many other BJT-based NIC circuits based on original Linvill's design (Figure 3-51 , [110]), which are compared in Table 4-1 Comparison of different designs of NIC with two BJT

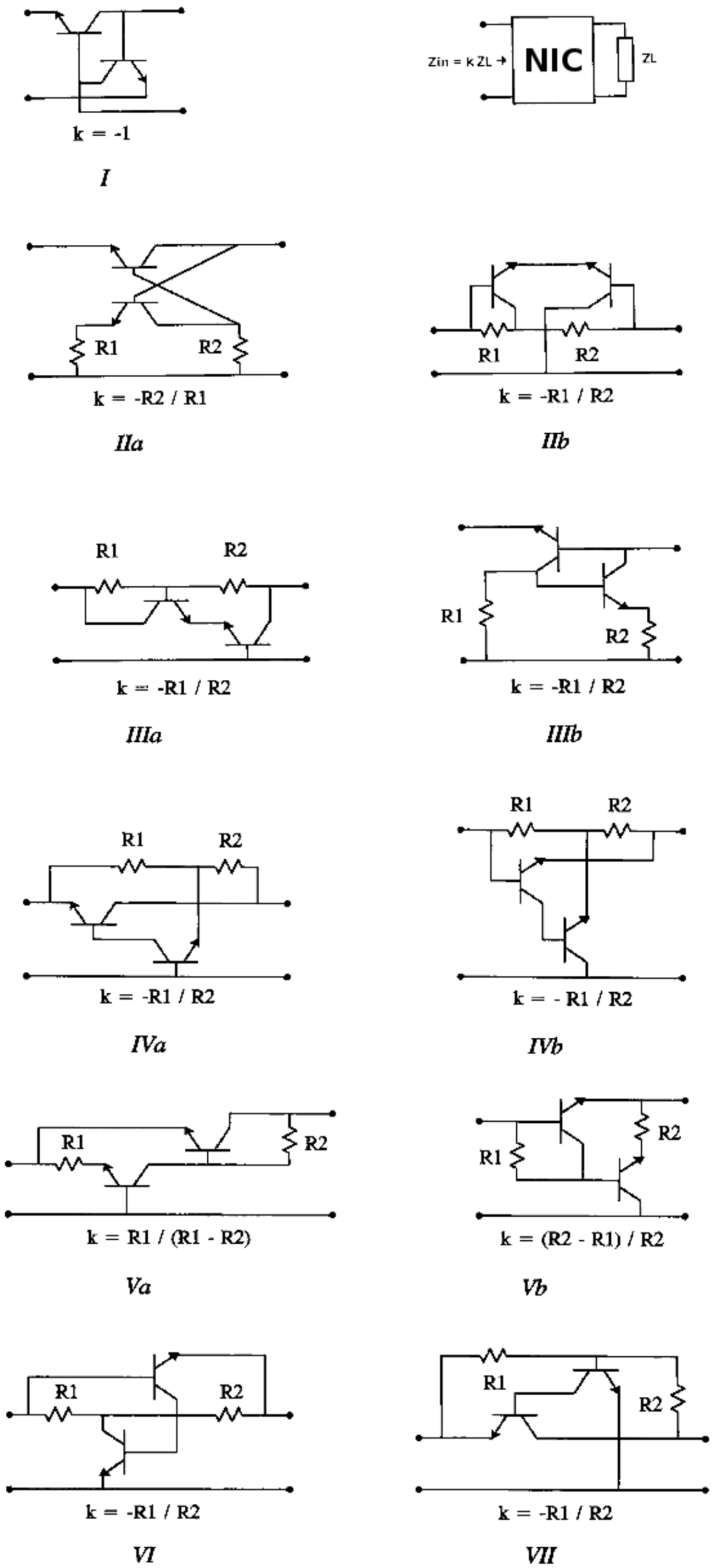

Figure 4-3 Different designs of NIC circuits with two BJTs (taken from [110])

Circuit No.	Author	Year	Equation for conversion factor k (transistors are assumed to have finite transconductance g_m)
I,IIa	Linvill	1953.	IIa: $k=\dfrac{1+g_mR_1-g_m^2R_2R_L}{g_m+g_m^2R_1}$
IIb,IIIa,IV	Myers	1965.	IIb,IIIa: $k=\dfrac{2(R_1+R_2+R_L)-g_mR_1R_L}{2+g_mR_2}$
IIIb	Yanagisawa	1957.	IIIb: $k=\dfrac{1+g_mR_2-g_m^2R_1R_L}{g_m+g_m^2R_2}$
IVa,Va,Vb	Hakim	1965.	Va: $k=\dfrac{2(R_1+R_2+R_L)-g_mR_1R_L}{2+g_mR_2}$ Vb: $k=\dfrac{1+g_m(R_1+R_L)-g_m^2R_1R_L}{2g_m+g_m^2(R_1-R_2)}$
IVb	Larky	1957.	k does not depend on g_m
VII	Nagata	1965.	k does not depend on g_m

Table 4-1 Comparison of different designs of NIC with two BJT (taken from [110])

All the circuits from Table 4-1 would operate equally well if they used the ideal transistors. However, one could expect significant differences in performances of practical realizations. Simulations in [110] revealed that only circuits IVa, IVb, VI and VII (Figure 4-1) do not depend on finite values of transconductance g_m. Of course, it is a consequence of thoughtful selection of negative feedback resistors that assure small conversion error. All other designs require (unrealistic) infinite value of g_m for achieving required conversion factor k.

4.1.3 Kolev-Meunier NII

Two basic NII topologies were analyzed in in Section 3.3.1. However, almost all known designs in practice use topology based on trans-conductance amplifiers (FETs) shown in Figure 3-33. A typical example of this NII is Kolev-Meunier topology [39][110], Figure 4-4.

Input impedance of this circuit is given by:

$$Z_{\text{in}}=\frac{V_1}{I_1}, \tag{4.3}$$

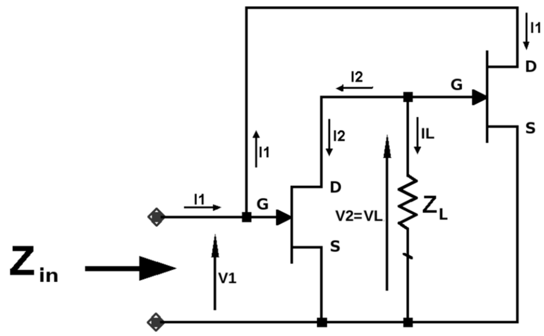

Figure 4-4 Kolev-Meunier NII

while the load impedance reads as:

$$Z_L = \frac{V_L}{I_L} \ . \tag{4.4}$$

The transconductances of the transistors M_1 and M_2 are given by:

$$g_{m1} = \frac{I_2}{V_1}, g_{m2} = \frac{I_1}{V_2} \qquad . \tag{4.5}$$

From (4.4) and (4.5) one gets:

$$Z_{\text{in}} = \frac{V_1}{I_1} = \frac{\frac{I_2}{g_{m2}}}{g_{m2} \cdot V_2} = \frac{1}{g_{m1} g_{m2}} \frac{I_2}{V_2} \tag{4.6}$$

Taking into account that $V_L = V_2$ and the currents I_2 and I_L flow in opposite directions, one finds the relationship between V_2 and I_2:

$$Z_L = \frac{V_L}{I_L} = -\frac{V_2}{I_2} \Rightarrow \frac{I_2}{V_2} = -\frac{1}{Z_L}. \tag{4.7}$$

By insertion of (4.7) into (4.6) one finally derives the expression for the input impedance:

$$Z_{\text{in}} = -\frac{1}{g_{m1} g_{m2} Z_L} \ . \tag{4.8}$$

It can be seen that Kolev-Meunier circuit behaves as an SCS NII. Conversion factor depends on the transconductances of used transistors. This appears to be a significant drawback of the design in discrete implementation because it is difficult to control value of g_m (it depends on I_D). However, in the microelectronic implementation, the transconductance can be controlled by a proper choice of FET dimensions or by active biasing techniques. The latter was used in very interesting implementation of microelectronic tunable negative inductance for operation in UHF range [108].

4.1.4. Other designs

There are also discrete NIC/NII circuits realizations in OPamp technology, which are used at very low frequencies. Nowadays, there are also very-fast OPamps that operate up to the frequency of 6 GHz or even more. Similar devices were used in some prototypes in our previous EOARD projects [27][43][44] and associated Miller NICs were able to operate in very broad frequency range (100 kHz -700 MHz). Clearly, this was a consequence of very carefully designed strong negative feedback that assures almost 'flat' gain, and, in turn, negligible values of parasitic impedance/admittance. It is interesting that there is no attempt of designing some kind of MMIC 'OPamp-like' amplifier in the literature. Such as amplifier would eventually enable construction of Miler NIC with low conversion error, at microwave frequencies. In Section 6.1. we report a first step towards this goal by design and fabrication of Miler negative capacitor in HCBT technology, operating from DC to 2GHz.

Finally, we have conducted a very detailed stability analysis of all above-mentioned BJT NIC circuits (and their FET-based counterparts), as well as the Kolev-Meuniere NII circuit. We found that there is no *a priory* preferred topology. More precisely, the NIC/NII topology should be chosen by taking into account particular type of external network and types of unstable poles (complex poles that cause self-oscillations, DC poles that cause growing exponential DC signal, a pole in the origin that cause DC offset Figure 4-5). It was noted that different NIC topologies yielded different range of external impedances needed for stable operation, but it was not possible to connect this property with particular design parameter.

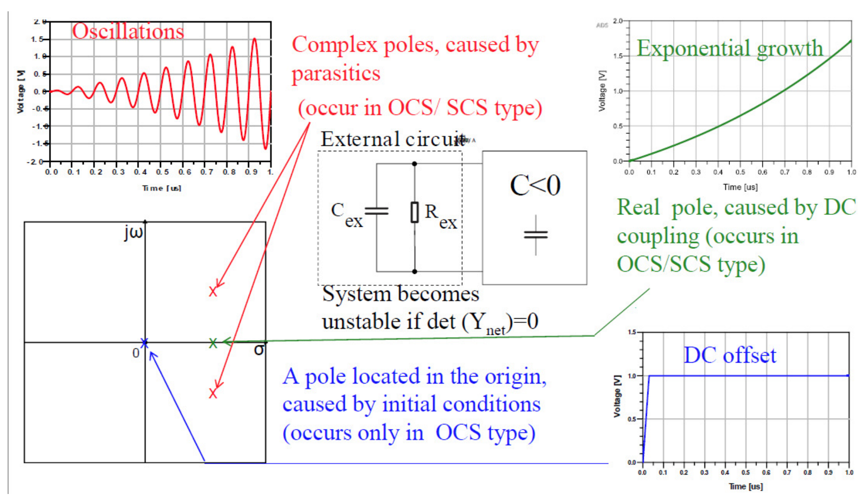

Figure 4-5 Possible types of unstable (RHS) poles that may occur in system that comprises NIC/NII and some external passive network. The graphs have been generated for the case of Miler negative capacitor loaded with external shunt RC network.

4.2. Review of previous research on relation between operating bandwidth and stability

In Section 3.4.4. it was shown that a two-pole model of NIC amplifier extends the range of permissible impedances of the external network, resulting in stable operation. At the same time, introduction of the second pole causes narrowing of operational bandwidth (Figure 3-52). So, it appears that the stability and bandwidth are inevitably connected. It is worth mentioning that the theoretical studies that would support this hypothesis (to the best of Authors' knowledge) are not available in the literature. On the other hand, it also appears that hypothesis on bandwidth-stability dependence is connected to our previous research on band-pass non-Foster capacitor.

Briefly, the main stability problems in negative capacitor occur due to unstable DC pole [43][44][96]. The basic idea of avoiding occurrence of unstable 'DC pole' is to prevent the generation of negative capacitance for ω=0. Thus, the active element should operate in some area of complex frequency plane (s-plane) that does not cover real axis (Figure 4-6). The simplest type of 'safe operation area' is rectangle, or in the real frequency domain, a band-pass transfer function.

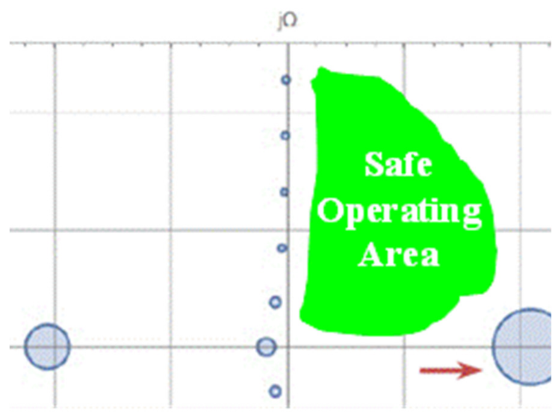

Figure 4-6 General strategy of improving stability properties of NIC/NIV circuits by avoiding potentially unstable areas in complex plane.

So, we decided to introduce NIC/NIV amplifier, a frequency characteristic of which is limited *for both high and low frequencies* (i.e. it is of 'band-pass' type Figure 4-7). More precisely, the gain should be lower than 1 at ω=0.

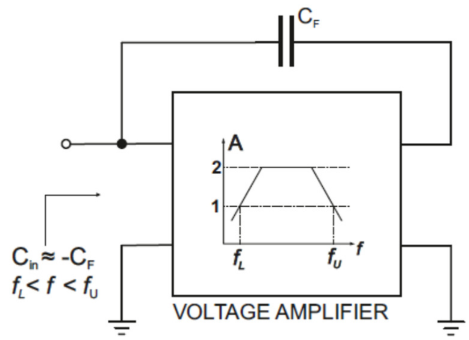

Figure 4-7 (taken from [96]) Implementation of a negative capacitor based on a voltage amplifier, using a 'bandpass' design that prevents occurrence of unstable 'DC pole'

For instance, a band-pass operation can be achieved by implementation of the amplifier transfer function A that has two time constants (τ_1 and τ_2):

$$A = \frac{A_0 s\tau_1}{(1+s\tau_1)(1+s\tau_2)}. \tag{4.9}$$

Here, s stands for a complex frequency (s=σ+jω). A straightforward derivation of input capacitance shows that it is positive for ω=0, preventing the existence of unstable 'DC pole'.

In the first step, the stability of proposed band-pass negative capacitor was investigated analytically. Again, it was assumed that a negative capacitor is shunted by external positive capacitor C_{EXT} and resistor R_{EXT}, and the system poles were sought. The derivation led to a cubic polynomial, the poles of which are enforced to reside in LHP of a complex plane by varying several system parameters. Some obtained results are shown in Figure 4-8 and Figure 4-9.

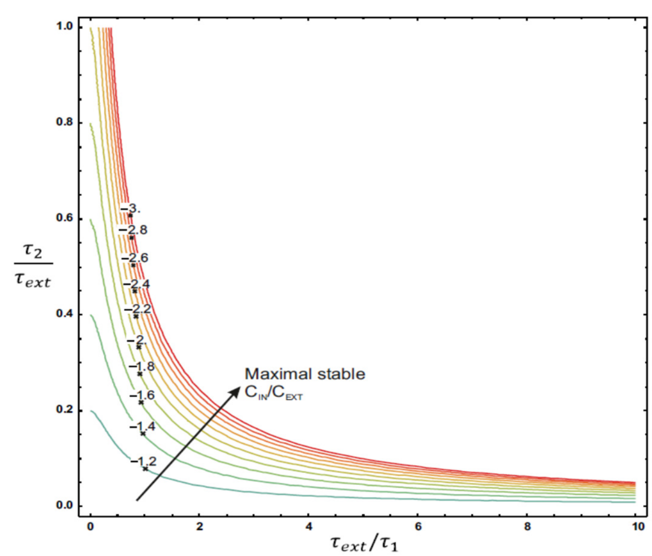

Figure 4-8 (taken from [96]) Bandpass negative capacitor – Contour plot of maximal stable normalized negative capacitance (obtained analytically)

Figure 4-8 depicts a contour plot of maximal normalized negative input capacitance (C_{IN}/C_{EXT}) as a function of both amplifier time constants, normalized to the external time constant:

$$\tau_{ext} = R_{ext}\, C_{ext}. \tag{4.10}$$

There are several important properties that can be deduced from Figure 4-8. Firstly, it is possible to generate a stable overall negative capacitance that (for the given set of parameters) can be as large as -3C_F.. At second, larger values of generated negative capacitance are possible by allowing higher losses in external circuit (i.e. by lowering R_{EXT}). At third, generated negative capacitance is inversely proportional to the amplifier bandwidth B (defined as ω_2/ω_1=τ_1/τ_2, $\omega_1$and ω_2 being lower and upper cut-off frequency, respectively).

The influence of the amplifier bandwidth on maximal generated negative capacitance can be understood in a more details with the help of Figure 4-9. It shows maximal stable normalized negative capacitance as a function of the amplifier bandwidth B, while the parameter τ_2/τ_{ext} is varied. It can be seen that higher values of normalized time constant enable larger absolute value of input negative capacitance. However, the increase of maximal absolute value of generated negative capacitance is accompanied with the decrease of bandwidth.

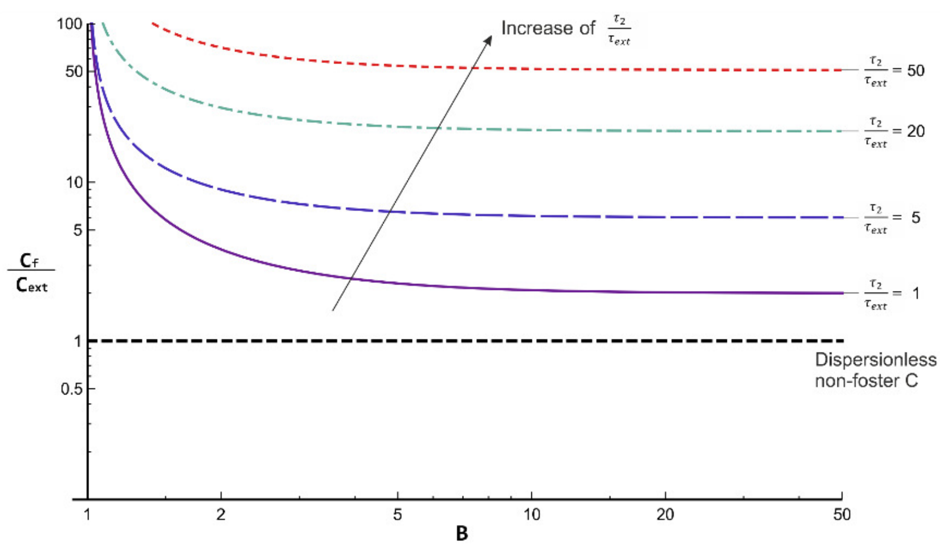

Figure 4-9 (taken from **[96]**) Bandpass negative capacitor - Maximal stable normalized negative capacitance as a function of amplifier bandwidth B with different values of τ_2/τ_{ext}

Study in [96] also reported experimental results in low RF range (100 kHz – 10 MHz) that support above theoretical prediction. The experiment in [96], it was easy to control the bandwidth since the NIC contained two high-speed OPamps and passive filter structure. Such implementation may be challenging in MMIC technology that, almost exclusively uses cross-coupled transistor pair (Linvill NIC).

4.3. Stability improvement of Linvill negative capacitor by band-pass design

Let us briefly comment on frequency characteristic of a simple OCS Linvill NIC with two BJTs (Figure 4-10a)).

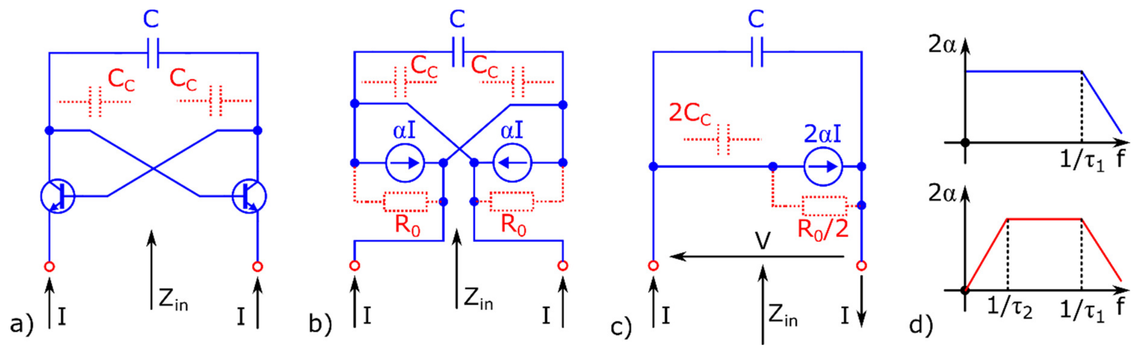

Figure 4-10. OCS negative capacitor based on Linvill's floating NIC
a) Simplified schematic; b) Decomposition into two CB current amplifiers; c) Equivalent single-stage NIC; d) Dispersion of one-pole (upper) and two-pole (lower) current amplifier model; Idealized NIC is shown in blue color, while additional elements that appear in real-word implementation, are given in red.

As already discussed in Section 3.5.1., the NIC system can be further decomposed into two ideal, zero-input-impedance current amplifiers with gain function α_0 (common base circuits) Figure 4-10b). This allows 'folding' into an equivalent single-stage amplifier with double gain ($2\alpha_0$) (Figure 4-10c), whose input impedance is given by:

$$Z_{in} = \frac{1}{sC}(1 - 2\alpha_0). \tag{4.11}$$

In the case of ideal dispersionless transistors (α_0=1), (4.1.1.) shows that a load capacitor C is converted into its 'negative image' ($-C$), as discussed before.

Let us now try to take into account the most pronounced NIC's non-idealities (final reactance of coupling capacitors (C_c) and finite output resistance (R_g) of the controlled current source, shown by red elements in Fig. 1). Looking at the 'folded' circuit input terminal one finds that C_c and R act as shunt elements of the controlled current source. They introduce a second time constant (τ_2), and therefore, the second pole into the transfer characteristic (lower part of Figure 4-10), which now reads as:

$$\alpha = \frac{\alpha_0 s \tau_2}{(1 + s\tau_1)(1 + s\tau_2)}, \tau_1 = \frac{1}{2\pi f_1}, \tau_2 = RC_c = \frac{1}{2\pi f_2}. \tag{4.12}$$

Obviously, the transfer functions (4.12) and (4.9) are identical. Therefore, the graphs in Figure 4-8 and Figure 4-9 are also valid for Linvill OCS NIC whose cross-coupling capacitors have finite values. Thus, we again conducted a stability analysis for generic ideal and non-ideal transistors and computed a range of allowable external loads (shunt RC combination) needed for stable operation. All these results (not shown here for the sake of clarity) show that narrower operating bandwidth of the NIC enables wider range of permissible external loads (this finding is similar to simulations presented in [110]). This is a very important conclusion that allows finding a compromise between stability and NIC operating bandwidth in practical implementations. Surprisingly, it appears that this possibility has not been employed so far. We use this strategy in design examples in Chapter 5 and Chapter 6.

As a by-product of above discussion we tried to develop equivalent circuit of OCS two-pole negative capacitor. To this end, we conducted methodology outlined in Section 3.4.4. Developed impedance function leads to some 'strange' element with $-Bs^2$) dispersion function (B being a constant). We have recognized similarity between this form and the form of the three-capacitor non-Foster *K* inverter [107], which leads to equivalent circuit in Figure 4-11.

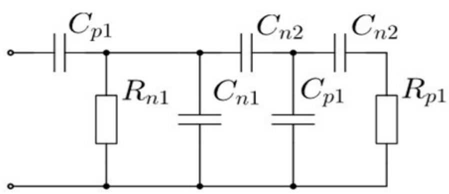

R_{p1}	$\frac{\tau_2}{2\alpha_0 C}$
R_{n1}	$-\frac{2\alpha_0\tau_1}{C}$
C_{p1}	C
C_{n1}	$-\frac{(\tau_1+\tau_2)C}{2\alpha_0\tau_1}$
C_{n2}	$-C$

Figure 4-11. (adapted from [107]). Equivalent circuit of 2-pole band-pass OCS negative capacitor

Chapter 5. STABILITY IMPROVEMENT – NOVEL DESIGN BASED ON COMPENSATED PASSIVE NETWORKS

Stability improvement – novel design based on compensated passive networks

In Chapter 2, it was mentioned that there are so-called unilateral non-Foster designs based on compensated lossy networks with anomalous dispersion [72][73]. In addition, there has been a theoretical proposal for bandpass non-Foster elements that were claimed to be absolutely stable [102]. These elements are similar in some sense to the bandpass non-Foster capacitors proposed in our earlier EOARD/AFRL-funded projects [27][43]. However, there is no clear physical connection between these two approaches. Intuitively, one might expect that the presence of resistive components (even if their losses are compensated by additional negative resistance/conductance) would improve stability properties. Therefore, we decided to study passive networks that exhibit dispersion similar to ordinary non-Foster behavior, but with inevitable losses. In Chapter 5, we show that based on the above idea, it is possible to design a non-Foster element with a range of allowable external impedances (admittances) larger than the circuits available in the literature.

5.1 Low-pass negative inductance

5.1.1. Passive RC network that emulates negative inductance – basic idea

Let us analyze the input admittance of the simple parallel combination of capacitance C_P and resistance R_P (Figure 5-1a). In the Laplace domain, this admittance reads:

$$Y_{in,RC}(s) = \frac{1}{\mathrm{R_P}} + sC_P, \tag{5.1}$$

where $s = \sigma + j\omega$ is complex frequency.

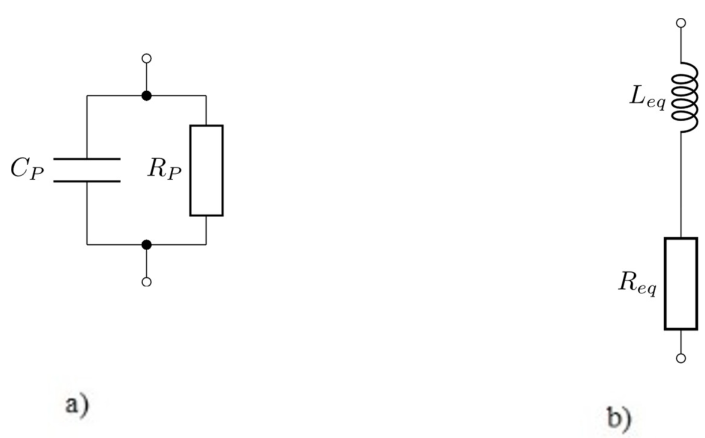

Figure 5-1 Schematic of parallel RC network (a) and its equivalent Z_{IN} **ω**(jω) representation in jω domain (b)

By setting $s = j\omega$ we can examine the behavior of the circuit from (Figure 5-1 a) in the frequency domain ($j\omega$). Input impedance is then given by the following expression:

$$Z_{in,RC}(j\omega) = \frac{1}{Y_{in}(s = j\omega)} = R_P \frac{1}{\left(\frac{\omega}{\omega_{rc}}\right)^2 + 1} - jR_P \frac{\frac{\omega}{\omega_{rc}}}{\left(\frac{\omega}{\omega_{rc}}\right)^2 + 1}, \tag{5.2}$$

where $\omega_{rc} = \frac{1}{R_P C_P}$ is circuit's cut-off frequency ('resonant' frequency).

Quick analysis of input impedance below the resonant frequency (ω_{rc}) simplifies (5.2) to:

$$Z_{in,RC}(j\omega) = Z_{in}(j\omega)|_{\omega \ll \omega_{rc}} \approx R_{\mathrm{p}} - jR_P \frac{\omega}{\omega_{rc}} = R_p + \mathrm{L_{eq0}}\omega. \tag{5.3}$$

From (5.3) we conclude that circuit behaves as series combination of positive resistance R_P and equivalent negative inductance $L_{eq0} = -R_P/\omega_{rc}$ (Figure 5-1b). To further analyze behavior of the circuit, we have plotted input impedance (5.2.) as a function of frequency normalized to resonant frequency (ω_{rc}) (Figure 5-2a). We can immediately distinguish two regions, one located below the resonant frequency ① and other one located above resonant frequency ②. In the region ① we can observe negative slope of the imaginary part (blue curve) of the input impedance, indicating non-Foster-like behavior. Strictly speaking, this is not a non-Foster circuit, since losses are present.

To further investigate this interesting behavior, we have calculated equivalent input inductance as $L_{eq}(j\omega) = \Im\{Z_{in}(j\omega)\}/\omega$, which is valid only in region ①. Equivalent inductance $L_{eq}(j\omega)$ and resistance $R_{eq}(j\omega) = \Re\{Z_{in}(j\omega)\}$ are plotted in Figure 5-2b. We see that value of $L_{eq}(j\omega)$ approaches $L_{eq0} = -R_P/\omega_{rc}$ as ω approaches 0. Furthermore, we see that value of equivalent negative inductance is accompanied by substantial loss determined by value of resistor R_P. Accompanying losses severely impact quality factor (Figure 5-2c) of the negative inductance and some loss compensation is needed.

a)

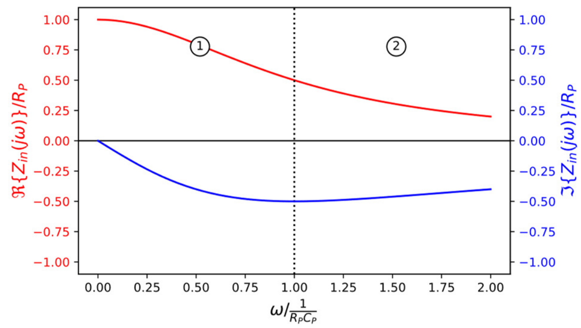

b)

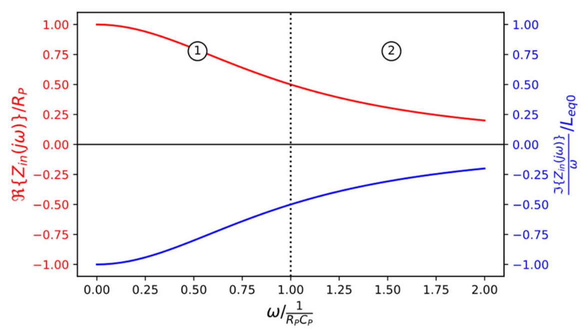

c)

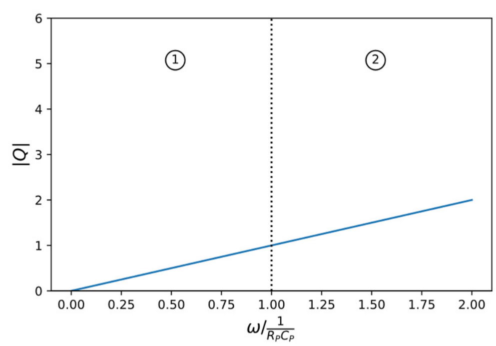

Figure 5-2 Real and imaginary part of input impedance of parallel C_P and R_P (a). Equivalent resistance and negative inductance (b). Quality factor Q of the circuit (c)

5.1.2. Passive RC network that emulates negative inductance – loss compensation

In order to compensate losses and increase the quality factor, the circuit was loaded with OCS NIC (Figure 5-3) with feedback resistance R_F . The NIC input impedance is given by:

$$Z_{in,NIC}(s) = R_F\left(1 - \frac{A_0}{1 + s\tau}\right) = R_F \cdot \frac{\frac{s}{\omega_{pu}} + \kappa}{\frac{s}{\omega_{pu}} + 1}, \tag{5.4.}$$

where $\kappa = 1 - A_0$ determines DC conversion factor of low-pass NIC and $\omega_{pu} = \frac{1}{\tau}$ is the upper pole of the OCS NIC conversion characteristics [103]. It should be noted that, for the sake of simplicity, we will take $A_0 = 2$ and subsequently $\kappa = -1$ (as it was already described in Section 3.2). Input impedance (Z_{in}) in $j\omega$ domain is obtained by setting $s = j\omega$ into (5.4), which yields:

$$Z_{in,NIC}(j\omega) = R_F \frac{-1 + \left(\frac{\omega}{\omega_{pu}}\right)^2}{1 + \left(\frac{\omega}{\omega_{pu}}\right)^2} + j2R_F \frac{\frac{\omega}{\omega_{pu}}}{1 + \left(\frac{\omega}{\omega_{pu}}\right)^2}. \tag{5.5.}$$

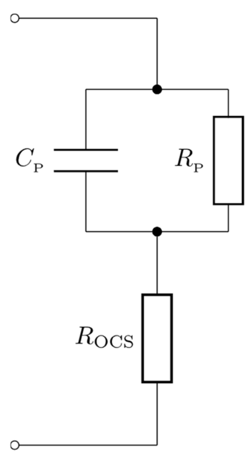

Figure 5-3 Schematic of parallel RC network compensated by OCS negative resistance.

Analysis of $Z_{in,NIC}(j\omega)$ (5.5.) below the pole frequency ω_{pu} shows that NIC input impedance behaves as a series connection of negative resistance $-R_F$ and equivalent positive inductance $L_{p,NIC}$:

$$Z_{in,NIC}(j\omega)\big|_{\omega \ll \omega_{pu}} \approx -R_F + j\frac{2R_F}{\omega_{pu}}\omega. = -\mathrm{R_F} + \mathrm{jL_{p,NIC}}\omega. \tag{5.6.}$$

This positive inductance $L_{p,NIC}$ can 'swamp' value of negative inductance generated by a circuit we wish to compensate. This would deteriorate properties of negative inductance. Therefore, great care should be taken in choosing NIC parameters. The parameters of entire network can be deduced by combining our knowledge of the RC circuit behavior below resonant frequency (5.3) and behavior of the OCS NIC circuit below pole frequency (5.6). After simple derivation, one finds a value of compensated (net) impedance:

$$\begin{aligned} Z_{in,com}(j\omega)\big|_{\substack{\omega \ll \omega_{pu},\\ \omega \ll \omega_{rc}}} &\approx R_P - R_F + j\left(-\frac{R_P}{\omega_{rc}} + \frac{2R_F}{\omega_{pu}}\right)\omega \\ &= \mathrm{R_P}(1-\alpha) + jL_{eq0}\left(-1+\frac{2\alpha}{\beta}\right)\omega, \end{aligned} \tag{5.7.}$$

where $\alpha = R_F/R_P$, $L_{eq0} = R_P/\omega_{rc}$, $\beta = \omega_{pu}/\omega_{rc}$. It can be shown that $\alpha \approx 1$ and $\beta \gg \alpha$, which simplifies (5.7) to $Z_{in,com}(j\omega) \approx -jL_{eq}\omega$. Therefore, for perfect cancelation, a value of negative resistance generated by NIC should be equal to the value of positive resistance R_P. Furthermore, NIC pole frequency (ω_{pu}) should be 'high enough'. This is needed in order to obtain negligible value of parasitic positive inductance generated by the NIC itself. Total input impedance in $j\omega$ domain of the compensated circuit is found by combining 5.2 and 5.5, which yields:

$$\begin{aligned} Z_{in,com}(j\omega) &= Z_{in,RC} + Z_{in,NIC} \\ &= R_P\left[\frac{1}{\left(\frac{\omega}{\omega_{rc}}\right)^2 + 1} + \alpha\frac{-1+\left(\frac{\omega}{\beta\omega_{rc}}\right)^2}{1+\left(\frac{\omega}{\beta\omega_{rc}}\right)^2}\right] \\ &\quad + jR_P\left[-\frac{\frac{\omega}{\omega_{rc}}}{\left(\frac{\omega}{\omega_{rc}}\right)^2+1} + 2\alpha\frac{\frac{\omega}{\beta\omega_{rc}}}{1+\left(\frac{\omega}{\beta\omega_{rc}}\right)^2}\right]. \end{aligned} \tag{5.8}$$

Input impedance (5.8.) is plotted as a function of frequency (Figure 5-4a) with parameters $\alpha = R_F/R_P = 1$ and $\beta = \omega_{pu}/\omega_{rc} = 200$. Figure 5-4a shows that, with selected design parameters, the input parasitic resistance is almost completely canceled at low frequencies. This is also confirmed by high quality factor ((Figure 5-4c). Furthermore, the slope of imaginary part of input impedance in region ① (blue line in (Figure 5-4 a)) is still negative, confirming non-Foster behavior. Equivalent inductance was also calculated (as in the previous uncompensated case) as $L_{eq}(j\omega) = \Im\{Z_{in}(j\omega)\}/\omega$,and normalized to value $L_{eq0} = R_P/\omega_{rc}$ ((Figure 5-4b).

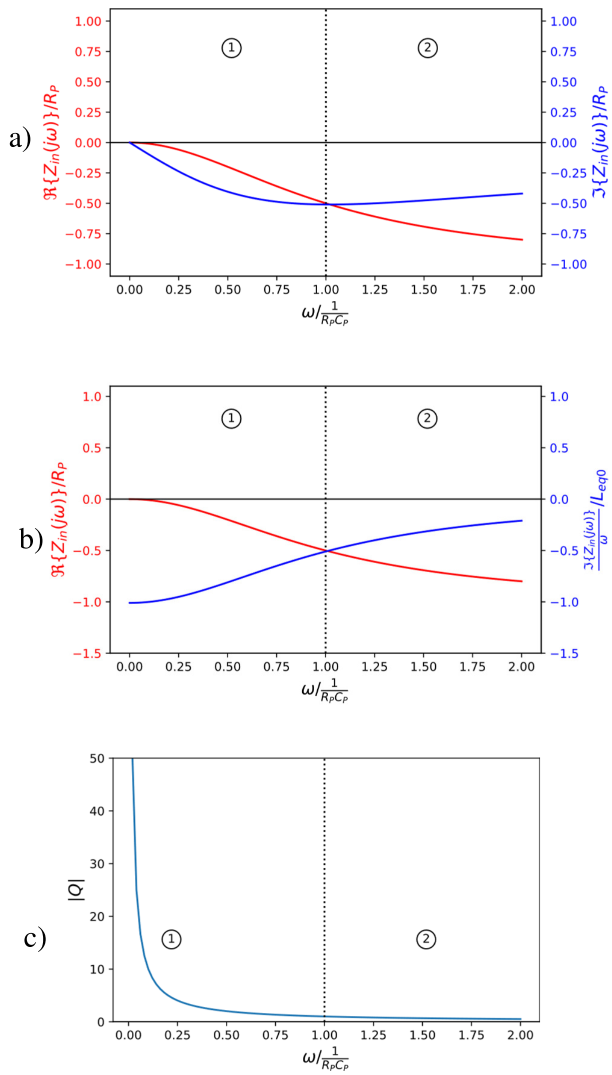

Figure 5-4 (a) Real and imaginary part of input impedance of parallel C_P and R_P **c**ompensated by OCS negative resistance. (b) Equivalent resistance and negative inductance. (c) Quality factor Q of the circuit. Plots are obtained with $A = R_F/R_P = 1$ and $\beta = \omega_{pu}/\omega_{rc} = 200$

5.1.3. Passive RC network that emulates negative inductance – stability analysis

To test the stability of the compensated structure, we have loaded it with external passive network that simulates realistic scenario in common applications such as matching of a small loop antenna. External network comprises positive compensating inductance L_L , and it is excited by voltage generator with internal impedance R_g ,as shown in Figure 5-5a.

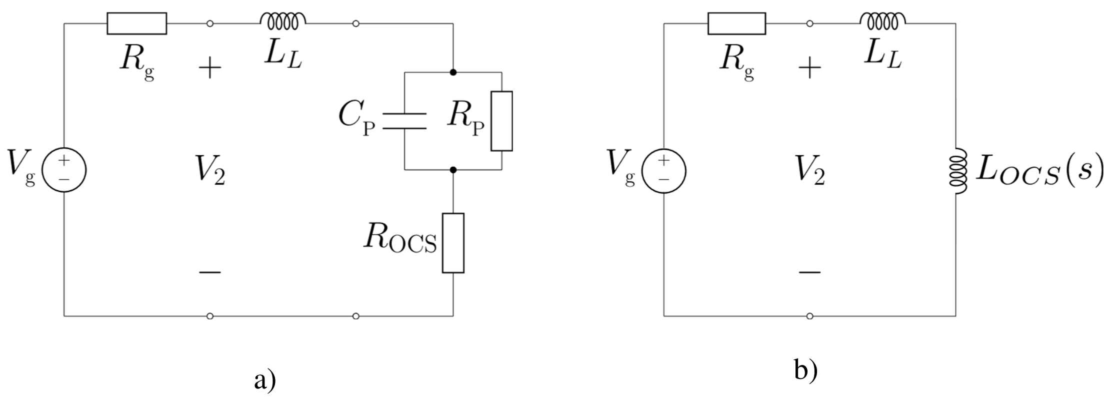

Figure 5-5 (a)Stability testing schematics for novel compensated RC network loaded with external network. (b)Stability testing schematic for 'classic' negative inductance constructed based on OCS NIC.

Transfer function of such a circuit can be written as:

$$H_V(s) = \frac{V_2}{V_g} = \frac{Z_{in}}{Z_{in} + R_g} = \frac{N(s)}{D(s)}. \tag{5.9.}$$

The characteristic equation governing the stability of the system is given by denominator $D(s)$ of (5.9.):

$$\begin{aligned} s^3 C_P L_L R_P \tau_u + s^2\left(C_P L_L R_P + C_P R_F R_P \tau_u + C_P R_P R_g \tau_u + L_L \tau_u\right) \\ + s\left(-C_P R_F R_P + C_P R_P R_g + L_L + R_F \tau_u + R_P \tau_u + R_g \tau_u\right) - R_F \\ + R_P + R_g \end{aligned} \tag{5.10.}$$

Poles of the system are given by solving (5.10.). As it is well known, any linear time-invariant system is stable if all the poles lie in the Left-Hand Side (LHS) of the complex plane [83][84][85]. In that case, associated transfer function (5.9) does not diverge. Since 5.10. is a cubic polynomial, obtaining analytical solution is possible but impractical. Thus, we have decided to use Routh-Hurwitz stability criterion that predicts stability of the system without solving characteristic equation. Routh-Hurwitz stability criterion for third order polynomial ($a_3\, s^3 + a_2\, s^2 + a_1\, s + a_0 = 0$) states:

$$a_0 > 0 \wedge a_1 > 0 \wedge a_2 > 0 \wedge a_3 > 0 \wedge a_1 a_2 - a_0 a_3 > 0. \tag{5.11.}$$

With assumption that values of all elements are positive and real, and then applying (5.11.) to (5.10.), one gets stability conditions:

$$\beta(1+\beta) + (1+\alpha+2\alpha\beta-\alpha\beta^2)\gamma + (\alpha+\alpha^2-\alpha^2\beta)\gamma^2 + (1+\beta)^2\gamma\delta + (1+2\alpha)\gamma^2\delta + (1+\beta)\gamma^2\delta^2 > 0 \ \wedge \delta > \alpha - 1, \tag{5.12.}$$

where $\alpha = R_F/R_P$, $\beta = \omega_{pu}/\omega_{rc}$, $\gamma = L_{eq}/L_L$, $\delta = R_g/R_P$. Here, α and β describe the behavior of compensated RC network and parameters γ and δ describe ratio of some parameters of external network and compensated network. Using (5.12.) we calculated stability area of the circuit with parameters which ensures maximum of quality factor ($\alpha = R_F/R_P = 1$ and $\beta = \omega_{pu}/\omega_{rc} = 200$) (Figure 5-4).

Stability properties can easily be interpreted from ‘stability map shown in Figure 5-6.

Let us compare stability condition (5.12.) to the one derived for network shown in Figure 5-5b. (a ‘classical’ one-pole OCS NIC loaded with positive inductance L_F). Stability condition of network in Figure 5-5b has a very simple form [44]:

$$|-L_F| < \frac{R_g}{\omega_{pu}} + L_L. \tag{5.13.}$$

Equation (5.13.) shows that it is possible to achieve overall negative inductance, but a factor R_g/ω_{pu} (which can be interpreted as equivalent 'internal' NIC inductance) limits the range of achievable negative inductances. For example, if we take $R_g = 50\ \Omega$ and NIC pole frequency $f_{pole} = 100\ GHz$, R_g/ω_{pu} has value of 79.57 pH which we can consider negligible for loading inductances (L_F) in order of nH, which are common in microwave regime. In this case, (5.13) reduces to $|-L_F| < L_L$. This is well-known criterion, which simply says that overall inductance is positive. On the contrary, in new design, total (net) inductance can be negative ($\frac{L_{eq}}{L_L} > 1$) for very broad range of normalized parameters of external passive network (Figure 5-6), which is impossible in classical design. So, from the stability point of view, presented novel design is significantly better than standard one-pole NIC designs from the literature.

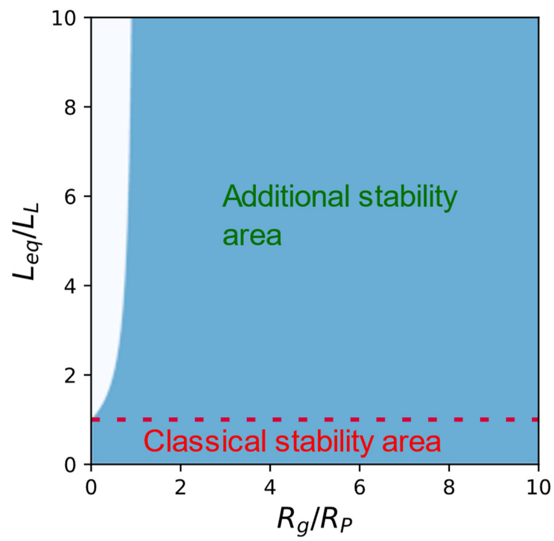

Figure 5-6 Stability area plot of compensated RC network loaded with positive inductance. Plot is generated with A = R_F/R_P = 1 and β= ω_{pu}/ω_{rc} = 200 Dark blue – range of normalized external impedances that cause stable operation; Light blue - range of normalized external impedances that cause unstable operation. Please note that in standard negative inductor based on one-pole NIC, maximal stability area would be bounded by L_{eq}/L_L<1

5.1.4. Passive RC network that emulates negative inductance – design example

The operation of proposed negative inductance was verified by design of negative inductance in 40 nm TSMC CMOS technology, with the help of Cadence Virtuoso™ [104], ADS™ [105], and STAN™ [106] software design tools. First, we have designed Linvill NIC (Figure 5-8), that should generate compensating negative resistance for RC passive network (analogous to R_{OCS} in basic circuit in Figure 5-3). Dimensions of both transistors ($W = 2\ \mu m \cdot 32 = 64\ \mu m, L = 40\ nm$) where optimized to achieve high values of transistor transconductance ($g_m = 30\ mS$) and transit frequency (f_T=125 GHz).

Designed Linvill NIC was configured to work in OCS configuration (the load comprising series combination of resistor R_F and inductor L_F) The inductance L_F is added to compensate for the NIC parasitic input inductance, as predicted in previous section (5.1.6). It was expected that this modification would increase the operating bandwidth of the compensated RC structure. Shunt RC structure was then loaded in series with OCS negative resistance (Figure 5-7).

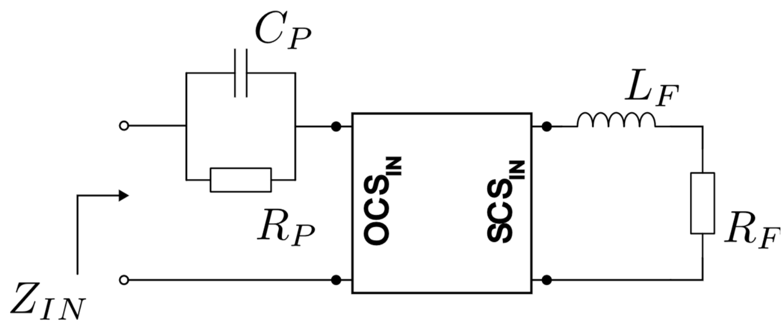

Figure 5-7 Compensated RC structure loaded with OCS negative resistance (based on Linvill NIC from **Figure 5-8**)

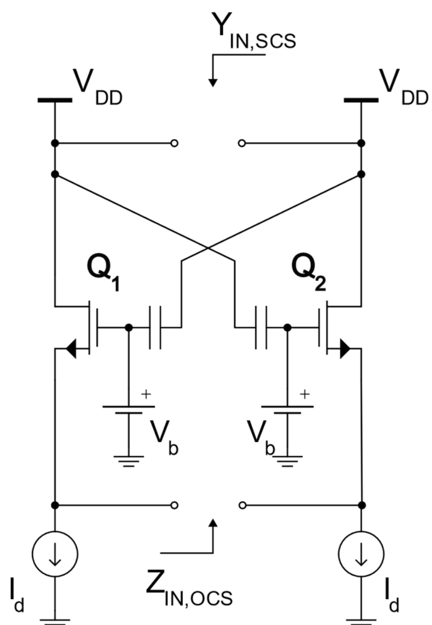

Figure 5-8 Linvill NIC used as compensating negative resistance of proposed negative inductor (designed in 40 nm CMOS technology; Q1 = Q2, W = 32 · 2 µm = 64 µm, L = 40 nm. (Gate bias networks are omitted for clarity).

The elements values were tuned to achieve generation of designed negative inductance in L band (1-2 GHz) (Figure 5-9) ($R_P = 303\ \Omega, C_P = 105\ fF, R_F = 405\ \Omega, L_F = 1.8\ nH$). It can be seen that value of R_F is larger than value predicted by theoretical analysis. This is caused by finite 'parasitic' resistance of NIC circuit, which was not taken into account in approximative analytical approach. This larger value of R_F increases the value of input parasitic inductance $\left(L_{par} = \frac{2R_F}{\omega_{pu}}\right)$ that can 'swamp' the value of negative equivalent inductance. Therefore, the series compensating inductance L_F is needed. After several optimization cycles, we were able to achieve value of equivalent negative inductance of -5 nH (Figure 5-9b) with negligible parasitic resistance as indicated by good Q factor across entire L band ((Figure 5-9c)

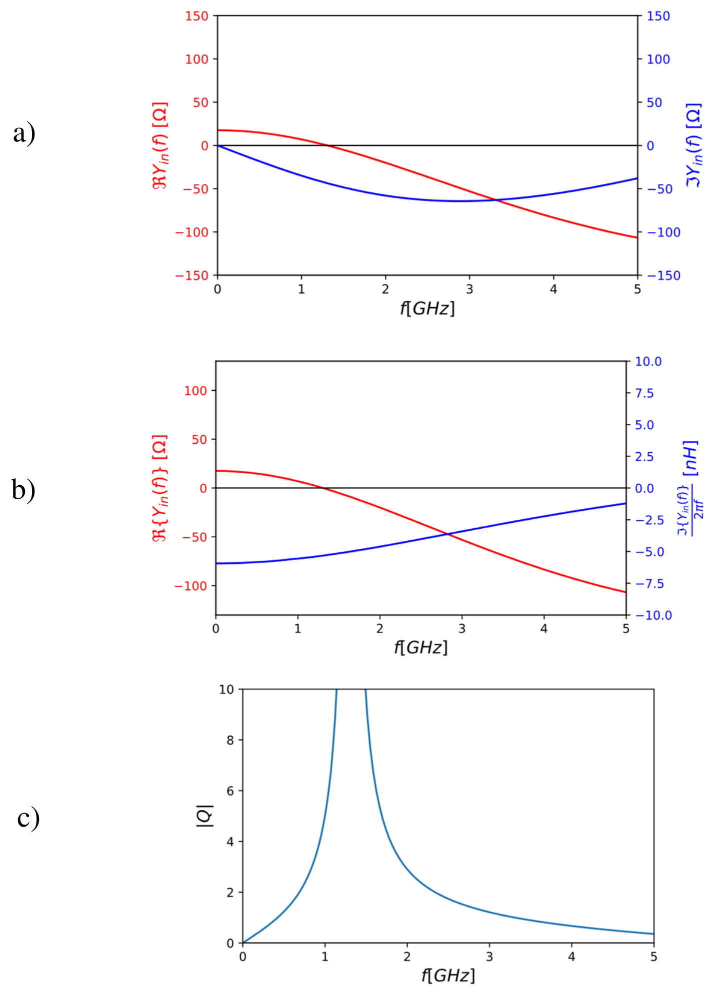

Figure 5-9 Real and imaginary part of input impedance of parallel C_P and R_P compensated by OCS negative resistance (a). Equivalent resistance and negative inductance (b). Quality factor Q of the circuit. Plots are obtained with $R_P = 303\ \Omega$, $C_P = 105$ fF, $R_F = 405\ \Omega$, $L_F = 1.8$ nH

In the next step, we check the stability of the designed negative inductance. To this end, we loaded the compensated structure with external passive network, following the methodology from chapter 5.1.3. The circuit was then excited with AC voltage generator in the frequency range from 1 MHz to 300 GHz and values of external network (L_L and R_g) were varied across 1:10 range. Signals V_g and V_2 were monitored and associated transfer function $H = V_2/V_g$ was calculated at each frequency using ADS™. This data was imported in commercial system identification software STAN™. STAN™ uses magnitude and phase of transfer function obtained by AC simulation and construct the transfer function in the Laplace domain by polynomial fitting. Obtained transfer function is then used to calculate the location of poles and zeros (pole-zero identification), that can be used for prediction of stability properties of the given circuit. Furthermore, STAN, along with poles and zeros of the transfer function, outputs the confidence factor (ρ) for each pole. The result of the multiple simulations is plotted in Figure 5-10 and overlayed above the results of simplified theoretical prediction given in Chapter 5.1.3. Each dot is a result of vector fitting of AC analysis simulation results. If all of the resulting poles of the fitted transfer function (for one particular set of external network parameters) are stable the dot is painted green, if any of the poles are unstable the dot is painted yellow, orange or red (depending on the confidence factor). Red and orange dots are good prediction of unstable behavior while yellow dots are likely caused by numerical errors and need further investigation with AC analysis with larger number of frequency points.

For this particular case, STAN™ gave the results which are in excellent agreement with simplified analytic prediction of stability. We assume that slight shift in the boundary between stable and unstable areas is caused by parasitic elements present in the realistic model of designed NIC.

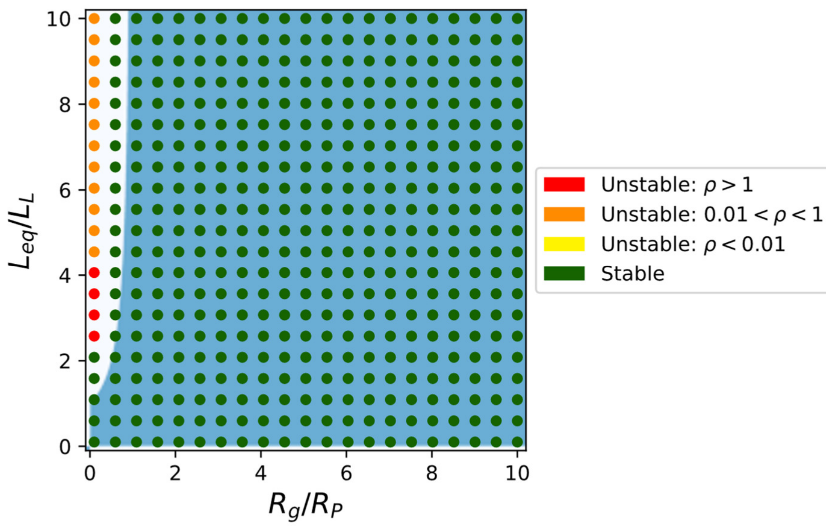

Figure 5-10 Stability area plot of compensated RC network loaded with positive inductance. Plot is generated with R_P = 303 Ω, C_P = 105 fF, R_F = 405 Ω, L_F = 1.8 nH**.** Painted areas are calculated using simplified analytical approach (Dark blue – range of external impedances that cause stable operation; Light blue - range of external impedances that cause unstable operation). Colored dots are results predicted by commercial system identification software tool STAN™.

It can be concluded that the stability properties of the proposed negative inductor, based on a compensated passive RC network, are indeed significantly better than the stability properties of all designs from the current literature. In addition, simplified analytical method of stability prediction gives very good results that can be used for subsequent numerical optimization.

5.2 Low-pass negative capacitance

5.2.1. Passive RL network that emulates negative capacitance – basic idea

In this section, we analyze passive network which is a dual of shunt RC network from Figure 5-1. The new network (Figure 5-11a) comprises simple series combination of inductance L_P and resistance R_P, and its input impedance in the Laplace domain reads:

$$Z_{in,RL}(s) = \mathrm{R_P} + sL_P, \tag{5.14}$$

where $s = \sigma + j\omega$ is complex frequency.

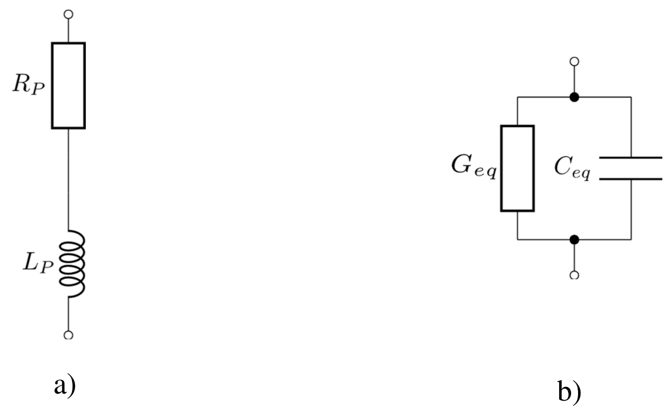

Figure 5-11 Schematic of series R_L network (a) and its equivalent $Y_{in}(j\omega)$ representation in jω domain (b)

The input admittance in the steady-state frequency domain ($s = j\omega$) is given by:

$$Y_{in,RL}(j\omega) = \frac{1}{Z_{in}(j\omega)} = G_P \frac{1}{\left(\frac{\omega}{\omega_{rl}}\right)^2 + 1} - jG_P \frac{\frac{\omega}{\omega_{rc}}}{\left(\frac{\omega}{\omega_{rl}}\right)^2 + 1}, \tag{5.15}$$

where $\omega_{rl} = \frac{R_P}{L_P}$ is circuit cut-off frequency ('resonant' frequency) and $G_P = \frac{1}{R_P}$ is conductance. We can now study the behavior of the circuit input admittance below the resonant frequency (ω_{rl}):

$$Y_{in,RL}(j\omega) = Y_{in}(j\omega)|_{\omega \ll \omega_{rl}} \approx G_P - j\frac{\mathrm{G_P}}{\omega_{rl}}\omega = R_p + \mathrm{C_{eq0}}\omega. \tag{5.16}$$

From (5.16) we conclude that circuit behaves as series combination of positive resistance R_P and equivalent negative capacitance $C_{eq0} = -G_P/\omega_{rl}$ (Figure 5-12b). To analyze behavior of this circuit, we have plotted input admittance (5.15) as a function of frequency normalized to resonant frequency ω_{rl} (Figure 5-12a). Analogous to the previous case (Section 5.1) we find negative slope of the imaginary part of input admittance $Y_{in,RL}$, below the resonant frequency ω_{rl} (region 1). This is non-Foster like behavior that can be interpreted as a negative capacitance. Value of equivalent capacitance is calculated as $C_{eq} = \Im\{Y_{in,RL}\}/\omega$ while parasitic conductance is taken as $G_{eq} = \Re\{Y_{in,RL}\}$ (Figure 5-12b). Again, we note that calculated equivalent capacitance is valid only below the resonant frequency, where the negative slope of imaginary part of input admittance is present. In addition, non-Foster negative capacitance is accompanied by losses governed by value of positive conductance G_P. Inherent loss of this circuit severely impacts the value of quality factor Q (Figure 5-12c), and some compensation is needed.

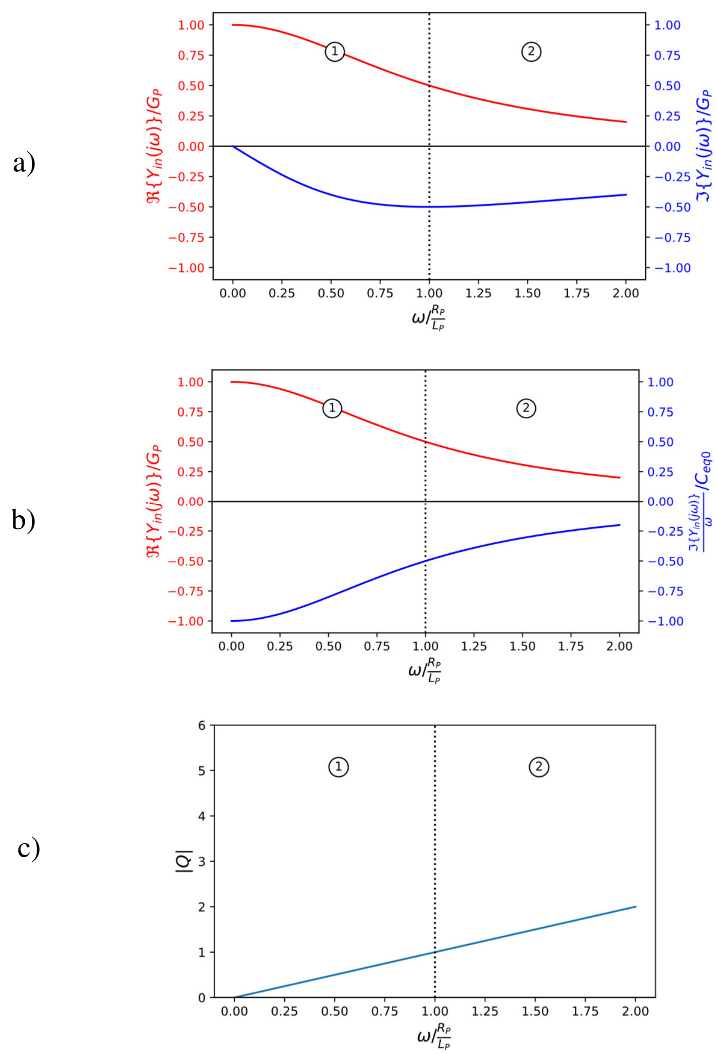

Figure 5-12 (a) Real and imaginary part of input impedance of series L_P and R_P. (b) Equivalent conductance and negative capacitance. (c) Quality factor Q of the circuit.

5.2.2. Passive RL network that emulates negative capacitance – loss compensation

In order to compensate losses and increase the quality factor the circuit was loaded with SCS NIC (Figure 5-13) with feedback conductance G_F .

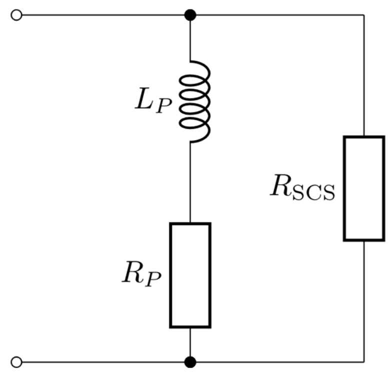

Figure 5-13 Schematic of series RL network compensated by SCS negative resistance.

The NIC input admittance is given by:

$$Y_{in,NIC}(s) = G_F\left(1 - \frac{A_0}{1 + s\tau}\right) = G_F \cdot \frac{\frac{s}{\omega_{pu}} + \kappa}{\frac{s}{\omega_{pu}} + 1}, \tag{5.17.}$$

where ω_{pu} is upper pole frequency of SCS NIC. Input admittance Y_{in} in $j\omega$ domain reads:

$$Y_{in,NIC}(j\omega) = G_F \frac{-1 + \left(\frac{\omega}{\omega_{\mathrm{pu}}}\right)^2}{1 + \left(\frac{\omega}{\omega_{\mathrm{pu}}}\right)^2} + j2G_F \frac{\frac{\omega}{\omega_{\mathrm{pu}}}}{1 + \left(\frac{\omega}{\omega_{\mathrm{pu}}}\right)^2}. \tag{5.18.}$$

Analysis of $Y_{in,NIC}(j\omega)$ (5.18.) below the pole frequency ω_{pu} shows that NIC input admittance behaves as shunt connection of negative conductance $-G_F$ and equivalent positive capacitance $C_{p,NIC}$:

$$Y_{in,NIC}(j\omega)\big|_{\omega \ll \omega_{pu}} \approx -G_F + j\frac{2G_F}{\omega_{pu}}\omega. = -\mathrm{G_F} + \mathrm{jC_{p,NIC}}\omega. \tag{5.19.}$$

Analogous to the previous case, NIC parasitic elements can ‘swamp’ value of generated negative capacitance and deteriorate properties of the entire system. Combining 5.19 and 5.16 one gets:

$$Y_{in,com}(j\omega)\Big|_{\substack{\omega\ll\omega_{pu},\\ \omega\ll\omega_{rl}}} \approx G_P - G_F + j\left(-\frac{G_P}{\omega_{rl}} + \frac{2G_F}{\omega_{pu}}\right)\omega$$
$$= G_P(1-\alpha) + jC_{eq0}\left(-1+\frac{2\alpha}{\beta}\right)\omega, \tag{5.20.}$$

where $\alpha = G_F/G_P$, $C_{eq} = G_P/\omega_{rl}$, $\beta = \omega_{pu}/\omega_{rl}$. We can now take α and β as design parameters and by setting $\alpha \approx 1$ and $\beta \gg \alpha$,(5.20) simplifies to $Y_{in,com}(j\omega) \approx -jC_{eq}\omega$.

Total input impedance of the compensated circuit is found by combining 5.15 and 5.18:

$$Y_{in,com}(j\omega) = Y_{in,RC} + Y_{in,NIC}$$
$$= G_P\left[\frac{1}{\left(\frac{\omega}{\omega_{rl}}\right)^2+1} + \alpha\frac{-1+\left(\frac{\omega}{\beta\omega_{rl}}\right)^2}{1+\left(\frac{\omega}{\beta\omega_{rl}}\right)^2}\right]$$
$$+ jG_P\left[-\frac{\frac{\omega}{\omega_{rl}}}{\left(\frac{\omega}{\omega_{rl}}\right)^2+1} + 2\alpha\frac{\frac{\omega}{\beta\omega_{rl}}}{1+\left(\frac{\omega}{\beta\omega_{rl}}\right)^2}\right]. \tag{5.21}$$

Input admittance was calculated using (5.21) and plotted as a function of frequency normalized to resonant frequency ω_{rl} (Figure 5-14a) with parameters $\alpha = G_F/G_P = 1$ and $\beta = \omega_{pu}/\omega_{rl} = 200$. Figure 5-14a shows that, with selected design parameters, the input parasitic conductance is almost completely canceled at low frequencies. This is also confirmed by calculated quality factor (Fig. 5.2.4c). Furthermore, the slope of imaginary part of input admittance is still negative, confirming non-Foster behavior. Equivalent capacitance is calculated as in previous uncompensated case as $C_{eq}(j\omega) = \Im\{Y_{in}(j\omega)\}/\omega$ and normalized to value $C_{eq0} = G_P/\omega_{rc}$ (Figure 5-14b).

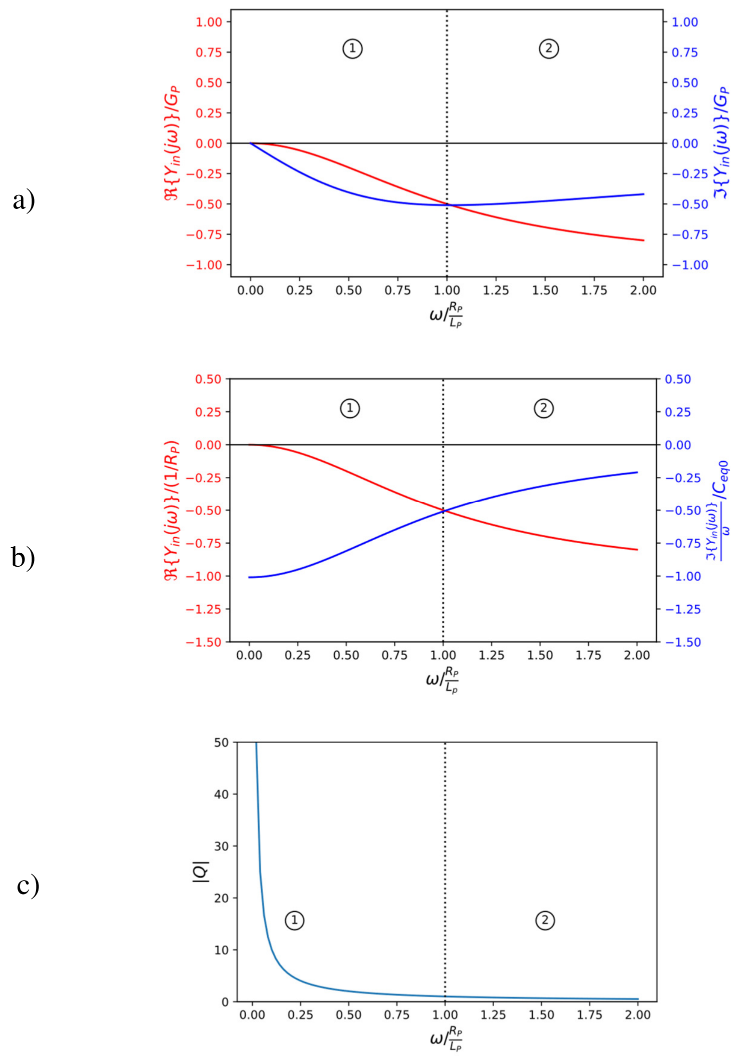

Figure 5-14 (a) Real and imaginary part of input impedance of series L_P and R_P compensated by SCS negative conductance. (b) Equivalent conductance and negative capacitance. (c) Quality factor of the circuit. Plots are obtained with $\alpha = G_F/G_P = 1$ and $\beta = \omega_{pu}/\omega_{rc} = 200$

5.2.3. Passive RL network that emulates negative capacitance – stability analysis

To test the stability of the compensated structure, we have loaded it with positive compensating capacitance C_L and excited the network by voltage generator with internal resistance R_g, as sketched in Figure 5-15a.

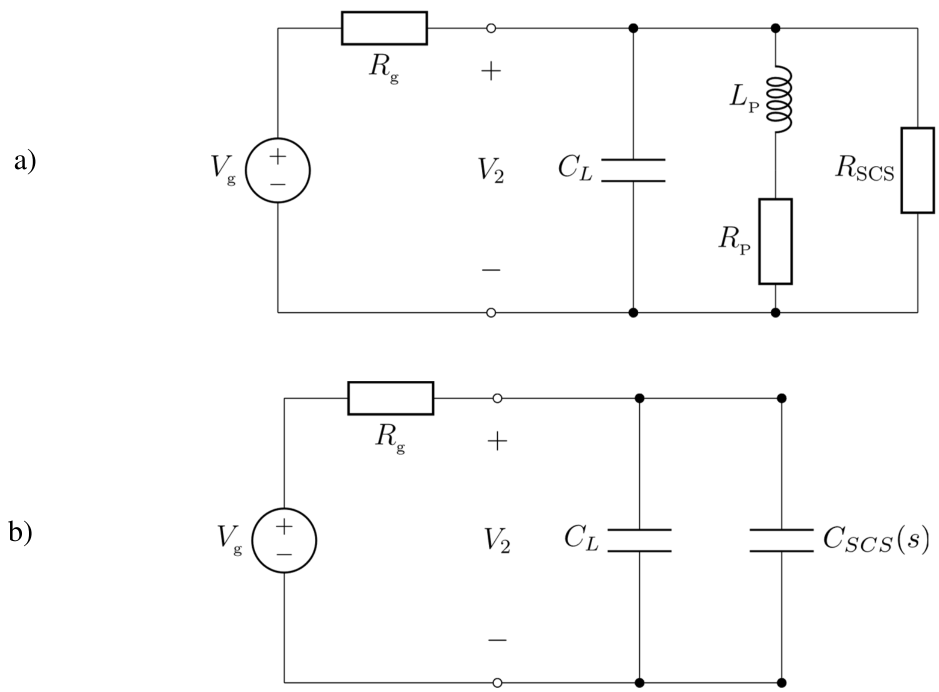

Figure 5-15 Networks used in stability analysis. a) Compensated RL network loaded with external network, b) 'Classical' negative capacitance constructed with SCS NIC

Transfer function of such a circuit can be written as:

$$H_V(s) = \frac{V_2}{V_g} = \frac{Z_{in}}{Z_{in} + R_g} = \frac{N(s)}{D(s)}. \tag{5.22.}$$

The characteristic equation governing the stability of the system is given by denominator $D(s)$ of (5.22.):

$$\begin{gathered} s^3 C_L L_P R_F R_g \tau_u + s^2\left(C_L L_P R_F R_g + C_L R_F R_P R_g \tau_u + L_P R_F \tau_u + L_P R_g \tau_u\right) + \\ s\left(C_L R_F R_P R_g + L_P R_F - L_P R_g + R_F R_P \tau_u + R_F R_g \tau_u + R_P R_g \tau_u\right) + R_F R_P + \\ R_F R_g - R_P R_g = 0 \end{gathered} \tag{5.23.}$$

Similarly to the previous case, the characteristic equation is in the form of cubic polynomial. Therefore, we again applied Routh-Hurwitz stability criterion to test the stability of the system. After applying (5.11) to (5.23) and some simplification, system stability criterion becomes:

$$\begin{gathered} \beta(1+\beta) + (1+\alpha+2\alpha\beta-\alpha\beta^2)\gamma + (\alpha+\alpha^2-\alpha^2\beta)\gamma^2 + (1+\beta)^2\gamma\delta \\ + (1+2\alpha)\gamma^2\delta + (1+\beta)\gamma^2\delta^2 > 0 \ \wedge \delta > \alpha - 1, \end{gathered} \tag{5.24.}$$

where $\alpha = G_F/G_P$, $\beta = \omega_{pu}/\omega_{rc}$, $\gamma = C_{eq}/C_L$, $\delta = G_g/G_P$. Using (5.24.) we have plotted stability area of the circuit with parameters $\alpha = G_F/G_P = 1$ and $\beta = \omega_{pu}/\omega_{rc} = 200$, which ensures good quality factor as shown before (Figure 5-14). We see from the plotted figure that total capacitance can be negative ($\frac{C_{eq}}{C_L} > 1$). Thus, the stable area in Figure 5-16 expands above the line $\frac{C_{eq}}{C_L} = 1$. We can now compare stability condition (4.2.9.) to the one derived for network shown in Figure 5-15b (a 'classical' one-pole OCS NIC loaded with positive capacitance C_F). Stability condition for network in fig 4.2.3b was derived in previous projects [44] and it states:

$$|-C_F| < \frac{G_F}{\omega_P} + C_L. \tag{5.25.}$$

From (5.25.) we see that it is possible to achieve overall negative inductance, but a factor $\frac{G_F}{\omega_P}$ (which can be interpreted as equivalent 'internal' NIC capacitance) limits the range of achievable negative capacitance. As the value of NIC pole frequency increases, the term $\frac{G_F}{\omega_P}$ tends to 0. In turn (4.1.10) reduces to well known stability criterion of hypothetical dispersionless NIC: $|-C_F| < C_L$ (the overall capacitance must be positive). On the contrary, in new design, total (net) capacitance can be negative ($\frac{C_{eq}}{C_L} > 1$) for very broad range of normalized parameters of external passive network (Figure 5-16), which is impossible in classical design. So, from the stability point of view, presented novel design is significantly better than standard one-pole NIC designs from the literature.

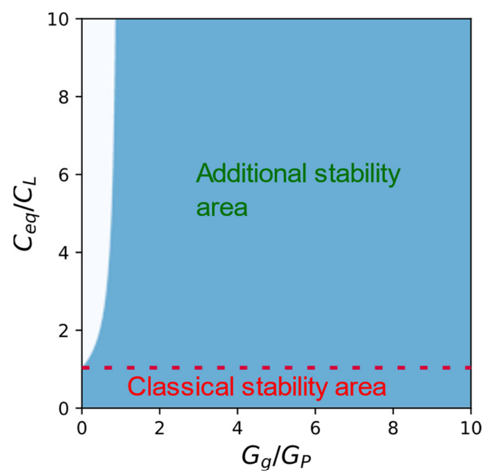

Figure 5-16 Stability area plot of compensated RL network loaded with positive inductance. Plot is generated with $\alpha = G_F/G_P = 1$ and $\beta = \omega_{pu}/\omega_{rc} = 200$. Dark blue – range of normalized external impedances that cause stable operation; Light blue - range of normalized external impedances that cause unstable operation. Please note that in standard negative inductor based on one-pole NIC, maximal stability area would be bounded by $C_{eq}/C_L<1$.

5.2.4. Passive RL network that emulates negative capacitance – design example

Proposed design was again verified using 40 nm CMOS technology. Previously designed NIC (Figure 5-8) was configured for operation in SCS configuration with shunt connection of resistance R_F and capacitance C_F. Shunt capacitance C_F is added to compensate for the parasitic input capacitance of SCS negative conductance Linvill circuit, as predicted in the section 4.2.5. This approach increases operating bandwidth of compensated RL structure. Series RL structure was then loaded in shunt with SCS negative conductance (Figure 5-17).

Values of the elements were tuned to achieve the value of equivalent required negative capacitance in L band (1-2 GHz) (Figure 5-18) ($R_P = 39\,\Omega, L_P = 1.21\,nH, R_F = 1\,\Omega, C_F = 111\,fF$.). Value of R_F is smaller than predicted by theoretical analysis, which is caused by finite 'parasitic' resistance of NIC circuit, not taken into account in simplified analysis. Smaller value of R_F causes larger value of parasitic conductance. This, in turn causes an increase of value of input parasitic capacitance $\left(C_{par} = \frac{2G_F}{\omega_{pu}}\right)$ that can 'swamp' the value of negative equivalent capacitance. Therefore, the parallel shunt capacitance C_F is needed. After several optimization cycles, we were able to achieve value of equivalent negative capacitance of -0.7 pF (Figure 5-18b) with negligible parasitic resistance as indicated by good Q factor (Figure 5-18 c)

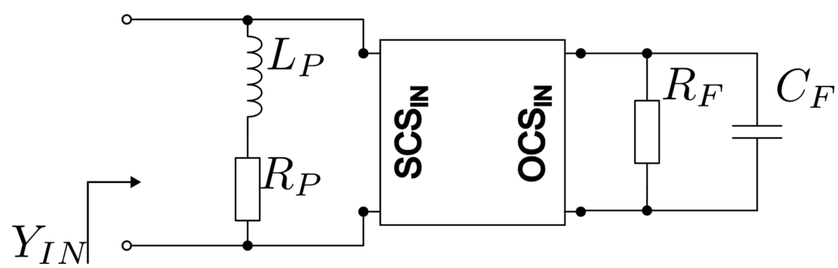

Figure 5-17 Compensated RL structure loaded with OCS negative resistance realized by Linvill NIC from Figure 5-8

Finally, stability of the entire circuit was again verified using STAN™ tool and compared with theoretical predictions, showing excellent agreement (Figure 5-19). So, it can again be noted that simplified analytical method of stability prediction can be used as starting point for subsequent numerical optimization.

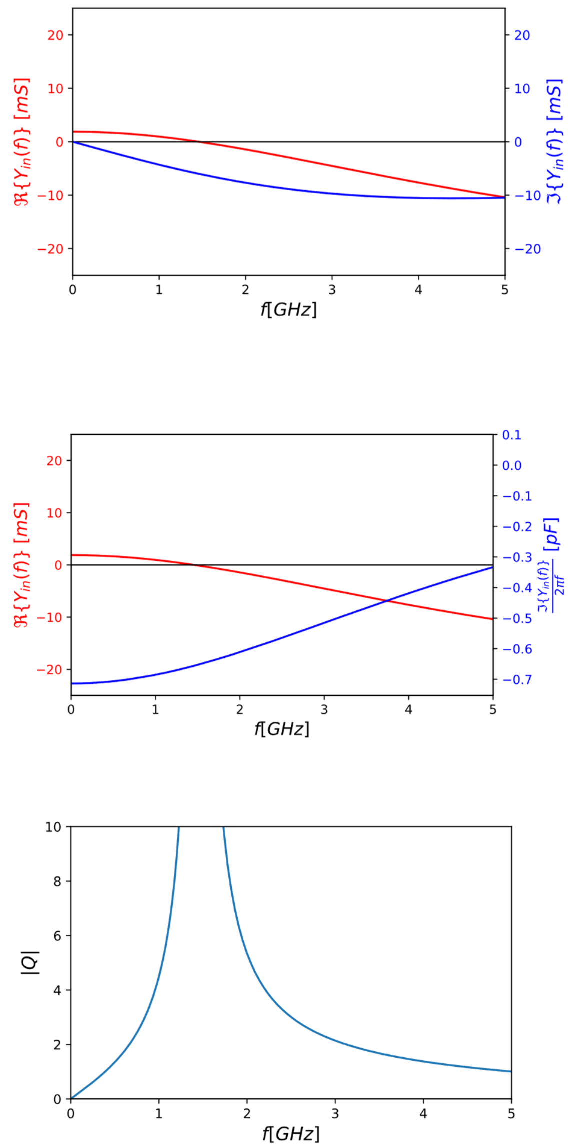

a)

b)

c)

Figure 5-18 a) Real and imaginary part of input impedance of series L_P and R_P compensated by SCS negative resistance. b) Equivalent resistance and negative inductance. c) Quality factor Q of the circuit. Plots are obtained with $R_P = 39\ \Omega$, $L_P = 1.21$ nH, $R_F = 1\ \Omega$, $C_F = 111$ fF

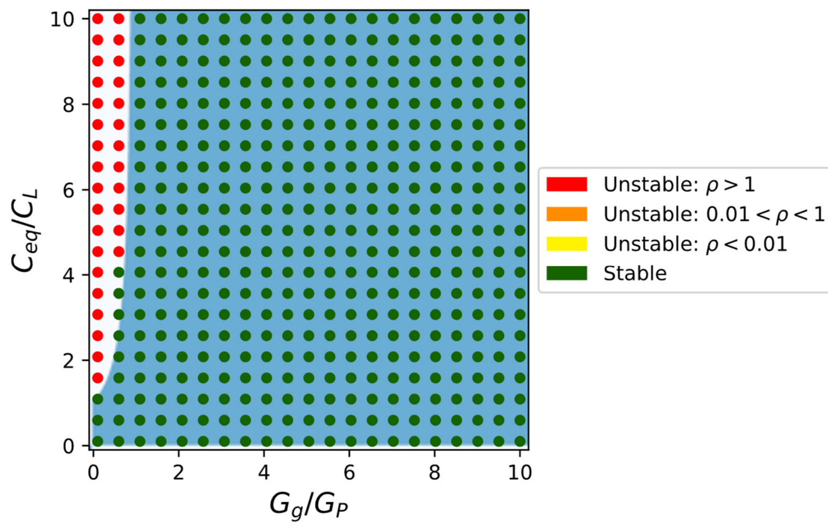

Figure 5-19 Stability area plot of compensated RL network loaded with positive inductance. Plot is generated with the following parameters $R_P = 39\ \Omega$, $L_P = 1.21$ nH, $R_F = 1\ \Omega$, $C_F = 111$ fF. Painted areas are calculated using simplified analytical approach (Dark blue – range of external impedances that cause stable operation; Light blue - range of external impedances that cause unstable operation). Colored dots are results predicted by commercial system identification software tool STAN^{TM}.

5.3 High-pass negative inductance

5.3.1. Passive RC network that emulates negative inductance – basic idea

Input admittance of the series combination of capacitance C_P and resistance R_P (Figure 5-20a), defined in the Laplace domain, is given by:

$$Z_{in,RC}(s) = R_p + \frac{1}{sC_p}, \tag{5.26}$$

where $s = \sigma + j\omega$ is complex frequency.

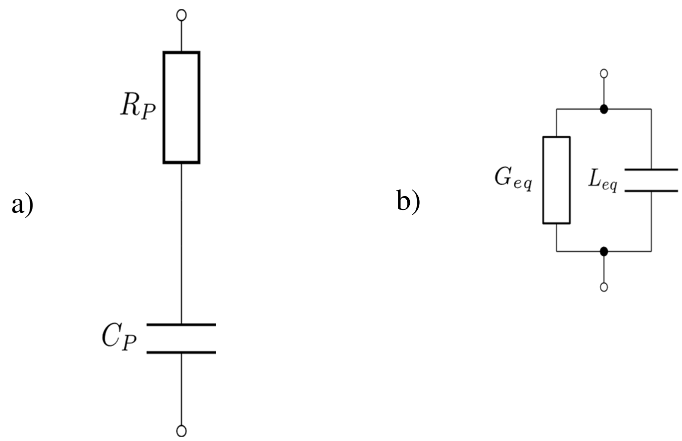

Figure 5-20 Schematic of series RC network (a) and its equivalent $Y_{in}(j\omega)$ representation in jω domain (b)

To study the circuit in the steady-state frequency domain we set $s = j\omega$ and derive the expression for input admittance:

$$Y_{in,RC}(j\omega) = \frac{1}{Z_{in,RC}(s = j\omega)} = G_P \frac{\left(\frac{\omega}{\omega_{rc}}\right)^2}{1 + \left(\frac{\omega}{\omega_{rc}}\right)^2} + jG_P \frac{\frac{\omega}{\omega_{rc}}}{1 + \left(\frac{\omega}{\omega_{rc}}\right)^2}, \tag{5.27}$$

where $G_p = \frac{1}{R_p}$ is conductance and $\omega_{rc} = \frac{1}{R_p C_p}$ is cut-off (resonant) frequency of RC circuit. Straightforward analysis shows that, above cut-off frequency (5.27), simplifies to:

$$Y_{in}(j\omega) = Y_{in,RC}\Big|_{\omega \gg \omega_{rc}} \approx \mathrm{G_p} + j\frac{1}{\frac{1}{G_P \omega_{rc}}\omega} = G_p + \frac{1}{jL_{eq0}\omega}. \tag{5.28}$$

Thus, above the cut-off frequency, input admittance can be interpreted as a parallel combination of equivalent negative inductance $L_{\mathrm{eq0}} = -\frac{1}{G_p \omega_{rc}}$ and ordinary positive conductance G_p (Figure 5-20b). To analyze behavior of the circuit, we have plotted input impedance in $j\omega$ domain (5.27) of proposed circuit (Figure 5-21a). One can distinguish a region with positive dispersion 1 and a region above the resonant frequency (ω_{rc}) with negative ('anomalous') dispersion that we can interpret as negative-inductance behavior 2. Negative inductance (present in region 2 of (Figure 5-21b) is calculated as $L_{eq}(j\omega) = -1/(\Im\{Y_{in}(j\omega)\}\omega)$, while equivalent parasitic conductance is taken as $G_{eq}(j\omega) = \Re\{Y_{in}(j\omega)\}$. Here we note that calculated equivalent inductance is valid only in the region 2. It can be noted that equivalent negative inductance in region 2 is almost dispersionless across extremely broad band and that it approaches the value (L_{eq0}) given in (5.28) as the frequency increases. However, it can also be seen that the value of 'parasitic' conductance is rather high and, consequently, quality factor is low (Figure 5-21c). Furthermore, it can be seen that the value of L_{eq0} is determined by the value of G_p (conductance of series resistor) while the resonance is controlled by values of series RC circuit. As in the previous cases, the compensation of 'parasitic' conductance is needed in order to improve the quality factor.

a)

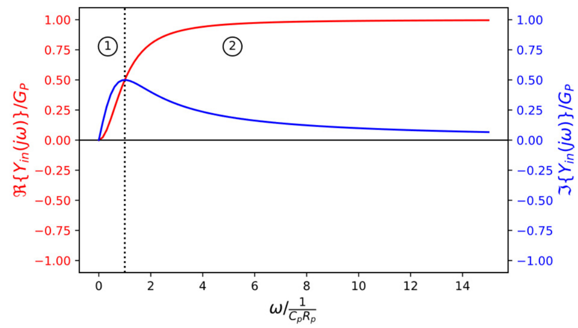

b)

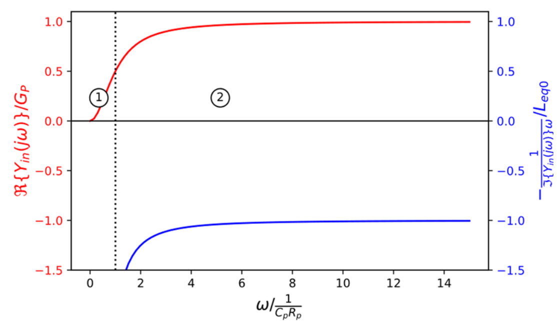

c)

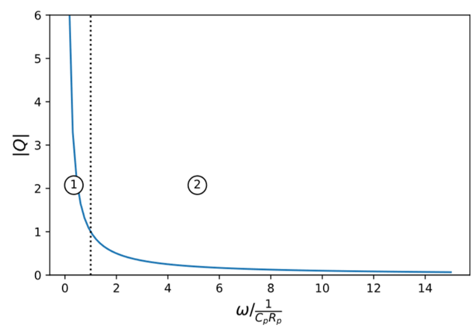

Figure 5-21 a) Real and imaginary part of input impedance of series C_P and R_P. b) Equivalent conductance and negative inductance. c) Quality factor Q of the circuit

5.3.2. Passive RC network that emulates negative inductance – loss compensation

In order to compensate losses and increase the quality factor the circuit was loaded with SCS NIC (Figure 5-22) with feedback conductance G_F. The NIC input admittance is given by (5.17.).

Combining (5.28.) and (5.19.) we get:

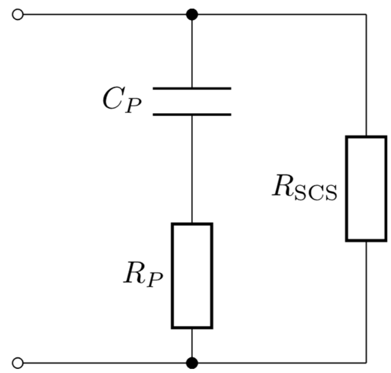

Figure 5-22 Schematic of series RC network compensated by SCS negative resistance.

$$Y_{in,com}(j\omega)\Big|_{\substack{\omega\ll\omega_{pu},\\ \omega\gg\omega_{rc}}} \approx G_P - G_F + j\left(\frac{G_P\omega_{rc}}{\omega} + \frac{2G_f}{\omega_{pu}}\omega\right) = G_{\mathrm{P}}(1-\alpha) + j\frac{1}{L_{eq0}}\left(\frac{1}{\omega} + \frac{2\alpha}{\beta\omega_{rc}}\omega\right), \tag{5.29.}$$

where $\alpha = G_F/G_P$, $L_{eq0} = 1/G_P\omega_{rc}$, $\beta = \omega_{pu}/\omega_{rc}$. Again, α and β will be taken as design parameters. From imaginary part of above expression, one derives approximate upper bound of operation as:

$$\frac{d\Im\left\{Y_{in,com}(j\omega)\Big|_{\substack{\omega\ll\omega_{pu},\\ \omega\gg\omega_{rc}}}\right\}}{d\omega} = \frac{1}{L_{eq0}}\left(-\frac{1}{\omega^2} + \frac{2\alpha}{\beta\omega_{rc}}\right) = 0 \rightarrow \omega_2 = \sqrt{\frac{\beta}{2\alpha}}\omega_{rc}. \tag{5.30.}$$

This calculated upper bound is an approximate expression that is valid for high values of β . However, it can be used as a good starting point in the design procedure.

Total input admittance of the compensated structure is given by combination 5.3.2. and 5.18. with applied simplifications for α and β:

$$Y_{in,com}(j\omega) = Y_{in,RC}(j\omega) + Y_{in,NIC}(j\omega) = G_P\left[\frac{\left(\frac{\omega}{\omega_{rc}}\right)^2}{\left(\frac{\omega}{\omega_{rc}}\right)^2 + 1} + \alpha\frac{-1 + \left(\frac{\omega}{\beta\omega_{rc}}\right)^2}{1 + \left(\frac{\omega}{\beta\omega_{rc}}\right)^2}\right] + jG_P\left[\frac{\frac{\omega}{\omega_{rc}}}{\left(\frac{\omega}{\omega_{rc}}\right)^2 + 1} + 2\alpha\frac{\frac{\omega}{\beta\omega_{rc}}}{1 + \left(\frac{\omega}{\beta\omega_{rc}}\right)^2}\right]. \tag{5.31}$$

To further study this circuit , the input admittance is plotted, by selecting $\beta = 200$ and $\alpha = 0.961$. So, the real part of (5.31) is negated at frequency $\frac{\omega}{\omega_{rc}} = 5.5$ (Figure 5-23a). At first, it is noticed that the 'parasitic' conductance (and, therefore, the loss) in region 2 was completely canceled at selected frequency, which significantly improves a quality factor (Figure 5-23c) of negative inductance. Also, there is occurrence of additional region with positive dispersion (region 3). Unwanted dispersion of input admittance in region 3 is caused by parasitic capacitance of NIC (caused by its pole), as it was discussed earlier. So, a series RC circuit compensated with negative resistance behaves as a band-pass negative inductance.

a)

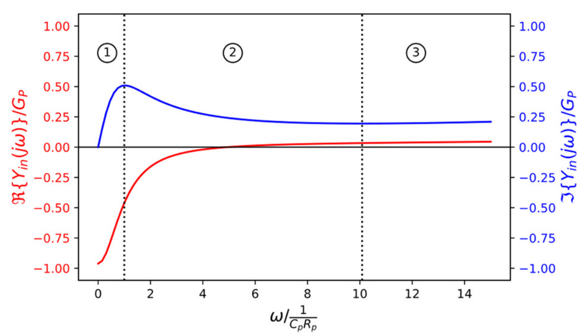

b)

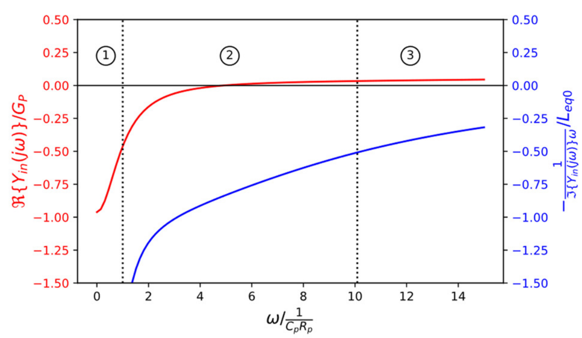

c)

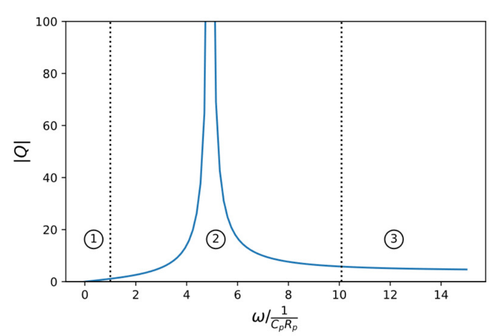

Figure 5-23 a) Real and imaginary part of input impedance of series C_P and R_P compensated by SCS negative conductance. b) Equivalent conductance and negative inductance. c) Quality factor Q of the circuit. Plots are obtained with $\alpha = G_F/G_P = 0.961$ and $\beta = \omega_{pu}/\omega_{rc} = 200$

Let us estimate the bandwidth of negative inductance. Upper frequency of operation is approximately given by (5.30) while lower frequency of operation is given by resonant frequency of RC circuit $\omega_1 = \omega_{rc}$, then we can define central frequency ω_c and fractional bandwidth FBW as:

$$\omega_c = \frac{\omega_1 + \omega_2}{2}, \tag{5.32 a}$$

$$FBW = \frac{\omega_2 - \omega_1}{\omega_c} = 2\frac{\omega_2 - \omega_1}{\omega_2 + \omega_1} = 2\frac{\sqrt{\frac{\beta}{2\alpha}} - 1}{\sqrt{\frac{\beta}{2\alpha}} + 1}. \tag{5.32 b}$$

Available bandwidth is plotted as a function of ratio of frequencies ω_{pu}/ω_{rc} and ratio of conductances $G_F/G_P = 0.961$ (Figure 5-24).

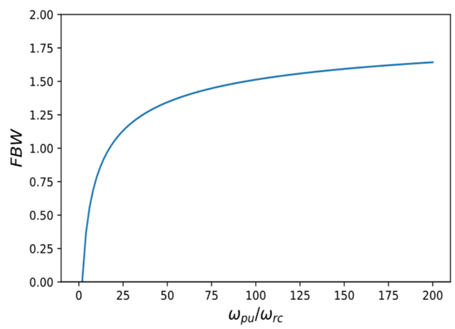

Figure 5-24 Plot of Fractional bandwidth (FBW) as a function of ratio of frequencies ω_{pu}/ω_{rc} and ratio of conductances $\alpha = G_F/G_P = 0.961$.

5.3.3. Passive RC network that emulates negative inductance – stability analysis

Stability of the proposed circuit was evaluated by loading it with external shunt inductance and excited with generator with internal resistance R_g (Figure 5-25a). Transfer function of such a circuit can be written as:

$$H_V(s) = \frac{V_2}{V_g} = \frac{Z_{in}}{Z_{in} + R_g} = \frac{N(s)}{D(s)}. \tag{5.33.}$$

The characteristic equation that determines the stability of the system is given by denominator of (5.33):

$$s^3(C_P L_L R_F R_P \tau_u + C_P L_L R_F R_g \tau_u + C_P L_L R_P R_g \tau_u) + s^2(C_P L_L R_F R_P + C_P L_L R_F R_g - C_P L_L R_P R_g + C_P R_F R_P R_g \tau_u + L_L R_F \tau_u + L_L R_g \tau_u) + s(C_P R_F R_P R_g + L_L R_F - L_L R_g + R_F R_g \tau_u) + R_F R_g = 0. \tag{5.34}$$

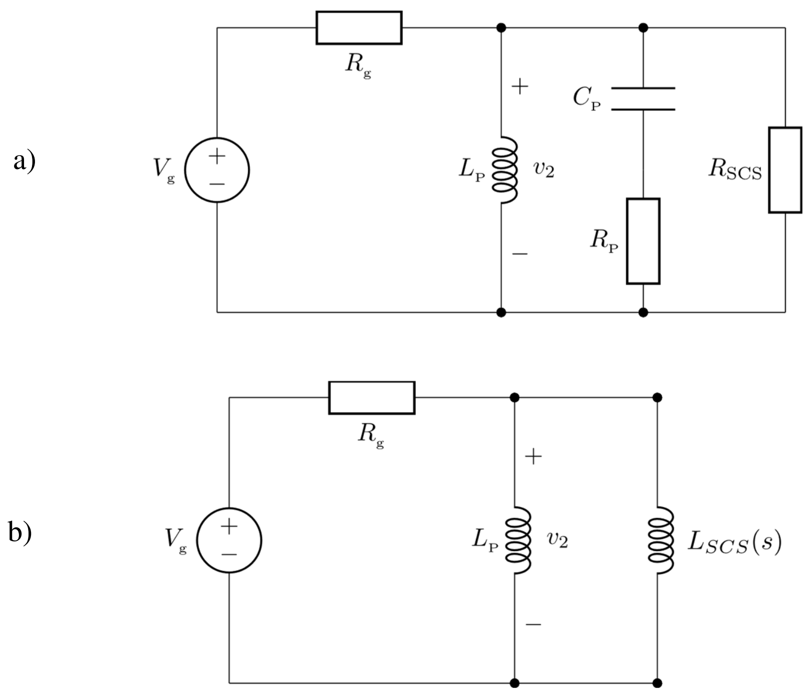

Figure 5-25 Stability testing schematics. a) Compensated RC network loaded with external network, b) ‘Classic’ negative capacitance constructed with SCS NIC

By applying Routh-Hurwitz stability criterion (5.11) to cubic polynomial (5.34) (with some simplifications), one gets the following inequalities:

$$\begin{gathered} 0 < \alpha \le \delta \wedge \beta > 1 \wedge \gamma > 0 \vee \\ \alpha > \delta \wedge \gamma > \frac{1}{2}\sqrt{\frac{\alpha^2\beta^4 + 2\alpha^2\beta^2 + \alpha^2 - 2\alpha\beta^4\delta - 2\alpha\beta^4 + 6\alpha\beta^2 + 2\alpha\delta + \beta^4\delta^2 + 2\beta^4\delta + \beta^4 - 2\beta^2\delta^2 - 2\beta^2\delta + \delta^2}{(\beta+1)^2}} \\ + \frac{\alpha\beta^2 + 2\alpha\beta - \alpha - \beta^2\delta - \beta^2 - 2\beta\delta - \delta}{2(\beta+1)}, \end{gathered} \tag{5.35.}$$

where $\alpha = G_F/G_P$, $\beta = \omega_p/\omega_{rl}$, $\gamma = L_{eq}/L_L$ and $\delta = G_g/G_F$. As in the previous cases, stability condition (5.35.) is plotted in the form of stability map (Figure 5-26) (with values $\alpha = 0.961$ and $\beta = 200$ that ensure good quality factor).

We have compared obtained results with stability of 'classical' SCS negative inductance based on one-pole NIC [2], using the same external RL network and the same methodology of stability prediction (Figure 5-25b). In the case of the negative SCS inductor (Figure 5-25b) the stability criterion simplifies to:

$$\frac{L_F}{L_E} > 1. \tag{4.36}$$

It can be seen that proposed design offers large additional area of impedances allowed for stable operation, that even enables the existence of net negative inductance.

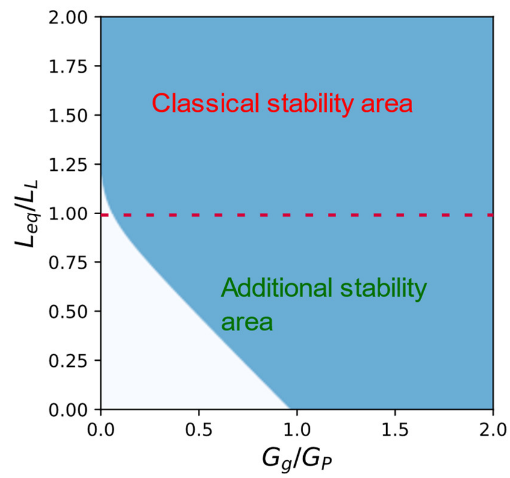

Figure 5-26 Comparison of stability regions of loaded compensated RC structure and loaded SCS negative inductance. Plot is generated with $\alpha = G_F/G_P = 0.961$ and $\beta = \omega_{pu}/\ \omega_{rc} = 200$. Dark blue – range of external impedances that cause stable operation; Light blue - range of external impedances that cause unstable operation.

5.3.4. Passive RC network that emulates negative inductance – design example

Proposed design was again verified using 40 nm CMOS technology. Previously designed NIC (Figure 5-8), operatively configured in SCS configuration loaded with shunt connection of resistance R_F and capacitance C_F was used (the role of these elements was already discussed in section 5.2.4. Series RC structure was then connected in parallel with SCS port of negative conductance (Figure 5-27).

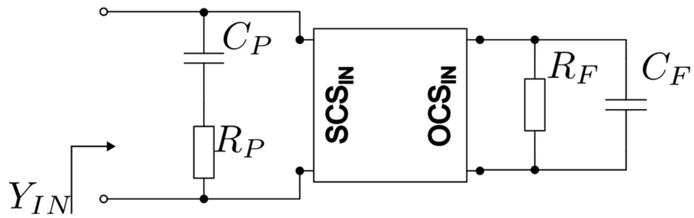

Figure 5-27 Compensated series RL structure loaded with OCS negative resistance.

In the first case, the values of elements were tuned to achieve the value of equivalent negative inductance in L band (1-2 GHz) (Figure 5-28b) ($R_P = 130\ \Omega, C_P = 2.43\ pF, R_F = 85\ \Omega, C_F = 128\ fF$.). We were able to achieve value of equivalent inductance of -40 nH in the specified frequency band (Figure 5-28b), with quality Q>2 (Figure 5-28c).

a)

b)

c)

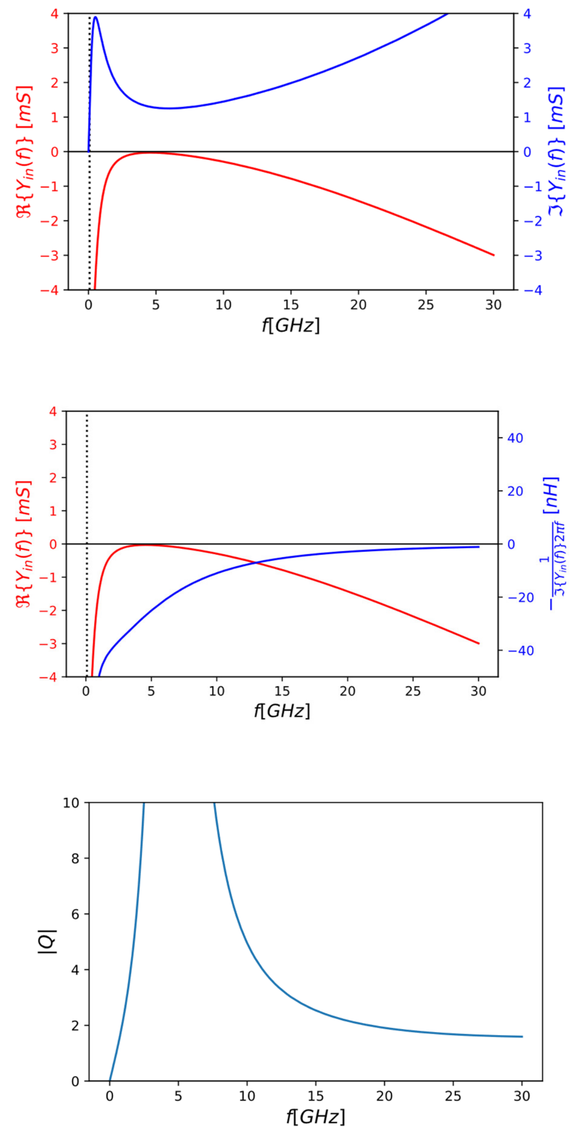

Figure 5-28 a) Real and imaginary part of input impedance of series C_P and R_P compensated by OCS negative resistance. b) Equivalent resistance and negative inductance. c) Quality factor Q of the circuit. Plots are obtained with R_P = 130 Ω, C_P = 2.43 pF, R_F = 85 Ω, C_F = 128 fF.

As in the previous cases, stability was verified using STAN™ and compared to theoretical prediction, showing good agreement (Figure 5-29).

In the second step, it was attempted to extend the design to the X-band (8 - 12 GHz). The goal was to achieve negative inductance of -5nH. The used parameters were: $R_P = 130\ \Omega, C_P = 2.43\ pF, R_F = 85\ \Omega, C_F = 128\ fF$. As it can be seen from Figure 5-30, obtained results show almost 'flat' characteristic of generated negative inductance gain with good Q factor.

We have also cross-checked the stability of X-band negative inductance (Figure 5-31) and again found very good agreement between theoretical predictions and results obtained by

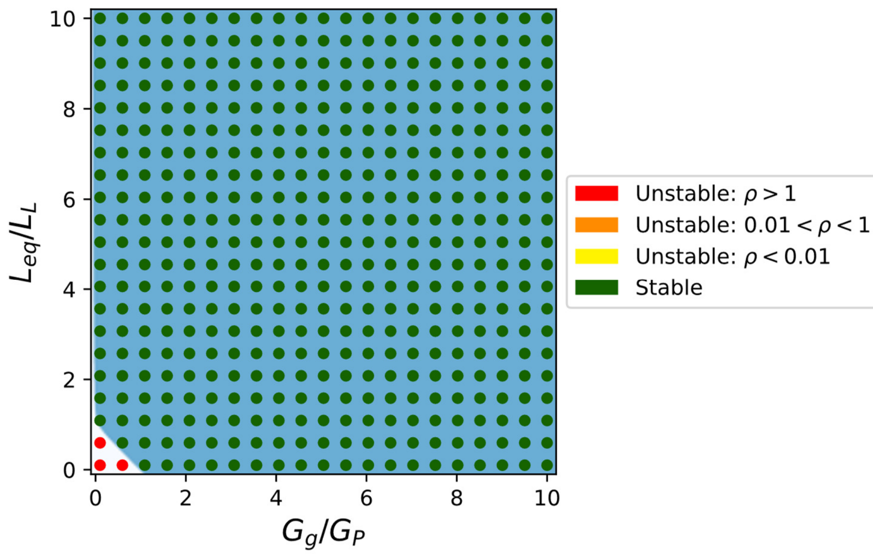

Figure 5-29 Stability area plot of compensated RC network loaded with positive inductance. Plot is generated $R_P = 130\ \Omega$, $C_P = 2.43$ pF, $R_F = 85\ \Omega$, $C_F = 128$ fF. Painted areas are calculated using simplified analytical approach (Dark blue – range of external impedances that cause stable operation; Light blue - range of external impedances that cause unstable operation). Colored dots are results predicted by commercial system identification software tool STAN™.

using STAN™ tool. This again shows that simplified analytical method of stability prediction can be used as starting point for subsequent numerical optimization.

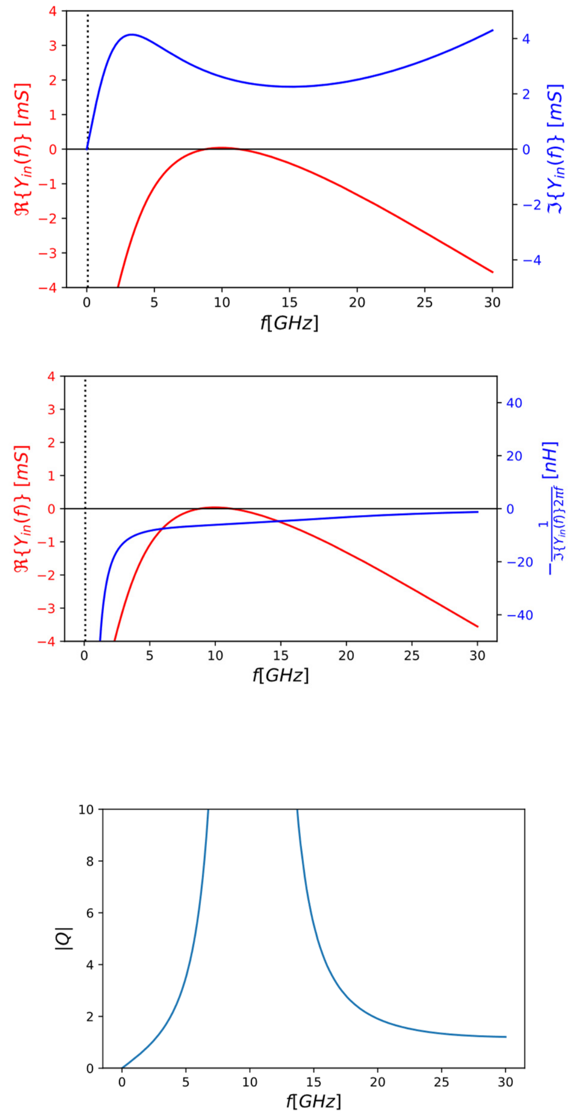

Figure 5-30 a) Real and imaginary part of input impedance of series C_P and R_P compensated by OCS negative resistance. b) Equivalent resistance and negative inductance. c) Quality factor Q of the circuit. Plots are obtained with $R_P = 120\ \Omega$, $C_P = 398$ fF, $R_F = 86\ \Omega$, $C_F = 122$ fF.

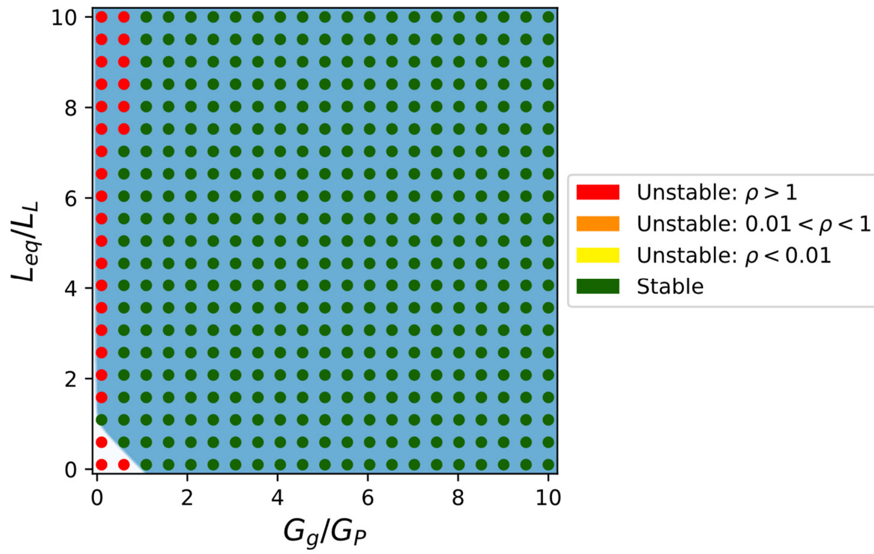

Figure 5-31 Stability area plot of compensated RC network loaded with positive inductance. Plot is generated using : $R_P = 120\ \Omega$, $C_P = 398$ fF, $R_F = 86\ \Omega$, $C_F = 122$ fF. Painted areas are calculated using simplified analytical approach (Dark blue – range of external impedances that cause stable operation; Light blue - range of external impedances that cause unstable operation). Colored dots are results predicted by commercial system identification software tool STAN™.

5.4 High-pass negative capacitance

5.4.1. Passive RL network that emulates negative capacitance – basic idea

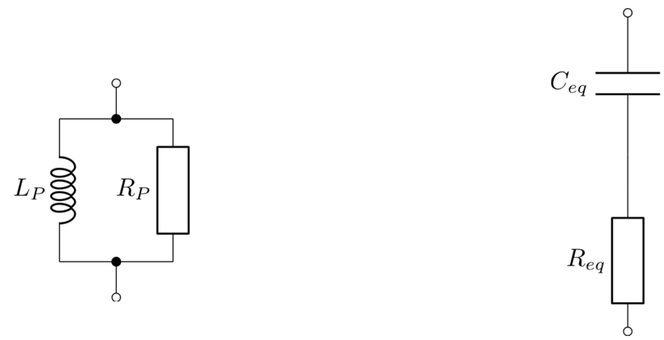

Figure 5-32 Schematic of parallel network (a) and its equivalent $\boldsymbol{Z_{in}(j\omega)}$ representation in $\boldsymbol{j\omega}$ domain (b)

Following the procedures outlined in the previous sections, we analyze a simple parallel connection of positive inductance L_P and resistance R_P (Figure **5**-**32**) whose input admittance Y_{in} in Laplace domain is given by:

$$Y_{in} = \frac{1}{\mathrm{R_P}} + \frac{1}{\mathrm{L_P\,s}}. \tag{5.37}$$

By setting $s = j\omega$ and analyzing input impedance $Z_{in}(j\omega)$ one gets:

$$Z_{in}(j\omega) = R_P \frac{\left(\frac{\omega}{\omega_{rl}}\right)^2}{\left(\frac{\omega}{\omega_{rl}}\right)^2 + 1} + jR_P \frac{\frac{\omega}{\omega_{\mathrm{rl}}}}{\left(\frac{\omega}{\omega_{rl}}\right)^2 + 1}, \tag{5.38}$$

where $\omega_{rl} = \frac{R_P}{L_P}$ is circuit cut-off frequency ('resonant' frequency). By assuming operation above the resonant frequency (5.38.) simplifies to:

$$\begin{aligned} Z_{in}(j\omega) &= \left(R_p \frac{\left(\frac{\omega}{\omega_{rc}}\right)^2}{1 + \left(\frac{\omega}{\omega_{rc}}\right)^2} + jR_p \frac{\frac{\omega}{\omega_{rc}}}{1 + \left(\frac{\omega}{\omega_{rc}}\right)^2} \right)\Bigg|_{\omega \gg \omega_{rc}} \approx \mathrm{R_p} + jR_P \frac{1}{\frac{\omega}{\omega_{rl}}} \\ &= R_p + \frac{1}{jC_{eq0}\omega}, \end{aligned} \tag{5.39}$$

where C_{eq} is equivalent negative capacitance defined by $C_{eq0} = -\frac{1}{\omega_{rl} R_P}$.

By using (5.38) we have plotted the input real and imaginary part of the input impedance $Z_{in}\ (j\omega)$ (Figure 5-33). It is immediately obvious this is dual case of the one shown in previous section. One can distinguish a region with positive dispersion ① and a region above the resonant frequency (ω_{rl}) with negative ('anomalous') dispersion that we can interpret as negative-capacitance behavior ②. Negative capacitance (present in region ② of (Figure 5-33b) is calculated as $C_{eq}(j\omega) = -1/(\Im\{Z_{in}(j\omega)\}\omega)$, while equivalent parasitic resistance is taken as $R_{eq}(j\omega) = \Re\{Z_{in}(j\omega)\}$. Here we note that calculated equivalent inductance is valid only in the region ②. It can be noted that equivalent negative capacitance in region ② is almost dispersionless across extremely broad band and that it approaches the value (C_{eq0}) given in (5.39) as the frequency increases. However, it can also be seen that the value of 'parasitic' resistance is rather high and, consequently, quality factor is low (Figure 5-33c). Furthermore, it can be seen that the value of C_{eq0} is determined by the value of R_p (resistance of parallel resistor) while the resonance is controlled by values of parallel RL circuit. As in the previous cases, the compensation of 'parasitic' resistance is needed in order to improve the quality factor.

a)

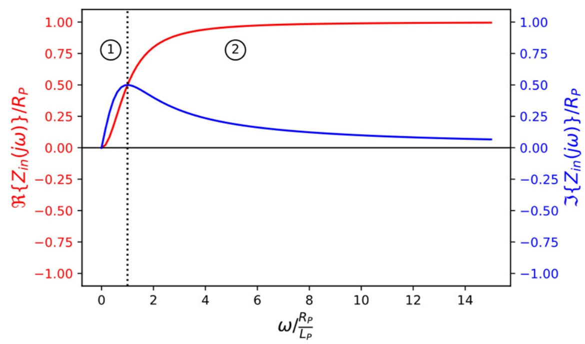

b)

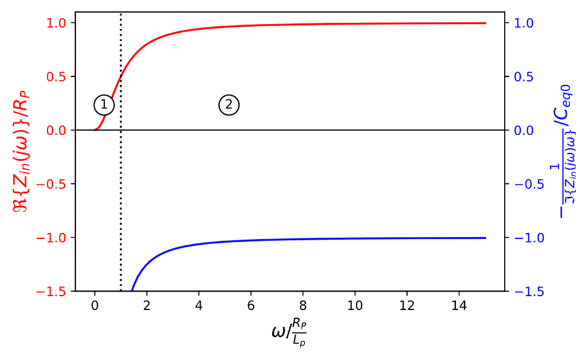

c)

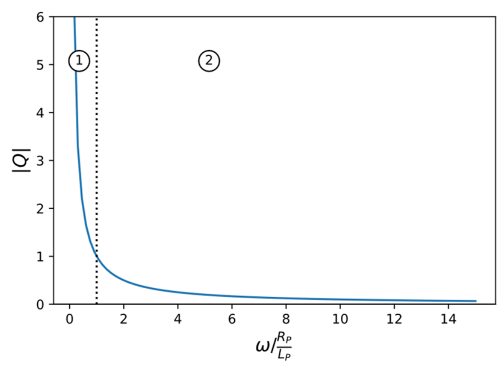

Figure 5-33 a) Real and imaginary part of input impedance of parallel L_P and R_P. b) Equivalent resistance and negative capacitance. c) Quality factor Q

5.4.3. Passive RL network that emulates negative capacitance – loss compensation

In order to compensate losses and increase the quality factor, the circuit was connected to Linvill OCS NIC (Figure 5-34) loaded with feedback resistance R_F . This NIC behaves as negative resistance, the impedance of which is given by (5.1.4.).

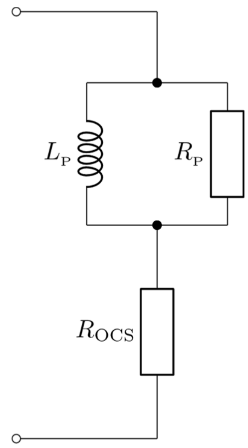

Figure 5-34 Schematic of shunt RL network that emulates negative capacitance, compensated by series OCS negative resistance.

Combining (5.39.) and (5.5.), one gets:

$$\begin{aligned} Z_{in,com}(j\omega)\Big|_{\substack{\omega\ll\omega_{pu},\\ \omega\gg\omega_{rc}}} &\approx R_P - R_F + j\left(\frac{R_P\omega_{rl}}{\omega} + \frac{2R_f}{\omega_{pu}}\omega\right) \\ &= R_{\mathrm{P}}(1-\alpha) + j\frac{1}{C_{eq0}}\left(\frac{1}{\omega} + \frac{2\alpha}{\beta\omega_{rl}}\omega\right), \end{aligned} \tag{5.40.}$$

where $\alpha = R_F/R_P$, $C_{eq0} = 1/R_P\omega_{rl}$, $\beta = \omega_{pu}/\omega_{rl}$. The expressions (5.29.) and (5.40.) are completely analogous. So, previously drawn conclusions about the upper pole frequency (5.30.) and the bandwidth (5.32.) are valid here, as well. Total input admittance of the compensated structure is given by combination of 5.27. and 5.18. Applying definitions of α and β , the input admittance reduces to:

$$\begin{aligned} Z_{in,com}(j\omega) &= Z_{in,RL}(j\omega) + Z_{in,NIC}(j\omega) \\ &= R_P\left[\frac{\left(\frac{\omega}{\omega_{rl}}\right)^2}{\left(\frac{\omega}{\omega_{rl}}\right)^2+1} + \alpha\frac{-1+\left(\frac{\omega}{\beta\omega_{rl}}\right)^2}{1+\left(\frac{\omega}{\beta\omega_{rl}}\right)^2}\right] \\ &\quad + jR_P\left[\frac{\frac{\omega}{\omega_{rl}}}{\left(\frac{\omega}{\omega_{rl}}\right)^2+1} + 2\alpha\frac{\frac{\omega}{\beta\omega_{rl}}}{1+\left(\frac{\omega}{\beta\omega_{rl}}\right)^2}\right]. \end{aligned} \tag{5.41}$$

Finally, input impedance (5.41.) is plotted as a function of frequency with $\beta = 200$ and $\alpha = 0.961$ so that real part of input impedance is totally canceled at the frequency $\frac{\omega}{\omega_{rl}} = 5.5$. It can be seen that, above the resonant frequency (region ②), there is a negative slope of imaginary part of input impedance, indicating non-Foster-like behavior. Additionally, there is additional region with positive slope of imaginary part of input impedance that determines upper boundary of the frequency of operation (region ③). This change of slope is caused by positive parasitic inductance of OCS NIC, given by 5.6. It can also be seen that the quality factor of the circuit is significantly improved in the vicinity of design frequency (Figure 5-35c).

a)
b)
c)

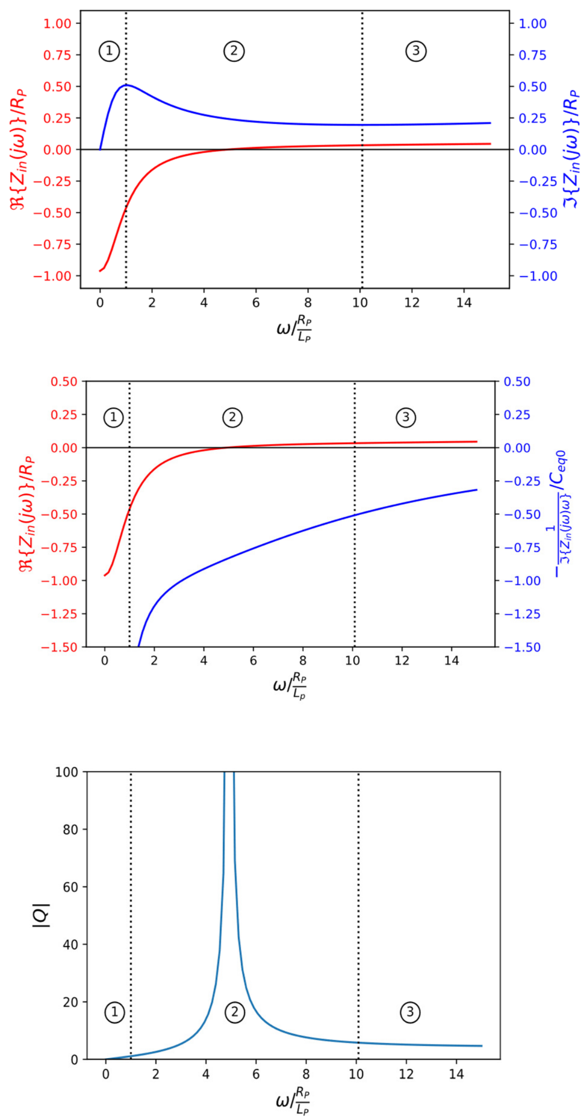

Figure 5-35 a) Real and imaginary part of input admittance of parallel combination of L_P and R_P, compensated by series negative resistance. c) Quality factor as a function of frequency of compensated circuit. Plot has been obtained with the following parameters $\alpha = R_F/R_P = 0.961$ and $\beta = \omega_{pu}/\omega_{rc} = 200$

5.4.4. Passive RL network that emulates negative capacitance - stability analysis

To test the stability of the compensated structure, we have loaded it with external positive capacitance C_L and excited it by voltage generator with internal resistance R_g (Figure 5-36a). This eternal network mimics realistic scenario in standard applications such as matching of a short dipole antenna.

a)

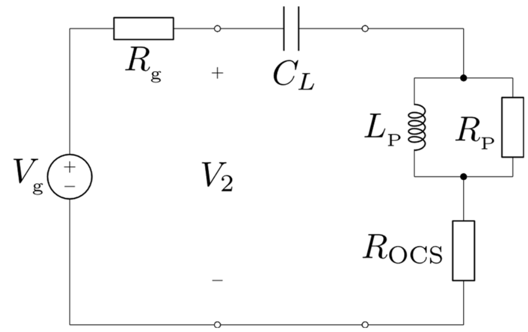

b)

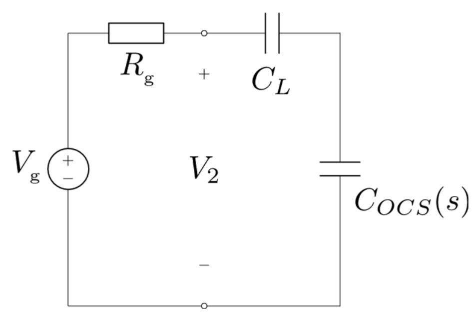

Figure 5-36 Stability testing schematics. a) Compensated RL network loaded with external network, b) 'Classic' negative capacitance constructed with OCS NIC

The circuit transfer function is defined as:

$$H_V(s) = \frac{V_2}{V_g} = \frac{Z_{in}}{Z_{in} + R_g} = \frac{N(s)}{D(s)}. \tag{5.42.}$$

The characteristic equation governing the stability of the system is given by denominator $D(s)$ of (5.42.):

$$\begin{aligned} s^3&\left(C_L L_P R_F + C_L L_P R_P + C_L L_P R_g\right) \\ &+ s^2\left(-C_L L_P R_F \omega_p + C_L L_P R_P \omega_p + C_L L_P R_g \omega_p + C_L R_F R_P \right. \\ &\left. + C_L R_P R_g + L_P\right) + s\left(-C_L R_F R_P \omega_p + C_L R_P R_g \omega_p + L_P \omega_p + R_P\right) \\ &+ R_P \omega_p = 0. \end{aligned} \tag{5.43.}$$

Again, this is cubic polynomial and Routh-Hurwitz stability criterion can be applied (5.11). After a long derivation and some simplifications, the stability conditions of the system is found to be:

$$0<\alpha\le\delta\wedge\beta>1\wedge\gamma>0\vee$$
$$\alpha>\delta\wedge\gamma>\frac{1}{2}\sqrt{\frac{\alpha^2\beta^4+2\alpha^2\beta^2+\alpha^2-2\alpha\beta^4\delta-2\alpha\beta^4+6\alpha\beta^2+2\alpha\delta+\beta^4\delta^2+2\beta^4\delta+\beta^4-2\beta^2\delta^2-2\beta^2\delta+\delta^2}{(\beta+1)^2}}+\frac{\alpha\beta^2+2\alpha\beta-\alpha-\beta^2\delta-\beta^2-2\beta\delta-\delta}{2(\beta+1)},\tag{5.44.}$$

where $\alpha=R_F/R_P$, $\beta=\omega_p/\omega_{rl}$, $\gamma=C_{eq}/C_L$ and $\delta=R_P/R_g$. As in the previous cases, stability condition (5.35.) is plotted in the form of stability map (Figure 5-37) (with values $\alpha=0.961$ and $\beta=200$ that ensure good quality factor).

We have compared obtained results with stability of 'classical' OCS negative inductance based on one-pole NIC [2], using the same external RC network and the same methodology of stability prediction (Figure 5-36b). In the case of the negative SCS inductor (Figure 5-36b) the stability criterion simplifies to:

$$\frac{C_F}{C_E}>1.\tag{5.45}$$

We can immediately see that this is completely dual case to the one presented in section 5.3.4 and all the conclusions are analogous.

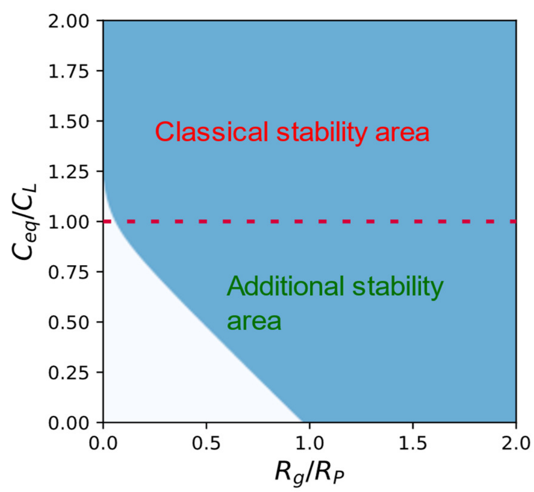

Figure 5-37 Stability area plot of compensated RC network loaded with positive inductance. Plot is generated with $\alpha = R_F/R_P = 0.961$ and $\beta = \omega_{pu}/\omega_{rc} = 200$. Dark blue – range of external impedances that cause stable operation; Light blue - range of external impedances that cause unstable operation. Please note that in standard negative inductor based on one-pole NIC, maximal stability area would be bounded by $C_{eq}/C_L>1$

5.4.5. Passive RL network that emulates negative capacitance – design example

This design was also verified in 40 nm CMOS technology. Previously designed Linvill NIC (Figure 5-8) was configured to operate in the OCS mode (its SCS port was loaded with series combination of resistance R_F and inductance L_F . The purpose of additional inductance L_F was to compensate for parasitic positive inductance at NIC input, as already explained in section

5.1.4. Parallel RL structure that shows non-Foster-like behavior, was then loaded in series with OCS port of Linvill negative resistance (Figure 5-38).

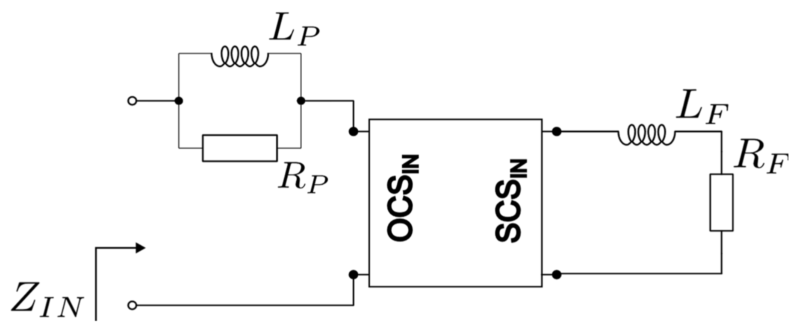

Figure 5-38 Compensated series RL structure loaded with OCS negative resistance.

We again attempted to design and test stability properties of two versions of negative capacitance: for operation in 2 GHz L band (Figure 5-39, Figure 5-40) and in 10 GHz X band (Figure 5-41, Figure 5-42). It can be concluded that main properties of this negative capacitor are similar to the properties of previously discussed non-Foster elements based on compensated passive networks. It is possible to optimize it either for minimal dispersion or for maximal Q Most importantly, the stability properties are again better than stability properties of external passive network.

a)

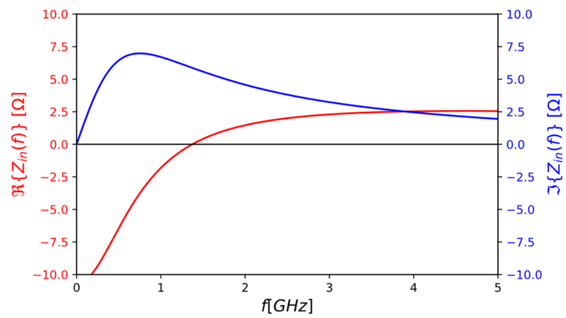

b)

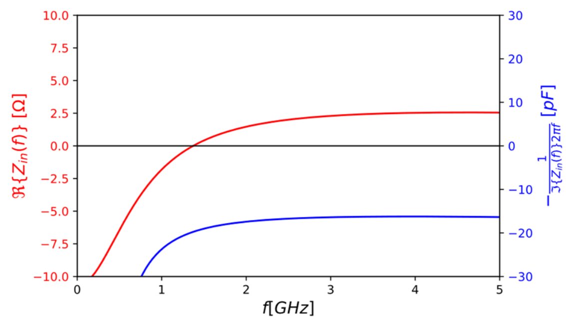

c)

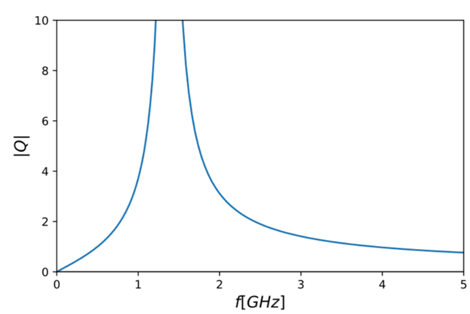

Figure 5-39 a) Real and imaginary part of input impedance of parallel C_P and R_P , compensated by OCS negative resistance. b) Equivalent resistance and negative inductance. c) Quality factor Q of the circuit. Plots are obtained with $R_P = 14\ \Omega$, $L_P = 2.96$ nH, $R_F = 54.5\ \Omega$, $L_F = 210$ pH

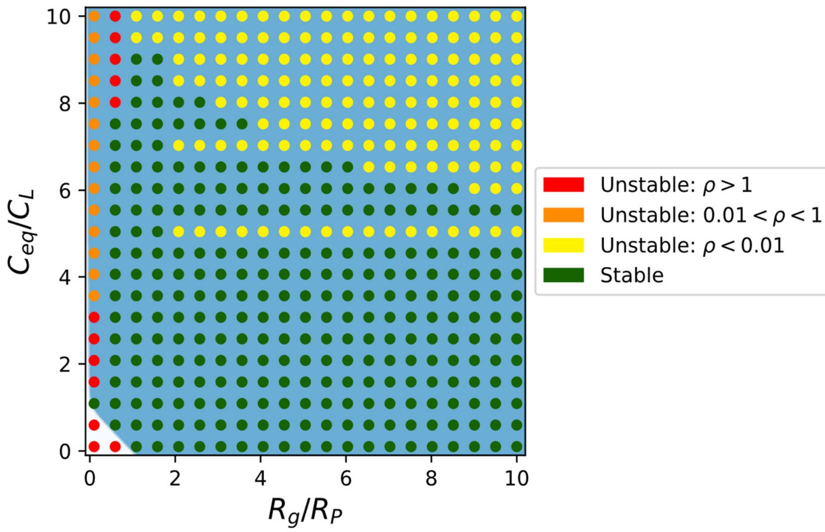

Figure 5-40 Stability area plot of compensated RC network loaded with positive inductance. Plot is generated $R_P = 14\ \Omega$, $L_P = 2.96$ nH, $R_F = 54.5\ \Omega$, $L_F = 210$ pH. Painted areas are calculated using simplified analytical approach (Dark blue – range of external impedances that cause stable operation; Light blue - range of external impedances that cause unstable operation). Colored dots are results predicted by commercial system identification software tool STAN™.

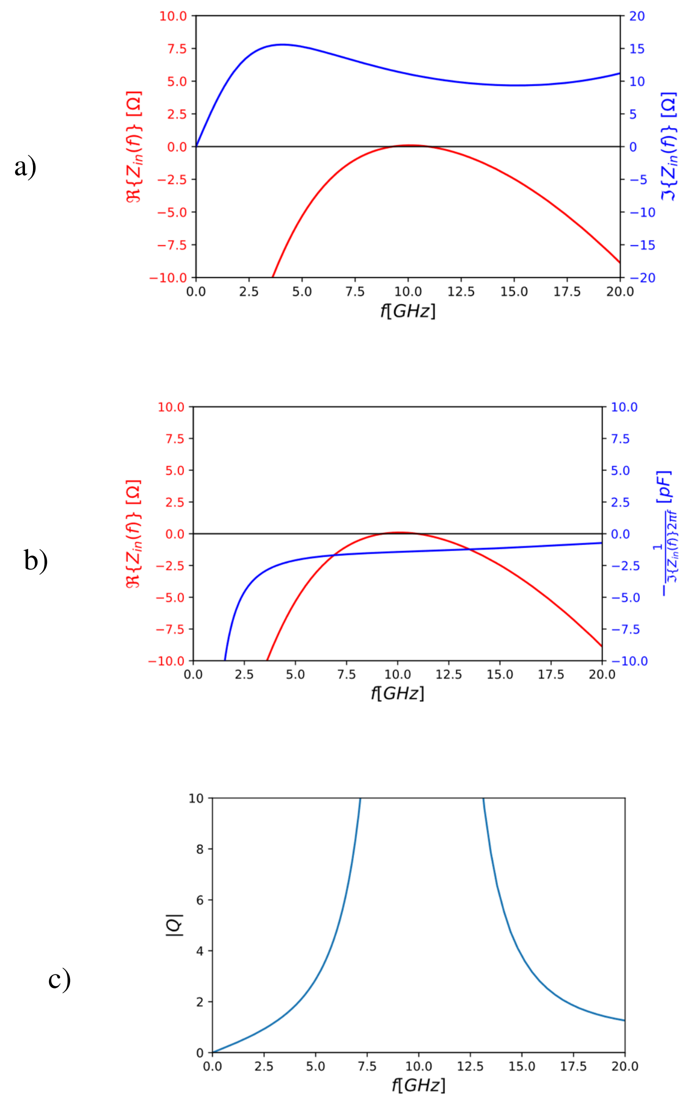

Figure 5-41 a) Real and imaginary part of input impedance of parallel C_P and R_P compensated by OCS negative resistance. b) Equivalent resistance and negative inductance. c) Quality factor Q of the circuit. Plots have been obtained with $R_P = 31.4\ \Omega$, $L_P = 1.22$ nH, $R_F = 70.5\ \Omega$, $L_F = 320$ pH.

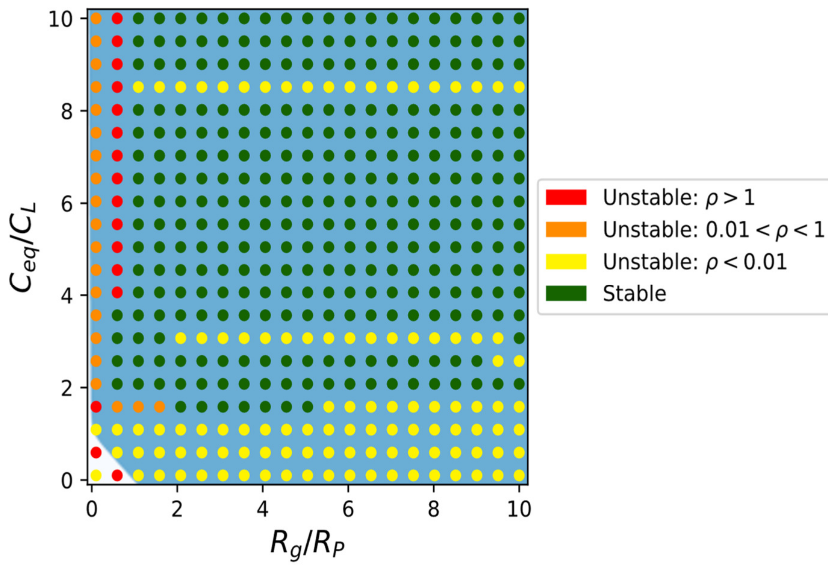

Figure 5-42 Stability area plot of compensated RC network loaded with positive inductance. Plot has been generated using: $R_P = 31.4\ \Omega$, $L_P = 1.22$ nH, $R_F = 70.5\ \Omega$, $L_F = 320$ pH. Painted areas are calculated using simplified analytical approach (Dark blue – range of external impedances that cause stable operation; Light blue - range of external impedances that cause unstable operation). Colored dots are results predicted by commercial system identification software tool STAN™.

One can conclude that, in above discussion, four novel types of non-Foster elements, based on compensated passive networks have been proposed (Figure 5-43).

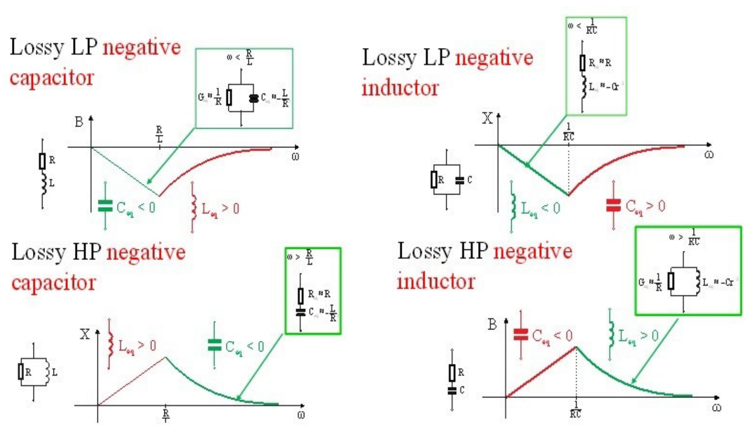

Figure 5-43 An overview of simple passive networks used for construction of stability-robust non-Foster elements.

The most important findings are summarized below:

- An imaginary part of equivalent admittance/impedance of simple series/parallel passive lossy networks (series RL and RC networks and parallel RL and RC networks) obeys non-Foster-like behavior.
- Non-Foster like behavior occurs within limited frequency band, which has either low-pass or high-pass behavior.
- If a circuit is loaded with negative conductance/resistance, it is possible to construct four classes of non-Foster elements (low-pass negative inductor, low-pass negative capacitor, high-pass negative inductor, high-pass negative capacitor).
- Stability properties of proposed novel designs are significantly better than stability properties of any designs from the literature.
- It is possible to use proposed novel circuits in RF tunable/broadband RF device. It was shown by four design examples (L-band and X-band low-pass and high-pass negative capacitors and negative inductors), in 40 nm CMOS technology.

Chapter 6. APPLICATIONS IN RF TUNABLE/WIDEBAND NETWORKS

Applications in RF tunable/wideband networks

6.1. General purpose RF Miller negative capacitor in HBCT technology

(*The results presented in Section 6.1 were achieved in collaboration with D. Muha from Metamaterials group and J. Žiljak, M. Koričić, and T. Suligoj, from Micro & Nano electronics lab, University of Zagreb, Faculty of Electrical Engineering and Computing).

As discussed in Section 4.1.4. there are discrete NIC/NII circuits realizations in OPamp technology, which are used at very low frequencies. Similar devices were used in some prototypes in our previous EOARD projects[27][43][44] and associated Miller NICs were able to operate in very broad frequency range (100 kHz -700 MHz). Clearly, this was a consequence of very carefully designed strong negative feedback that assures almost 'flat' gain, and, in turn, negligible values of parasitic impedance/admittance. It is interesting that there is no attempt of designing some kind of MMIC 'OPamp-like' NIC amplifier in the literature. Such as amplifier would eventually enable construction of Miler NIC with low conversion error, at microwave frequencies. Here we report a first step towards this goal by design and fabrication of Miler negative capacitor in HCBT technology, operating from DC to 2GHz.

A basic idea is sketched in Figure 6-1. It depicts very basic ('rudimentary') OPamp-like configuration that uses HCBT technology [1]. The unit HCBTs used in design have the emitter area of 0.1×1.8 μm^2. The collector current of the unit HCBT is 200 μA, and base-emiter voltage is 0.9 V, assuring f_T of approximately 45 GHz. Amplifier gain is adjusted by negative feedback resistors R_F and R_3. A load capacitor C_F is placed in positive feedback loop, which is responsible for generation of negative capacitance.

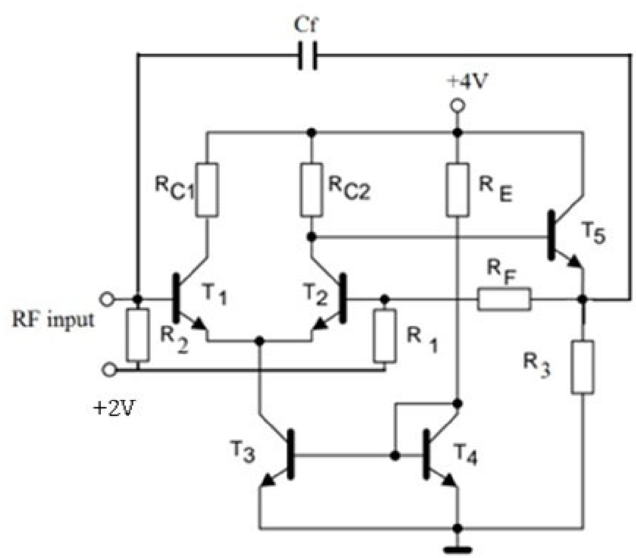

Figure 6-1 Simple SCS Miller negative capacitor that mimics low-freqeuncy OPamp approach. The circuit is designed in HCBT technology.

A photo of fabricated chip as is shown in Figure 6-2.

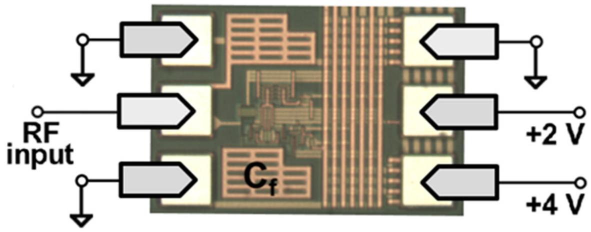

Figure 6-2 A microphotograph of fabricated SCS Miller negative capacitor that mimics low-frequency OPamp approach.

The RF input is at the left side of the chip while the feedback capacitor C_F (300 fF) is located at the bottom. There is also additional 'swamping' capacitor that prevents instabilities during testing. The capacitors are implemented by two aluminum metal layers of standard CMOS interconnect fabrication. The intermetal oxide layer between them serves as capacitor dielectric. The relatively small metal layer thickness (d = 0.5 um) and proximity of the silicon substrate limits the quality factor and the area of the capacitors. The oxide layer between the metal layers has dielectric constant ε_r=4 and the thickness of 0.75 um. The total stabilization capacitance (a

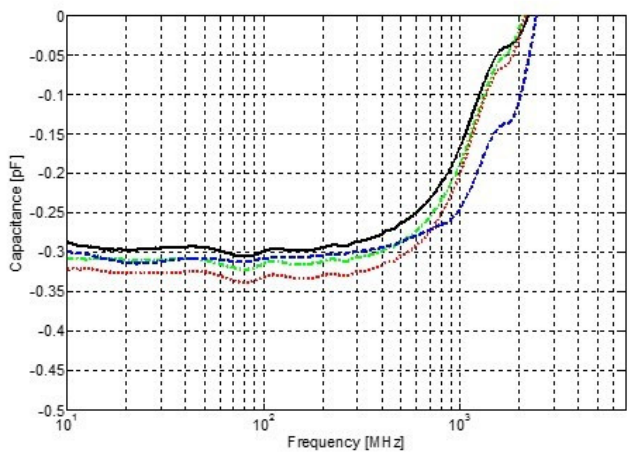

Figure 6-3 Measured input capacitance of SCS Miller negative capacitor integrated circut with HCBTs with different f_T (f_T=33 GHz – dash-dotted green curve, solid black, f_T=35 GHz –solid black curve, f_T=36 GHz –dotted red curve, ft=45GHz, –dotted blue curve.

shunt combination of 'swamping' capacitance and contact pad capacitance is 700 fF. A representative sample of measuring results is shown in Figure 6-3.

It can be seen that the NIC generates negative capacitance up to 2 GHz, while 'flat' nearly dispersion-less operation is possible up to 1 GHz. These results are similar to their low-frequency counter-parts, presented in [27][43][44]. Thr results are also compatible with widely-used $f_p/10$ 'rule of thumb' (f_p being the freqeuncy of the first pole) and can be improved by the use of floating Linvill topology.

6.2. General purpose RF Kolev tunable negative inductor in CMOS technology

Idea of variable negative inductance was tested for use in 40 nm CMOS technology by loading Kolev design of NII with varactor diode Figure 6-6.

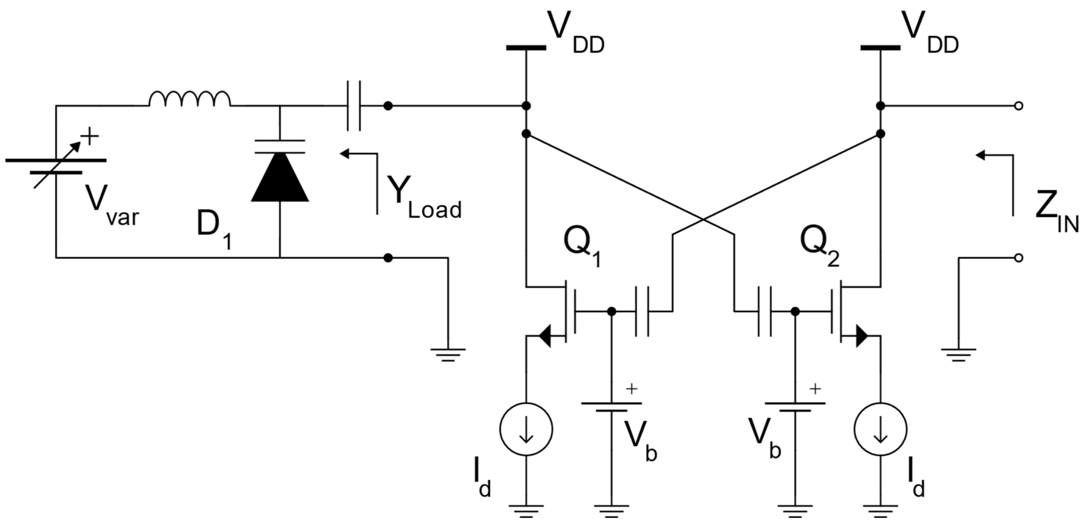

Figure 6-4 RF Kolev tunable negative inductor in 40 nm CMOS technology. Gate bias networks are omitted for clarity. $Q_1 = Q_2$: W = 32 · 2 µm = 64 µm, L = 40 nm. D_1: W = 2 µm, L = 2 µm, multiplier = 20

Negative impedance inverter was chosen as it allows us to design negative inductance without of use of inductor making this realization suitable for radio frequency integrated circuits. In the first step we modified the Linvill NIC used in Chapter 5 to work in grounded NII configuration. Dimensions of the transistors where kept the same ($Q_1 = Q_2: W = 2\ \mu m \cdot 32 = 64\ \mu m, L = 40\ nm$) to achieve large transconductance and high transfer frequency ($f_t = 125\ GHz$). Designed NII was loaded with varactor diode with capacitance range $7\ fF - 47\ fF, (-1.1V: 1.1V)$ ($W = L = 2\ \mu m$), with 20 diodes in parallel so the total range of the diode is $140\ fF - 940\ fF$. The varactor diode was biased with simple bias tee in the voltage range $-1.1V: 1.1V$. Circuit was simulated using Cadence™ simulations and values of input negative inductance and resistance where extracted ($L_{in}(f) = \Im\{Z_{in}(f)\}/2\pi f,\ R_{in}(f) = \Re\{Z_{in}(f)\}$) and plotted (Figure 6-5). Plot of extracted negative inductance shows variation from $-350\ pH: -85\ pH$ that is flat up to 10 GHz. For smaller values of load capacitance acquired values of input negative inductance stay flat up to 40 GHz (black lines in Figure 6-5). Parasitic resistance present at the input of NII (full lines in Figure 6-5) are consequence of the transformation characteristic of the NII (similar to the transformation characteristic of the NIC as discussed throughout Chapter 5), and it depends on the value of load capacitance. For this reason, the input resistance changes slope depending on the value of the load capacitance (determined by bias voltage).

Consequence of the change in the slope of the input resistance curve is the change of the frequency where we have the maximum value of quality factor, as the zero-crossing frequency of resistance curve changes. This could be mitigated by modeling a varactor diode with equivalent lumped element network and designing appropriate loading network to compensate for parasitic elements (similar to approach outlined in Chapter 5). Nevertheless, results obtained with simple load varactor diode still show very good results.

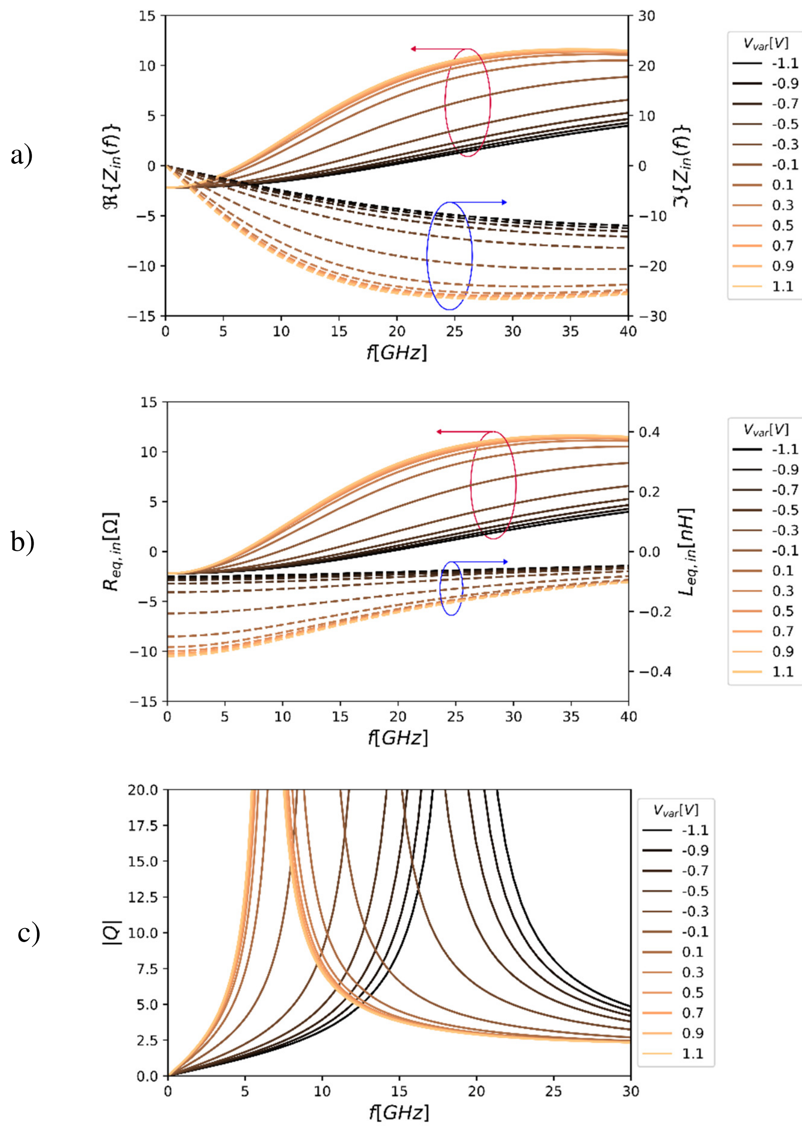

Figure 6-5 Tunable variable inductor obtained with Kolev NIV a) Real and imaginary part of input impedance . b) Equivalent resistance and negative inductance. c) Quality factor Q of the circuit.

To further explore the possibilities of this approach, we have decided to design floating variable negative inductance. To achieve this we have simply mirrored existing design to get the floating circuit Figure 6-6 Floating variable negative inductance, designed in 40 nm CMOS technology. Gate bias networks are omitted for clarity $Q_1 = Q_2$: W = 32 · 2 µm = 64 µm, L = 40 nm. D_1: W = 2 µm, L = 2 µm, multiplier = 20. The dimensions of the transistors and varactor diode where kept the same. The circuit was simulated using the same methodology as in the previous, single-ended case. Simulated results are plotted in Figure 6-7, where we see identical results to the one shown in Figure 6-5.

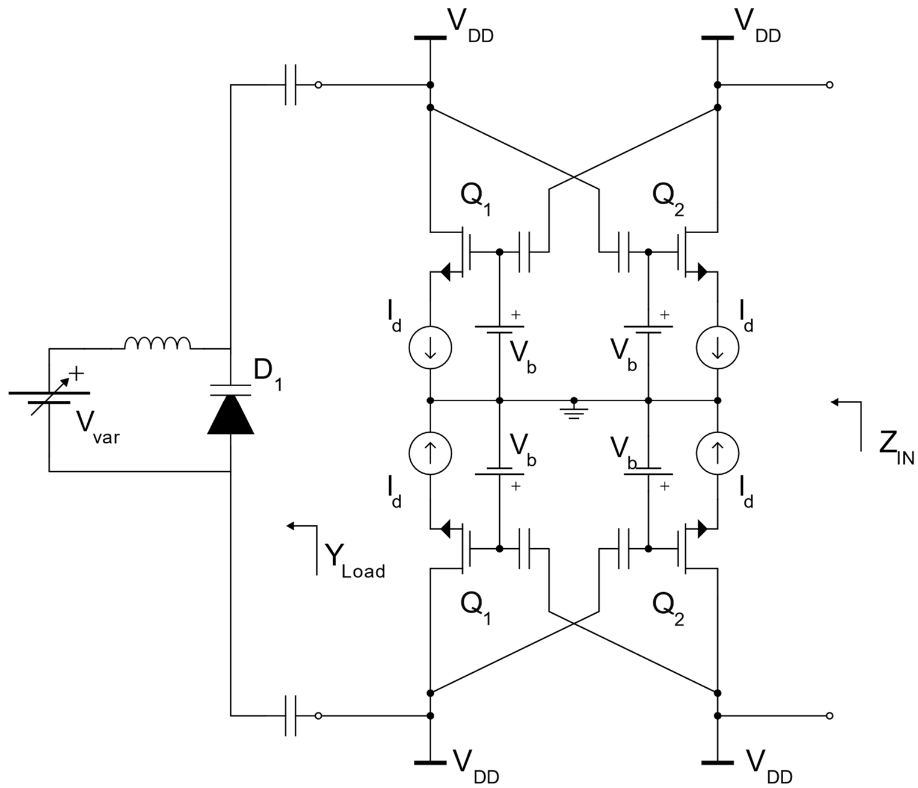

Figure 6-6 Floating variable negative inductance, designed in 40 nm CMOS technology. Gate bias networks are omitted for clarity $Q_1 = Q_2$: W = 32 · 2 µm = 64 µm, L = 40 nm. D_1: W = 2 µm, L = 2 µm, multiplier = 20

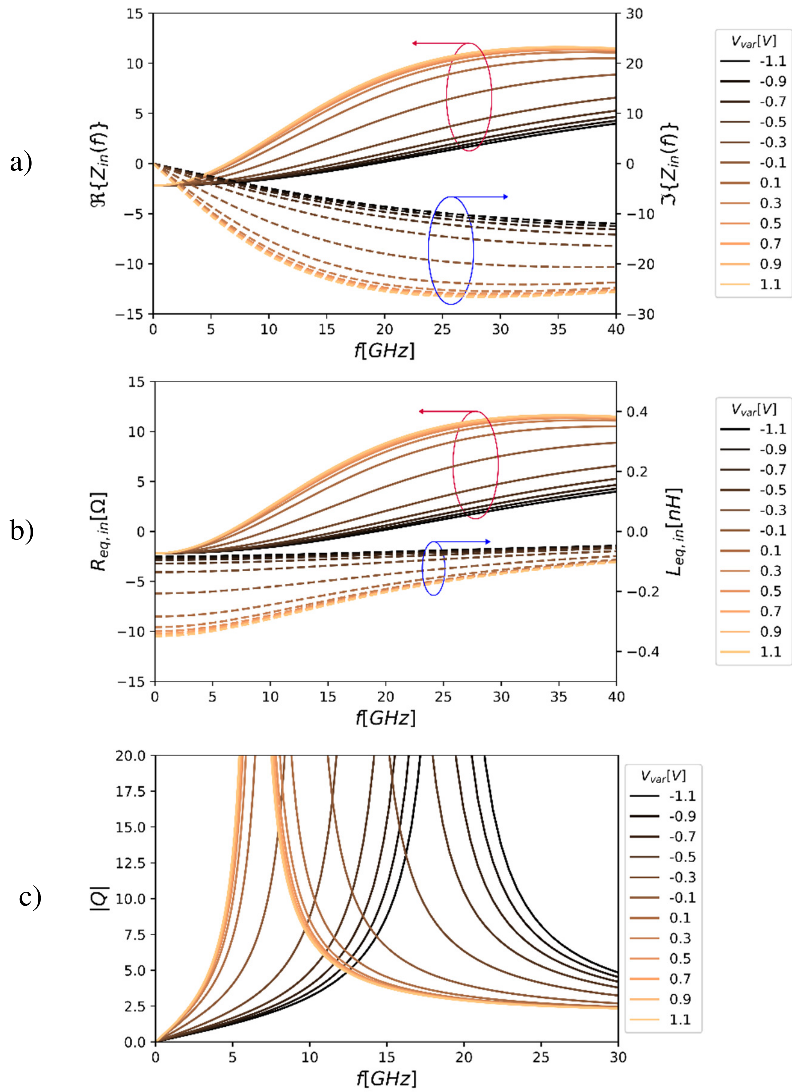

Figure 6-7 Tunable variable inductor obtained with Kolev NIV a) Real and imaginary part of input impedance . b) Equivalent resistance and negative inductance. c) Quality factor Q of the circuit..

6.3. Tunable bandpass filter with negative-capacitor-based inverter in CMOS technology

As it was discussed in Introduction and Section 2.1, there is a need for RF tunable filters and – tunable matching networks [9]. Such a structure usually comprises several resonant circuits that are mutually isolated by impedance inverters.

Impedance inverters are inevitable components of almost every multi-stage filter [127][128][129]. Conventional designs employing passive reactive elements or transmission lines (i.e. Foster networks) are inherently narrowband. Furthermore, they suffer from limited impedance transformation to external networks (resonators), which may cause poor matching properties of the associated filter. Furthermore, in the case of a tunable filter, narrowband inverter properties may limit tunability of the central frequency and bandwidth. Few years back, it was suggested that an inverter may also be constructed using non-Foster elements, which may enhance the system performances [128].

Therefore, we present a tunable wideband bandpass filter with a negative capacitor based impedance inverter. The filter is of Chebyshev two-pole bandpass type and it comprises series LC-resonators mutually coupled via impedance inverter (Figure 6-8a).

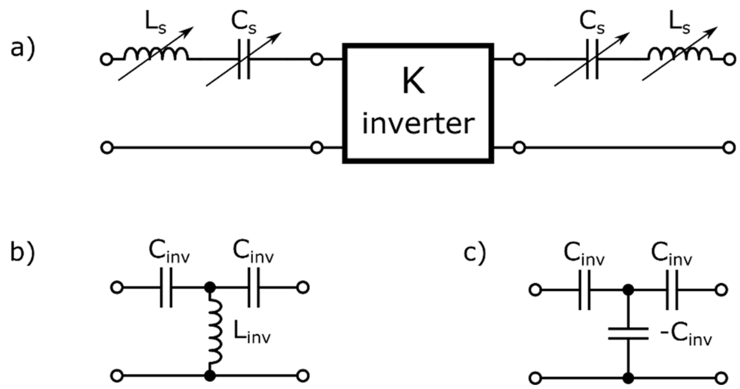

Figure 6-8 (a) Circuit diagram of a two-pole bandpass filter with an impedance inverter and two LC-resonators (L_sC_s). (b) Realization of a T-circuit impedance inverter where an equivalent inductor L_{inv} is used for the shunt branch. (c) Realization of an impedance inverter comprising two positive capacitors (C_{inv}) located in series branch and a negative ($-C_{inv}$) capacitor located in the shunt branch.

Ideal impedance inverters are used to isolate neighboring resonators and provide a ±90° phase shift (depending on the realization). Practical impedance inverter from Figure 6-8a can be realized with a T-circuit made out of 3 capacitors, where the sign of the capacitors in either series or shunt branch is 'flipped' with regards to the other branch. Thus, either capacitors in series branches are negative and a capacitor in shunt branch is positive, or vice-versa. We opted for the realization with only one negative capacitor located in the shunt branch. This allows use of grounded NIC/NII circuits, and, furthermore, avoids that the series negative capacitors get 'absorbed', by the capacitors C_s of the LC resonators.

A common limitation of an impedance inverter is its limited operating frequency of ±10% around central frequency, due to the variation of the input impedance, thus making them narrowband. For comparison presented here, we tested this implementation of the filter from Figure 6-8a. with the negative capacitor realized by: (i) a positive inductance L_{inv} (with the value of admittance being equal to the corresponding value of negative capacitance at the central frequency, so $L_{inv}=1/\omega^2 C_{inv}$ (f_0=2.45 GHz) (Figure 6-8b); (ii) ideal dispersionless negative capacitor (Figure 6-8c); and (iii) a realization of the negative capacitance based on OCS NIC compensated passive RL network (depicted in Figure 5-38 and extensively discussed in Section 5.4.1., Figure 6-9e and Figure 6-9f).

Design methodology of two-pole Chebyshev filter can be found in standard textbooks such as [127]. In addition, a possible application of non-Foster elements in these type of filters is discussed in several recent papers [107][129].

Calculated values of filter elements are given in Table 6-1, Table 6-2 and Table 6-3, depending on the used inverter, with K being the transformation factor between the load and input impedance ($Z_{in}=K^2/Z_{load}$ or $K=1/\omega C_{inv}$). Taking C_{inv} of 1.15pF yields K=56.48Ω at 2.45 GHz.

In Figure 6-9 we present the comparison between different implementations of the impedance inverter used in the filter: (i) using ordinary inductor for the place of negative capacitor (Figure 6-9a and Figure 6-9b), (ii) ideal dispersionless negative conductor (Figure 6-9c and Figure 6-9d) and (iii) a stable negative capacitance based on OCS NIC compensated passive RL network, depicted in Figure 5-38 and described in chapter 5.4.1. Values of used elements for designed negative capacitance are given in Table 6-3. In each of the three cases we started with a central frequency of 2.45 GHz and 10% bandwidth. Thus, the values of LC-resonators are different between each case but show the best obtainable possibilities of each case.

In the case of a 2-pole filter with a K-inverter made using an inductor L_{inv} in the shunt branch in place of a negative capacitor (Figure 6-8b, Figure 6-9a and Figure 6-9b), we have limited tunability of the bandwidth and central frequency, as expected. This is because an inductor can represent a negative capacitor only at a single frequency, as a consequence of basic energy-dispersion constraints. Clearly, dispersion characteristics of these two realizations of inverters are fundamentally different. For example, at a lower frequency an inductor placed in place of a negative capacitor will 'act' as a capacitor with larger capacitance, while at a higher frequency it will 'act' as a capacitor with smaller capacitance, further diminishing the matching of the inductor and deteriorating filter performances. Let us take a reasonable limit for usability of such a filter as a bandwidth of 10% (at least) and abs (S_{11}) <15dB. Looking at Figure 6-9a and Figure 6-9b, we see that for the inverter that uses an inductor in place of a negative capacitor, possible change of the central frequency is limited to 10% tunability of the central operating frequency and to 30% of fractional bandwidth ($\Delta f/f_0$). Additionally, the frequency characteristics are not symmetrical. Values of the parameters are given for this case are given in Table 6-1.

Cinv, pF	Linv [nH]	f0, GHz	Δf/f0, %	Ls, nH	Cs, pF
1.15	3.67	2.45	10	22.5	0.194
			20	9.64	0.517
			30	5.55	1.26
		2.205 (10% lower)	-9 / +11.2	22.5	0.243
		2.695 (10% higher)	-9.2 / +11.13	22.5	0.152

Table 6-1 Values of used filter parameters for the inverter using an inductor Linv instead of a negative capacitor.

Let us now look at the frequency characteristics given in Figure 6-9c and Figure 6-9d for the case where the K-inverter in the filter contains an ideal, dispersionless negative capacitor ($-C_{inv}$), as presented in Figure 6-8a and Figure 6-8c. We immediately find that, when compared to the previous case using an inductor instead of a negative capacitor, the frequency characteristics are symmetrical, owing to the same dispersion of the used capacitors in the inverter. Return loss (Figure 6-9c) is approximately -20dB for 10, 20 and 30% of fractional bandwidth. However, the tunability of the central frequency is limited to 10% (Figure 6-9d). Tunability is limited due to a decrease in the return loss at lower frequencies. One should bear in mind that an ideal, dispersionless capacitor is not causal and, therefore, cannot be constructed in practice. So, practical designs may have small, but inevitable dispersion that spoils predicted ideal results. Values of the parameters for this design case are given in Table 6-2.

C_{inv}, pF	f_0, GHz	$\Delta f/f_0$ %	L_s, nH	C_s, pF
1.15	2.45	10	25.5	0.164
		20	12.9	0.316
		30	8.5	0.464
	2.205 (10% lower)	-12.7 / +12.6	25.5	0.202
	2.695 (10% higher)	-8.12 / +8.64	25.5	0.135

Table 6-2 Values of filter parameters for the inverter using an ideal, dispersionless negative capacitor.

For the case of negative capacitance based on OCS NIC compensated passive RL network from chapter 5.4.1. used in the K-inverter, the frequency characteristics of the proposed filter are given in Figure 6-9e and Figure 6-9f. The return loss is slightly worse than one in the case of an ideal negative capacitor. This happens due to additional losses in the system (one cannot get negative capacitance without some accompanying loss/gain) in the form of a 'parasitic' real part of impedance. We can see that the frequency characteristics are symmetrical and rather similar to the case where an ideal negative capacitor was used. In Figure 6-9f we can see that the tunability of the central frequency is much larger than in all previous cases. Range of tunability of the central operating frequency is 20% (the shift towards lower and higher frequencies). We also noticed that the bandwidth is larger than one observed in the case of an ideal negative capacitor. Interestingly, the symmetry of the bandpass curve is maintained over the whole tuning bandwidth. Designed negative capacitance surely has some dispersion, but this can be controlled with the value of the resistor at the NIC load (this can be thought of as an additional degree of freedom).

Values of the filter parameters and negative capacitance values are given in Table 6-3. In order to keep the symmetry of the bandpass curve we slightly tuned R_{FL}, in order to keep the negative capacitance working in the regime of small positive parasitic resistance (R_{eq}>0).

C_{inv}, pF	f_0, GHz	$\Delta f/f_0$ %	L_s, nH	C_s, pF	R_{FL}, Ω	C_{eq} at f_0, pF	R_{eq} at f_0, Ω
1.15	2.45	10	25.4	0.166	157	-1.183	2.996
		20	12.56	0.337	154	-1.193	5.314
		30	8.17	0.529	149.7	-1.208	8.639
	2.205 (10% lower)	-10.88 / +11.93	25.4	0.206	151	-1.281	3.237
	1.96 (20% lower)	-13 / +13.2	25.4	0.27	142.2	-1.408	4.559
	2.695 (10% higher)	-8.7 / +9	25.4	0.139	162.8	-1.098	2.068
	2.94 (20% higher)	-7.84 / +8.06	25.4	0.114	167	-1.026	1.723

Table 6-3 Values of filter parameters for the inverter using an high pass OCS negative capacitor with equivalent values of generated negative capacitance C_{eq} and R_{eq}. Values for the negative capacitance in Figure 5-38 in chapter 5.4.1. are L_p=15nH, R_p=120Ω, for the passive negative capacitance and values for the loss compensation NIC load are L_{FL}=0.72nH, with R_{FL} given in the table (value was adjusted to give symmetric shape to S_{11}).

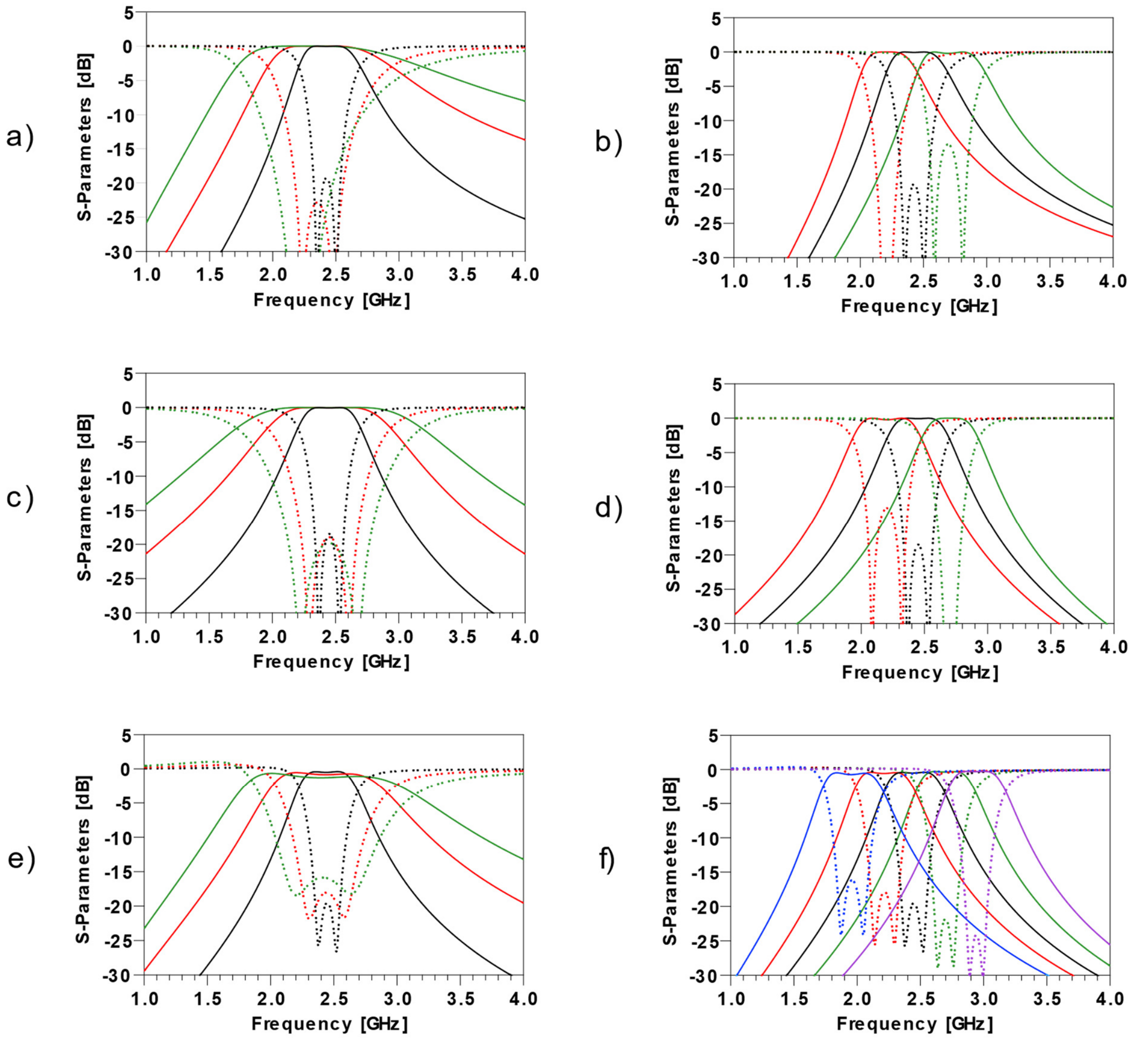

Figure 6-9 Frequency characteristics of different realizations of the proposed filter (S21 in solid lines, S11 in dotted lines). (a) Change of fractional bandwidth for the K-inverter using an inductor (10% black, 20% red, 30% green) and (b) tuning of central frequency (in black) 10% lower (red) and 10% higher (green). (c) Change of fractional bandwidth for the K-inverter using an ideal, dispersionless negative capacitor (10% black, 20% red, 30% green) and (d) tuning of central frequency (in black) 10% lower (red) and 10% higher (green). (e) Change of fractional bandwidth for the K-inverter using loss-compensated negative capacitance from chapter 5.4.1. (10% black, 20% red, 30% green) and (f) tuning of central frequency (in black) 10% lower (red), 20% lower (blue), 10% higher (green) and 20% higher (purple).

Lastly, in Figure 6-10 we present the stability analysis of the whole filter depicted in Figure 6-8a where the inverter comprises a loss-compensated negative capacitance (design given in chapter 5.4.1.). Stability was tested using a commercial system identification tool STAN^{TM} for a range of presented values of parameters.

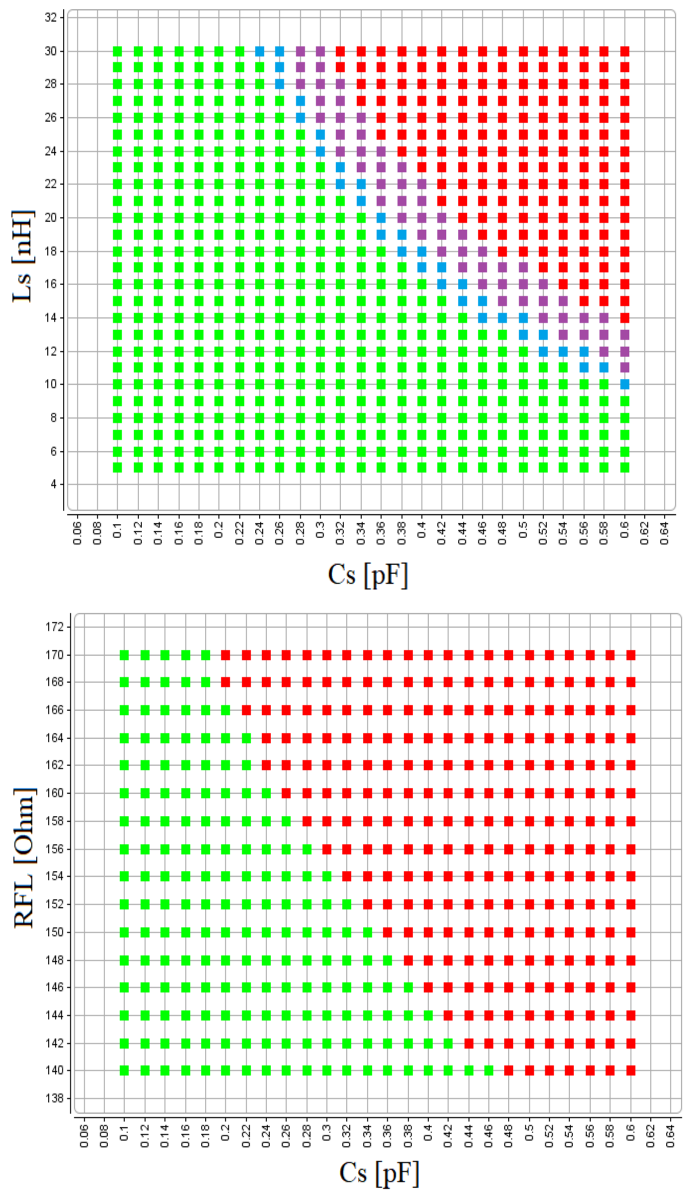

Figure 6-10 Stability analysis of the proposed tunable filter. The results are presented with respect to: (upper) Change of LC-resonator values C_s and L_s depicting the change of fractional bandwidth obtainable while having stable operating conditions. For R_{FL}=157Ω only green part is stable, while others are unstable, for R_{FL}=154Ω both blue and green are stable combinations while purple and red are unstable and for R_{FL}=149Ω only red part is unstable while all rest depict stable operations. (lower) Change of LC-resonator capacitor Cs and R_{FL} used in the negative capacitance depicting the tunability of the central frequency.

Shortly, we have demonstrated tunability of the center frequency up to 20% and bandwidth up to 30%, with return loss of more than 15 dB. A very important feature is that the symmetry of the bandpass curve is maintained over the tuning bandwidth, which is not possible with a standard passive design. Additionally, it was found that proposed design of non-Foster capacitor based on compensated passive network is indeed stability-robust.

6.4. Possible applications in active antennas and PT-symmetry systems

In addition to applications in RF tunable/broadband networks, we have also found that the developed methodology can be extended to self-oscillating active antennas and PT -symmetric systems. These could be interesting topics for further projects in the future. Since these additional findings were not covered by the original research objectives, they are outside the scope of this report. However, they can be found in Appendix, which contains all publications produced during the course of the projects, with appropriate acknowledgements.

Chapter 7. CONCLUSIONS AND FUTURE WORK

Conclusions and future work

This study reports on a 24-month research effort whose fundamental goal is to develop a simple methodology for a design of stable broadband non-Foster matching networks for tunable RF devices such as filters and/or power amplifiers.

This research is certainly novel since it deals with three well-known problems in non-Foster technology of broadband matching:

- Selection the most stability-robust NIC/NII topology for every particular application
- Design of stable tunable negative inductance
- Design of stable non-Foster reactive matching network for wideband tunable MMIC filters

As far as we know, there are almost no publicly available studies on the above topics. In particular, the idea of a tunable broadband microwave non-Foster filter is still in its infancy, and there are almost no studies on it in the literature. If successful, the proposed efforts could pave the way for fabrication of broadband non-Foster-based RF devices such as filters, combiners, splitters, hybrid junctions, and PAs.

As a short summary, the realized outcomes of the project are:

- We have shown that all electronic circuits that mimic negative immittance (NICs and NIIs) rely on the superposition of the original signal and assisting signal. Since these signals must be coherent, all classical circuits use positive feedback, which often leads to instability. It is extremely important to make a clear distinction between electronic admittance (associated with SCS properties) and electronic impedance (associated with OCS properties). We have also shown that a simple one-pole model of the NIC/NII amplifier is a useful approximation for both prediction of dispersion properties for frequencies below the pole frequency and for stability predictions. It was found that the dispersion of all the circuits analyzed is negligible when the maximum operating frequency is below one-tenth of the frequency of the first pole. The "parasitic" real part of the input impedance/admittance of the negative capacitor/inductor is negative in the SCS design and positive in the OCS design. This "parasitic" conductance/resistance can be compensated by an additional passive load network.
- We have reviewed all known methods of stability prediction and proposed a simple, straightforward method to develop simple equivalent circuits for all one-pole non-Foster and negative elements. We have also studied the most common realizations of NIC/NII circuits and performed a very thorough analysis of their stability properties. As expected, the stability properties were found to depend on both the NIC/NII topology and the passive external network topology. It was found that both OCS and SCS DC coupled negative capacitors/inductors/resistors based on NICs or NIIs always have an unstable DC pole that degrades the stability robustness. In addition, the DC coupled negative OCS capacitor and negative SCS inductor have a pole at the origin that causes DC offset at the input. The overall conclusion is that there is no such thing as the "most robust NIC/NII topology", *per se*.

- We have investigated the possibilities of improving the stability properties and found that the introduction of a bandpass mode significantly improves the stability properties. It turns out that the operating bandwidth is always inversely proportional to the range of allowable external impedances, i.e., to the stability robustness. We have applied this finding to the well-known Linvill NIC and shown that the stability characteristics can be improved by adjusting the operating bandwidth through proper selection of cross-coupling capacitors. We have also developed a very simple and accurate equivalent circuit for this modified Linvill negative capacitor.
- We have presented a novel design of non-Foster and Negative elements based on some very simple LP and HP passive series/shunt networks that exhibit non-Foster 'inverse' dispersion such that they behave as band-limited 'lossy negative capacitors/inductors. The losses of these passive 'negative' networks can be compensated by an additional negative series/shunt resistance/conductance. These novel non-Foster elements have shown stability properties better than the stability properties of all classical (NIC/NIV-based) non-Foster elements in the literature. The correctness of the proposed approach has been verified using four independent designs of negative capacitors and negative inductors in L and X frequency bands, in 40-nm CMOS technology. The generated negative capacitance capacitances and negative inductance ranged from -0.5 pF to -1 pF and -1 nH to -5 nH, respectively.
- In addition, we have shown applications of the proposed non-Foster elements in some RF tunable/broadband devices. We have designed and fabricated a general negative Miler capacitor using HCBT technology that produces capacitance from -0.3 pF to -0.1 pF in the frequency range from DC to 2GHz. We have also developed a tunable negative inductor that can be tuned between -100 pH and -300 pH in the range of 5-15 GHz. Finally, we have developed a tunable non-Foster-based bandpass filter for the 2.5-GHz band using 40-nm CMOS technology. We have demonstrated tunability of the center frequency up to 20% and bandwidth up to 30%, with return loss of more than 15 dB. A very important feature is that the symmetry of the bandpass curve is maintained over the tuning bandwidth, which is not possible with a standard passive design.

In addition to applications in RF tunable/broadband networks, we have found that the developed methodology can be extended to self-oscillating active antennas, PT -symmetric systems, and time-varying systems. In future research projects, we plan to develop a general, unified methodology that can be used to design all of these systems .

Chapter 8. BIBLIOGRAPHY

Bibliography

[1] L. Larson, ``RF and microwave hardware challenges for future radio spectrum access," Proc. IEEE, Vol. 102, No. 3, pp. 321-333, March 2014
[2] D.M. Pozar, “Microwave Engineering”, Willey, 1998
[3] M. K. Kazimierczuk “RF Power Amplifiers”, 2nd edition, Willey, 2015.
[4] L. D. Landau, E. M. Lifshitz, “Electrodynamics of Continuous Media”, 2nd edition, Buttterwoth Heinmann, Oxford, 2002
[5] S. Tretyakov, “Meta-Materials with Wideband Negative Permittivity And Permeability”, Microwave Opt. Technol. Lett., Vol. 31, No. 3, pp. 163-165, 2001
[6] R. M. Foster, “A reactance theorem”, Bell Labs Syst. Tech. J., Vol. 3, No. 2, pp. 259-267, 1924
[7] S. Hrabar, “First Ten Years of Active Metamaterial Structures with ‘Negative’ Elements”, accepted to EPJ Applied Metamaterials Journal, 2018
[8] S. E. Sussman-Fort, “Non-Foster Impedance Matching of Electrically-Small Antennas”, IEEE Trans. Antennas and Propagation, Vol. 57, No. 8, pp. 2230-2241, August 2009
[9] R. Aigner, "Tunable filters? Reality check!", IEEE Microwave Magazine, Vol. 16, No. 7, pp. 82-88, August 2015.
[10] M. Latour, “Negative impedance device,” US Patent (US1 687 253A), Nov 20, 1923.
[11] M. M. Dolmage, “Negative resistance,” US Patent (1 863 566), Jan 13, 1927.
[12] R. C. Mathes, “Negative impedance circuit,” US Patent (US1 779 382A), Aug 1, 1927
[13] B. van der Pol, “A new transformation in alternating-current theory with an application to the theory of audition”, Radio Eng. Proc. Inst., Vol. 18, No. 2, pp. 220-230, 1930
[14] L. Verman, “Negative circuit constants”, Radio Eng. Proc. Inst., Vol. 19, No. 4, pp. 676–681, 1931
[15] J. L. Merrill, “Theory of the negative impedance converter”, Bell System Technical Journal, Vol. 30, No. 1, pp. 88–109, 1951
[16] J. G. Linvill, “Transistor negative impedance converters”, Proc. IRE, Vol. 41, pp. 725-729, June 1953
[17] A. K. Perry, “Broadband antenna systems realized from active circuit conjugate impedance matching”, AD-769 800, Naval Postgraduate School, Monterey, September 1973
[18] S. E. Sussman-Fort, “Matching Network Design Using Non-Foster Impedances”, Presentation slides
[19] S. E. Sussman-Fort, “Matching Network Design Using Non-Foster Impedances”, International Journal RF and Microwave CAE, Vol. 16, No. 2, pp. 135-142, March 2006
[20] G. Skahill, R. M. Ruish, et. al., “Electrically Small, Efficient, Wide-Band, Low-Noise Antenna Elements”, Proc. on the 1998 Antenna Applications Symposium (in AFRL-SN-RS-TR-1999-86 Final Technical Report), UMAS 1998, pp. 214- 213
[21] J. Aberle, R. Lomak, “Antennas with non-Foster Matching Networks”, Morgan & Claypool, 2007
[22] N. Zhu, R. W. Ziolkowski, “Broad-bandwidth electrically small antenna augmented with an internal non-Foster element”, IEEE Ant. Wirel. Propag. Lett., Vol. 11, pp. 1116-1120, 2012
[23] N. Zhu, R. W. Ziolkowski, “Broad bandwidth, electrically small, non-Foster element-augmented antenna designs, analyses, and measurements”, IEICE Tran. on Comm., Vol. 96, No. 10, pp. 2399-2409, 2013
[24] F. Albarracín-Vargas, V. Gonzalez-Posadas, F. Javier Herraíz-Martinez, D. Segovia-Vargas, “Design Method for Actively Matched Antennas with Non-Foster Elements”,

IEEE Tran. Ant. Prop., Vol. 64, No. 9, pp. 4118-4123, 2016
[25] H. Mirzaei, G. V. Eleftheriades, “A resonant printed monopole antenna with an embedded non-Foster matching network”, IEEE Trans. on Ant. and Prop., Vol. 61, No. 11, pp. 5363-5371, 2013
[26] O. O. Tade, “Negative impedance converter for antenna matching”, PhD thesis, University of Birmingham, 2014
[27] S. Hrabar, I. Krois, I., Bonic, A., Kiricenko, E. U. Munoz, “Broadband Epsilon-Near-Zero (ENZ) and Mu-Near-Zero (MNZ) Active Metamaterial”, Final Report for Contract FA 8655-10-1-3030, EOARD/AFRL, August 2011
[28] D. Muha, S. Hrabar, I. Krois, I. Bonic, A. Kiricenko, D. Zaluski, “Design of UHF Microstrip Non-Foster Leaky-wave Antenna”, Proc. on ICECOM (Dubrovnik, 2013), pp. 134.
[29] S. Hrabar, “Leaky-wave Antenna based on Non-Foster Metamaterial - Is Stable Operation Feasible?”, Proc. on IWAT (Seoul, 2015), pp. 7
[30] H. Mirzaei, G. V. Eleftheriades, “Arbitrary-angle squint-free beamforming in series-fed antenna arrays using non-Foster elements synthesized by negative-group-delay networks”, IEEE Trans. Ant. and Propag., Vol. 63, No. 5, pp. 1997-2010, 2015
[31] S. Keum-Su, R. G. Rojas, “Electrically small wire monopole antenna with Non-Foster impedance element”, Proceedings of the Fourth European Conference on Antennas and Propagation (EuCAP), pp. 1-4, 12-16, April 2010
[32] Z. Ning, R. W. Ziolkowsky, “Design and measurements of an electrically small, broad bandwidth, non-Foster circuit-augmented protractor antenna”, Appl. Phys. Lett. Vol. 101, No. 2, 024107, 2012
[33] L. Batel, L. Rudant, J. F. Pintos, A. Clemente, C. Delaveaud, K. Mahdjoubi, “High directive compact antenna with Non-Foster elements”, International Workshop on Antenna Technology (iWAT), Seoul, Republic of Korea, 4-6 March 2015
[34] M. M. Jacob, D. F. Sievenpiper, “Non-Foster matched antennas for high-power Applications”, IEEE Tran, on Antennas and Propagation, Vol. 65, pp. 4461-4469, 2017
[35] S. Hrabar, T. Debogovic, “Broadband Fabry-Pérot antenna with non-Foster metasurface - how to test the basic idea?”, Antennas and Propagation & USNC/URSI National Radio Science Meeting, 2015 IEEE International Symposium, pp. 798-799, July 2015
[36] A. Ghadiri, K. Moez, Ghadiri, “Gain-Enhanced Distributed Amplifier Using Negative Capacitance”, Circuits and Systems I: Regular Papers, IEEE Transactions on, pp. 2834–2843, Vol. 57, Issue: 11, November 2010
[37] 10. Q. Wu, T.K. Quach, A. Mattamana et al. “Frequency tuning range extension in LC-VCOs using negative-capacitance circuits”, IEEE Trans. Circuits Syst. II: Express Briefs, Vol. 60, No. 4, pp. 182-186, April 2013
[38] Q. Wu, “Analysis and Design of Wide Tuning Range Low Phase Noise mm-wave LC-VCOs”, Ph.D. thesis, The Ohio State University, 2013.
[39] S. Kolev, B. Delacressonniere, J. Gautier, “Using a Negative Capacitance to Increase the Tuning Range of a Varactor Diode in MMIC Technology”, IEEE Tran. on Microw. Theory and Tech., Vol. 49, No. 12, pp. 2425-2430, 2001
[40] M. W. Yung, D. A Hitko, “Non-Foster Impedance Power Amplifier”, US patent 8,374,561 B1
[41] S. Lee, H. Park, K. Choi, Y. Kwon, “A Broadband GaN pHEMT Power Amplifier Using Non-Foster Matching”, IEEE Trans. Microw. Theory Tech, Vol. 63, No. 12, pp. 4406-4413, December 2015.

[42] D. Kholodnyak, “The State of the Art of Electronically Tunable Compact Bandpass Filters Design”, 2017 IEEE MTT-S International Microwave and RF Conference, pp. 263-266, 2017.

[43] S. Hrabar, I. Krois, I. Bonic, A. Kiricenko, D. Muha, “Active Reconfigurable Metamaterial Unit Cell Based on Non-Foster Elements”, Final Report for Contract FA8655-12-1-2081, EOARD /AFRL, October 2013

[44] S. Hrabar, I. Krois, J. Loncar,L. Vincelj, “Non-Foster Source-load Networks and Metasurfaces”, EOARD/AFRL, Final Report for Contract FA9550-15-1- 0120, EOARD /AFRL, July 2018

[45] N. Engheta, R. Ziolkowsky, (ed.), “Metamaterials: Physics and Engineering Explorations”, Wiley 2006

[46] G. V. Eleftheriades, K.G. Balman, (ed.), “Negative Refraction Metamaterials: Fundamental Principles and Applications”, Wiley 2005

[47] C. Caloz, T. Itoh, “Electromagnetic Metamaterials: Transmission Line Theory and Microwave Applications”, Wiley 2006

[48] H.-T. Chen, A. J. Taylor, N. Yu, “A review of metasurfaces: physics and applications”, Reports on progress in physics, Vol. 79, No. 7, pp. 1-40, 2016

[49] S. Hrabar, I. Krois, B. Ivsic, D. Zaluski, G. Pavlaković, “Active Dispersionless ‘Plasmonic’ Metamaterial - a Step Towards Broadband Cloaking”, Proc. of the 2008 IEEE AP-S International Symposium and USNC/URSI National Radio Science Meeting, pp. 203-20, San Diego, 2008

[50] S. Hrabar, “Active Dispersionless Metamaterials - a Path towards Broadband Cloaking”, Proc. on 2009 REME Workshop, pp. 108, Madrid, 2009

[51] S. Hrabar, I. Krois, A. Kiricenko, “Towards Active Dispersionless ENZ Metamaterial for Cloaking Applications”, Metamaterials, Vol. 4, No. 2-3, pp. 89-97, August-September 2010

[52] J. C. Soric, A. Alù, “Wideband tunable and non-Foster mantle cloaks”, presented at USNC-URSI Nat Radio Sci Meeting, Boulder, CO, USA, January 8–12, 2014

[53] S. Hrabar, Z. Sipus, I. Malcic, “Broadening of cloaking bandwidth by passive and active techniques”, A chapter in ‘Transformation Electromagnetics and Metamaterials', D. Werner, D. Kwon (editors), Springer, London, 2013

[54] P. Y. Chen, C. Argyropoulos, A. Alù, “Broadening the cloaking bandwidth with non-Foster metasurfaces”, Phys. Rev. Lett., Vol. 111, 23-6, 233001-1~233001-5, 2013

[55] S. A. Tretyakov, T. G. Kharina, “The perfectly matched layer as a synthetic material with active inclusions”, Electromagnetics, Vol. 20, No. 2, pp. 155-166, 2000

[56] F. Auzanneau, R. W. Ziolkowski, “Artificial composite materials consisting of nonlinearly loaded electrically small antennas: Operational-amplifier-based circuits with applications to smart skins”, IEEE Tran. on Antennas and Propagation, Vol. 47, No. 8, pp. 1330-1339, 1999

[57] S. Hrabar, “Active non-Foster Metamaterials: From Intriguing Background Physics to Real-world Applications”, A plenary talk, Proc. on Metamaterials Congress, pp. 601-603, Sankt Petersburg, 2012

[58] S. Hrabar, “Active radiofrequency metamaterial structures — Pros, cons and future trends”, Proc. on Metamaterials Congress, pp. 418, Oxford, 2015

[59] B. Okorn, S. Hrabar, I. Krois, “Investigation of basic physics of non-Foster negative capacitance in time domain”, Proc. on ELMAR, pp. 373, Zadar, 2011

[60] B. Okorn, S. Hrabar, I. Krois, “Physically sound model of a non-Foster negative capacitor”, Automatika: Journal for Control, Measurement, Electronics, Computing and Communications, Vol. 55, No. 2, pp. 244-252, 2017

[61] S. Hrabar, I. Krois, I. Bonic, A. Kiricenko, “Negative Capacitor Paves the way to Ultra-broadband Metamaterials”, Appl. Phys. Lett., Vol. 99, No. 25, 25403~25403-4, 2011

[62] S. Hrabar, I. Krois, I. Bonic, A. Kiricenko, “Ultra-broadband simultaneous superluminal phase and group velocities in non-Foster epsilon-near-zero metamaterial”, Appl. Phys. Lett., Vol. 102, No. 5, 05408-1~05408-5, 2013

[63] J. Long, M. Jacob, D. Sievenpiper, “Broadband fast-wave propagation in a non-Foster circuit loaded waveguide”, IEEE Trans. Microw. Theory Techn., Vol. 62, No. 4, pp. 789-798, 2014

[64] A. Niang, A. de Lustrac, S. N. Burokur, “Superluminal wave propagation in a non-Foster negative capacitor loaded transmission line”, Electronic Letters, Vol. 53, No. 8, pp. 547-549, 2017

[65] J. Long, “Non-Foster Circuit Loaded Periodic Structures for Broadband Fast and Slow Wave Propagation”, PhD Thesis, University of California, San Diego, 2015

[66] S. Hrabar, I. Krois, I. Bonic, A. Kiricenko, “Non-Foster elements - new path towards broadband ENZ and MNZ metamaterials”, Proc. on EUCAP, pp. 2674, Prague, 2011

[67] J. Long, D. Sievenpiper, “Low-profile and low-dispersion artificial impedance surface in the UHF band based on non-foster circuit loading”, IEEE Trans. Ant. and Propag., Vol. 64, No. 7, pp. 3003-3010, 2016

[68] J. Mou, Z. Shen, “Design and experimental demonstration of non-Foster active absorber”, IEEE Trans. Ant. and Propag., Vol. 65, No. 2, pp. 696-704, 2017

[69] J. Mou, Z. Shen, “Broadband and thin magnetic absorber with non-Foster metasurface for admittance matching”, Scientific Reports, Vol. 7, pp. 1-9, 2017

[70] M. Barbuto, A. Monti, F. Bilotti, A. Toscano, “Design of a non- Foster actively loaded SRR and application in metamaterial inspire components”, IEEE Trans. Ant. and Propag., Vol. 61, No. 3, pp. 1219-1227, 2013

[71] D. F. Sievenpiper, “Superluminal Waveguides Based on Non-Foster Circuits for Broadband Leaky-Wave Antennas”, IEEE Ant. and Wirel. Prop. Lett.,Vol. 10, pp. 231-234, 2011

[72] H. Mirzaei, G. V. Eleftheriades, “Realizing non-Foster reactive elements using negative-group-delay networks”, IEEE Trans. Microw. Theory Techn., Vol. 61, No. 12, pp. 4322-4332, 2013

[73] H. Mirzaei, “Negative-group-delay and non-Foster electromagnetic structures”, PhD dissertation, Dept. Elect. Comput. Eng., Toronto Univ., Toronto, ON, Canada, 2015

[74] S. Hrabar, “Is Stable Dispersionless non-Foster DNG Metamaterial Indeed Impossible?”, Proc. on Metamaterial Congress (Copenhagen, 2014), pp. 13.

[75] S. Hrabar, “Metamaterial Structures based on ‘Negative’ Elements - What Do We Know After a Decade of Research?”, Proc. on Metamaterial Congress (Rome, 2017), pp. 197

[76] Y. Fan, “Research and Design of Non-Foster Active Metamaterials”, PhD Thesis, Queen Mary University, United Kingdom, 2013

[77] S. Saadat, M. Adnan, H. Mosallaei, E. Afshari, “Composite metamaterial and metasurface integrated with non-Foster active circuit elements: A bandwidth-enhancement investigation”, IEEE Trans. Ant. and Propag., Vol. 61, No. 3, pp. 1210-1218, 2013

[78] T. P. Weldon, K. Miehle, R. S. Adams, K. Daneshvar, “A wideband microwave double-negative metamaterial with non-Foster loading”, Proceedings of IEEE SoutheastCon, pp. 1-5, 15-18 March 2012

[79] J. D. Brownlie, “On the Stability Properties of a Negative Impedance Converter”, IEEE Trans. CT-13, pp. 98-99, March 1966

[80] R. F. Hoskin, “Stability on Negative Impedance Converters”, Elec. Lett. 2, 3U1, September 1966

[81] A. F. Schwarz, “On the Stability Properties of a Negative-Immittance Converter”, IEEE

Trans. CT-1, 77, March 1967

[82] E. Ugarte-Muñoz, S. Hrabar, D, Segovia-Vargas, A. Kiricenko, “Stability of Non-Foster Reactive Elements for use in Active Metamaterials and Antennas”, IEEE Tran. on AP-S, Vol. 60, No. 7, pp. 3490-3494, 2012

[83] S. D. Stearns, “Counterintuitive Aspects of Non-Foster Networks”, Presentation slides, Adelphi Antenna Workshop on Electrically Small Antennas, Clarksville, MD, July 8-9, 2010

[84] S. D. Stearns, “Non-Foster Circuits and Stability Theory”, Proc. on IEEE APS/URSI (Spokane, 2011), pp. 1942-1945

[85] S. D. Stearns, “Incorrect Stability Criteria for Non-Foster Circuits”, Proc. on IEEE APS/URSI (Chicago, 2012), pp. 1

[86] S. Tretyakov, S. Maslovski, Veselago Materials: “What is Possible and Impossible about the Dispersion of the Constitutive Parameters”, IEEE Ant. and Prop. Mag., Vol. 49, No. 1, pp. 37-43, 2007

[87] J. Loncar, S. Hrabar, A. Kiricenko, “Stability of Metasurface-Based Parity-Time Symmetric Systems”, Proc. on Metamaterial Congress (Crete, 2016), pp. 738

[88] Y. Ràdi, D. L. Sounas, A. Alù, S. A. Tretyakov, “Parity-Time Symmetric Teleportation”, Phy. Rev. B, Vol. 93, 235427-235434, 2016

[89] Q. Tang, H. Xin, “Stability Analysis of Non-Foster Circuit Using Normalized Determinant Function”, IEEE Tran. Microw. Theory and Techn., Vol. 65, No. 9, pp. 3269-3277, 2017

[90] S. R. Rengarajan, C. R. White, “Stability analysis of superluminal waveguides periodically loaded with non-Foster circuits”, IEEE Anten. and Wireless Prop. Lett., Vol. 12, pp. 1303-1306, 2013

[91] J. Loncar, S. Hrabar, D. Muha, “Stability of simple lumped-distributed networks with negative capacitors”, IEEE Tran. on Ant. and Prop., Vol. 65, No. 1, pp. 390-395, 2017

[92] K. Z. Rajab, Y. Hao, D. Bao, C. G. Parini, C. Vazquez, J. Philippakis, M. Philippakis, “Stability of active magnetoinductive metamaterials”, J. Appl. Phys., Vol. 108, No. 5, 054904-1~054904-6, 2010

[93] S. D. Stearns, “Stable Band-pass Non-Foster Circuits”, Proc. on IEEE APS/URSI (Vancouver, 2015), pp. 1386

[94] S. D. Stearns, “Circuit Analysis of the Stability of a Two-Element Non-Foster Impedance Matching Network”, Proc. on IEEE APS/URSI (San Diego, 2017), pp. 1

[95] J. Loncar, D. Muha, S. Hrabar, “lnfluence of Transmission Line on Stability of Networks Containing ldeal Negative Capacitors”, Proceedings on Antenna and Propagation Society International Symposium (IEEE APSURSI), Vancouver, July 2015

[96] S.Hrabar, I. Krois, D. Zanic, “Improving Stability of Negative Capacitors for use in Active Metamaterials And Antennas”, Proc. of the 2018 IEEE Int. Symp. on Ant. and Prop. (APS / URSI), July 2018

[97] Stephen E. Sussman-Fort, Ron M. Rudish, “Non Foster Impedance Matching for Transmit Applications”, 2006 IEEE International Workshop on Antenna Technology, pp. 53-56, March 2006

[98] S. E. Sussman-Fort, R. M. Rudish, “Increasing Efficiency or Bandwidth of Electrically-Small Transmit Antennas by Impedance Matching With Non-Foster Circuits”, PIERS 2006, Mar. 26-29, 2006

[99] S. Hrabar and A. Kiricenko, “Towards Broadband Tunable non-Foster Radiating Systems”, 10th International Congress on Metamaterials, 2016, 133-135

[100] S. Hrabar, A. Kiricenko, I. Krois, “Antenna-transmitter based on Non-Foster Source”,

Proc. on IEEE APS/URSI (San Diego, 2017), pp. 875
[101] S. Hrabar, I. Krois, L. Vincelj, "Two-element Non-Foster Antenna-transmitter Array", Proceedings of the 2018 IEEE International Symposium on Antennas and Propagation (APS / URSI), July 2018
[102] S. D. Stearns, "Stable band-pass non-Foster circuits," in 2015 IEEE International Symposium on Antennas and Propagation and URSI Meeting, pp. 1386–1387, July 2015.
[103] F. Schwarz, "Negative resistors and negative conductors", Doctoral Dissertation, Delft University of Technology, 1969.
[104] ----- https://www.cadence.com
[105] ----- https://www.keysight.com
[106] ----- https://www.amcad-engineering.com/software-module/stan
[107] B. Buiantuev, N. Kalmykov, D. Kholodnyak, A. Brizic, L. Vincelj and S. Hrabar, "Physically Oriented Design of Negative Capacitors Based on Linvill's Floating Negative Impedance Converter (NIC)", in IEEE Trans. on Microwav. Theory and Techniq., vol. 70, no. 1, pp. 139-154, Jan. 2022
[108] C. R. White, J. W. May, J. S. Colburn, "A variable negative-inductance integrated circuit at UHF frequencies", IEEE Microw. Wireless Compon. Lett., Vol. 22, No. 1, pp. 35-37, 2012
[109] S. Saadat, H. Aghasi, E. Afshari, H. Mosallaei, "Low-power negative inductance integrated circuits for GHz applications", IEEE Microw. Wireless Compon. Lett., Vol. 25, No. 2, pp. 118-120, 2015
[110] S. E. Sussman-Fort, "Gyrator-Based Biquad Filters and Negative Impedance Converters for Microwaves", International Journal RF and Microwave CAE, Vol. 8, No. 2, pp. 86-101, 1998
[111] D. S. Nagarkoti, Y. Hao, D. P. Steenson, L. Li, E. H. Linfield, K. Z. Rajab, "Design of broadband non-Foster circuits based on resonant tunneling diodes", IEEE Ant. Wirel. Propag. Lett., Vol. 15, pp. 1398-1401, 2015
[112] D. Gregoire, C. White, J. Colburn, "Wideband Artificial Magnetic Conductors Loaded With Non-Foster Negative Inductors", IEEE Ant. and Wirel. Prop. Lett., Vol. 10, pp. 1586-1589, 2011
[113] D. J. Gregoire, C. R. White, J. S. Colburn, "A coaxial TEM cell for direct measurement of UHF artificial magnetic conductors", IEEE Ant. and Prop. Mag., Vol. 54, No. 2, pp. 251-259, 2012
[114] C. K. Kuo, "Realization of negative-immittance converters and negative resistances with controlled sources", PhD Thesis, Georgia Institute of Technology, December 1967
[115] J. Lončar, J. Vuković, I. Krois, and S. Hrabar, "Stability Constraints on Practical Implementation of Parity-Time-Symmetric Electromagnetic Systems", Photonics, vol. 8, no. 2, p. 56, Feb. 2021.
[116] A. Brizic and S. Hrabar, "A tunable high-pass filter employing the effects of negative capacitance and inductance", 2021 Fifteenth International Congress on Artificial Materials for Novel Wave Phenomena (Metamaterials), 2021, pp. 068-069, doi: 10.1109/Metamaterials52332.2021.9577157.
[117] D. Zanic, K. Lebo and S. Hrabar, "Open circuit stable non-Foster negative inductor", 2021 Fifteenth International Congress on Artificial Materials for Novel Wave Phenomena (Metamaterials), 2021, pp. 21-23, doi: 10.1109/Metamaterials52332.2021.9577184.
[118] D. Zanic and S. Hrabar, "Stability-improved Non-Foster Inductance based on Compensated Passive Structure", 2022 Sixteenth International Congress on Artificial

Materials for Novel Wave Phenomena (Metamaterials), Siena, Italy, 2022, pp. 193-195, doi: 10.1109/Metamaterials54993.2022.9920773.

[119] A. Brizic, K. Lebo and S. Hrabar, “Equivalent-circuit-based Stability Analysis of Non-Foster Open Circuit Stable Negative Inductor”, 2020 International Symposium ELMAR, 2020, pp. 13-16, doi: 10.1109/ELMAR49956.2020.9219036.

[120] A. Brizic and S. Hrabar, “Equivalent-circuit-based Stability Analysis of non-Foster SCS Negative Capacitor”, 2020 Fourteenth International Congress on Artificial Materials for Novel Wave Phenomena (Metamaterials), 2020, pp. 060-062, doi: 10.1109/Metamaterials49557.2020.9284966.

[121] H. Park, S. Lee, J, Lee, N, Sangwook, “A 0.1-1 GHz CMOS Variable Gain Amplifier Using Wideband Negative Capacitance”, IECE Trans. Electron., Vol. E92-C, No.10, pp. 1311-1314, October 2009

[122] D. Zanic, A. Brizic, E. Iakovenko, N. Kalmykov, D. Kholodnyak and S. Hrabar, “Equivalent Circuit of OCS Negative Capacitor based on Linvill’s Floating NIC”, 2022 IEEE International Symposium on Antennas and Propagation and USNC-URSI Radio Science Meeting (AP-S/URSI), Denver, CO, USA, 2022, pp. 1306-1307, doi: 10.1109/AP-S/USNC-URSI47032.2022.9886844.

[123] Y. Kwisung, M. Mohammed, et. al., “Negative impedance circuit and its application to inductorless resonant oscillators”, Pro. Int SOC Conference in Seoul, pp. 13-16, 2007

[124] M. M. Jacob, L. Jiang, D. F. Sievenpiper, “Nonlinear effects of non-Foster matching networks”, Proc. of the 2015 IEEE AP-S USNC/URSI, pp. 1248–1249, 2015

[125] H. Khoshniyat, A. Abdipour, G. Moradi, “Nonlinear modeling, time-domain analysis and simulation of non-Foster elements”, International Journal of Microwave and Wireless Technologies, Vol. 9, No. 4, pp. 1-9, September 2016

[126] T. Suligoj, M. Koricic, H. Mochizuki, S. Morita, K. Shinomura and H. Imai, "Horizontal Current Bipolar Transistor With a Single Polysilicon Region for Improved High-Frequency Performance of BiCMOS ICs," in IEEE Electron Device Letters, vol. 31, no. 6, pp. 534-536, June 2010.

[127] A. I. Zverev, Handbook of Filter Synthesis. Wiley-Interscience, 2005.

[128] Ante Brizic, Silvio Hrabar, Dominik Zanic, Igor Krois, “Investigation of impedance inverter based on band-pass non-Foster negative capacitor” 23rd International Conference on Applied Electromagnetics and Communications (ICECOM), Dubrovnik, Croatia, 2019, doi: 10.1109/ICECOM48045.2019.9163644

[129] Nikita Kalmykov, Dmitry Kholodnyak, “Non-Foster Elements Pave the Way to Design Novel Wideband and Tunable Bandpass Filters”, 2022 Asia-Pacific Microwave Conference (APMC), Yokohama, Japan, 2022, doi: 10.23919/APMC55665.2022.9999939